LIGHTWEIGHT ENERGY ABSORBING STRUCTURES FOR CRASHWORTHY DESIGN

Conor Francis O'Neill

Submitted for the Degree of Doctor of Philosophy

January 2018

SCHOOL OF MECHANICAL & SYSTEMS ENGINEERING

LIGHTWEIGHT ENERGY ABSORBING STRUCTURES FOR CRASHWORTHY DESIGN

Conor Francis O'Neill

Summary

The application of lightweight composite materials into the rail industry requires a stepwise approach to ensure rail vehicle designs can make optimal use of the inherent properties of each material. Traditionally, materials such as steel and aluminium have been used in railway rolling stock to achieve the energy absorption and structural resistance demanded by European rail standards. Adopting composite materials in primary structural roles requires an innovative design approach which makes the best use of the available space within the rolling stock design such that impact energies and loads are accommodated in a managed and predictable manner.

This thesis describes the innovative design of a rail driver's cab to meet crashworthiness and structural requirements using lightweight, cost-effective composite materials. This takes the application of composite materials in the rail industry beyond the current state-of-the-art and delivers design solutions which are readily applicable across rolling stock categories. An overview of crashworthiness with respect to the rail industry is presented, suitable composite materials for incorporation into rolling stock designs are identified and a methodology to reconfigure and enhance the space available within rail vehicles to meet energy absorption requirements is provided.

To realise the application of composite materials, this body of work describes the pioneering application of aluminium honeycomb to deliver unique solutions for rail vehicle energy absorbers, as well as detailing the use of lightweight composite materials to react the structural loads into the cab and carbody. To prove the capability of the design it is supported by finite element analysis and the construction of a full-scale prototype cab which culminated in the successful filing of two patents to protect the intellectual property of the resulting design.

To my family and friends

Acknowledgements

I would like to thank the following for their assistance in this programme of research:

- My academic and industrial supervisor **Prof. Mark Robinson** whose guidance and support has been key to delivering this successful project.

- My academic supervisor **Dr. Jack Hale** whose input and suggestions have helped guide and shape this work.

- **Prof. John Roberts** of Bombardier Transportation (UK) for passing on his extensive knowledge of rail vehicle crashworthiness to me.

- **Dr. Jan Prockat** of Bombardier Transportation (Germany) for assessing the ongoing designs and providing a critical analysis of key aspects of the derived solutions.

- **Guy Simmonds** of Anthony, Patrick & Murta Lda for producing the full-scale prototype cab and insisting on my involvement in its manufacture.

- **Dr. Marzio Grasso** of Frederico II University of Naples for his work on the dynamic simulations of the cab design solutions.

- The **European Commission** whose Framework 6 funded project “De-Light” (Contract Number 031483) forms the basis of this work.

- The **technicians** in the School of Mechanical & Systems Engineering for their assistance in undertaking the experimental work contained within this project.

- Those who have been involved in proof reading this manuscript: **Katherine O’Neill**, **Karen McTigue**.

- And to **everyone else** who supported me in this undertaking.

Nomenclature

a	Perpendicular height of triangle
A	Area
A_{load}	Load area
A_{tot}	Total area
A_{upp}	Upper absorber load area
b	Length of base of triangle
D	Depth
E_{abs}	Energy absorbed
H	Height
L	Length
m	Slope of a line
n	Integer
$P_{crush\text{-}mean}$	Mean crush load
P_{proof}	Proof load
r_{cd}	Die fillet radius
r_o	Internal tube radius
R	Radius
s_{crush}	Crush distance
V_f	Fibre volume fraction
V_{lc}	Maximum train unit operational speed at a level crossing
V_{tot}	Total volume
W	Width

σ_{crush} stress, being defined as the stress experienced by the energy absorber under dynamic crush load conditions and determined from:

$$\sigma_{crush} = \frac{P_{crush-mean}}{A_{upp}}$$

σ_{stat} stress, being defined as the stress experienced by the energy absorber under static load conditions and determined from:

$$\sigma_{stat} = \frac{P_{proof}}{A_{load}}$$

TABLE OF CONTENTS

LIST OF FIGURES

LIST OF TABLES

Chapter 1: Introduction

1.1. Crashworthiness

Instances of frontal and rear-end collisions between rail vehicles can be traced back as far as the mid-1800s. The 1844 Midland Railway coal wagon collision at Nottingham-Beeston is one of the earliest documented crashes involving two rail vehicles in a head-on collision. Reports from the time stated that *"…[the station-master] got upon the engine with the driver of the down train, and proceeded slowly towards Nottingham, but owing to a very heavy fog which prevented them from seeing many yards, they came into collision with an up train coming out on the down line, when two passengers were killed and several very severely wounded"* [1].

Such collisions continue to occur to this day, for example the 2008 head-on collision at Chatsworth, California, where a Union Pacific freight train and a Metrolink commuter train collided leading to the deaths of 25 passengers with another 126 injured (Figure 1). The accident report which resulted from the investigation stated that "*The force of the collision caused the locomotive of train 111 [Metrolink] to telescope into the lead passenger coach by about 52 feet*" [2].

Figure 1: Aerial view of the 2008 Chatsworth collision in California, U.S.A. [3]

This incident, which itself was preceded by the 2005 Metrolink crash at Glendale, California [4] prompted the US Federal Railroad Administration to research and implement crash energy management and energy absorbing devices into new rolling stock for the system [5].

On a global level there is evidence that the rate of occurrence of railway disasters has increased significantly over the past 100 years, with 88% of all collisions occurring in the past 40 years (1970 - 2009) [6]. In the UK however, this trend is not readily evident with a notable decrease in the total number of potentially high risk train accidents (PHRTAs) as shown in Figure 2 (data from UK Department of Transport [7]).

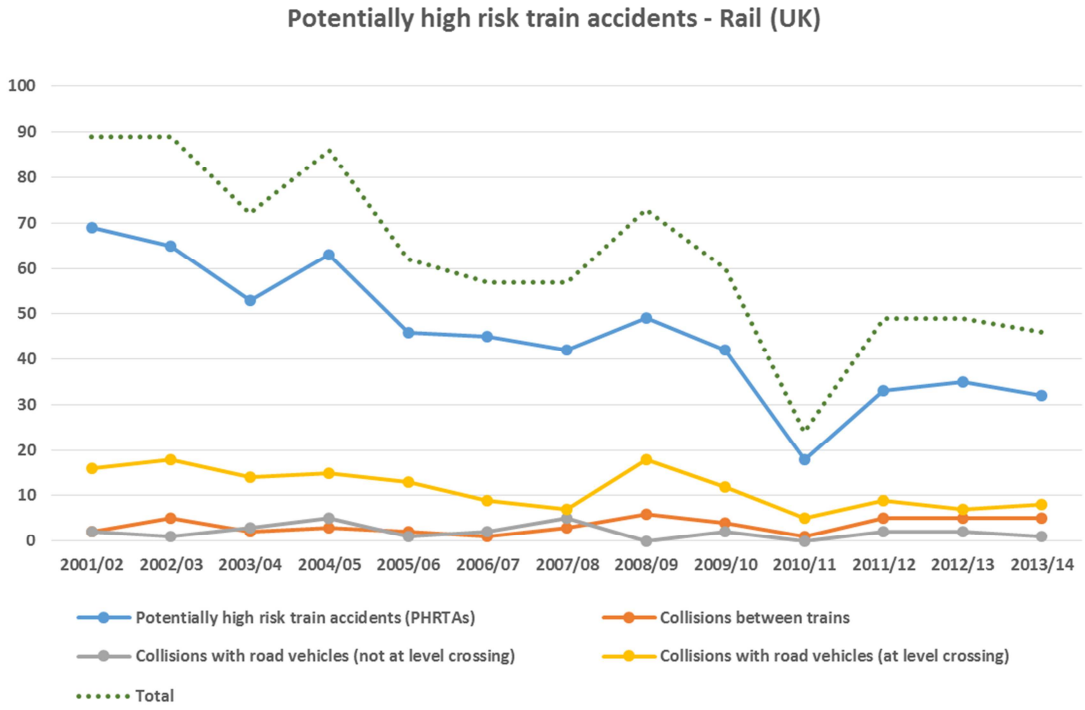

Figure 2: Potentially High Risk Train Accidents in the UK between 2001 and 2014 [7]

However, this should not lead to complacency - within the same period there were 12 fatalities, 65 passengers with major injuries and almost 70,000 passengers suffering minor injuries as a result of train collisions. Of note is the sharp increase in the past decade (2004-2014) of the number of minor injuries suffered (Figure 3) as a consequence of passengers physically impacting with internal fixtures during the collision. Such incidents prompted research by the European Commission through the EURailSafe initiative [8] and the SAFEINTERIORS project [9] which focused on delivering improved passive safety for rail passengers.

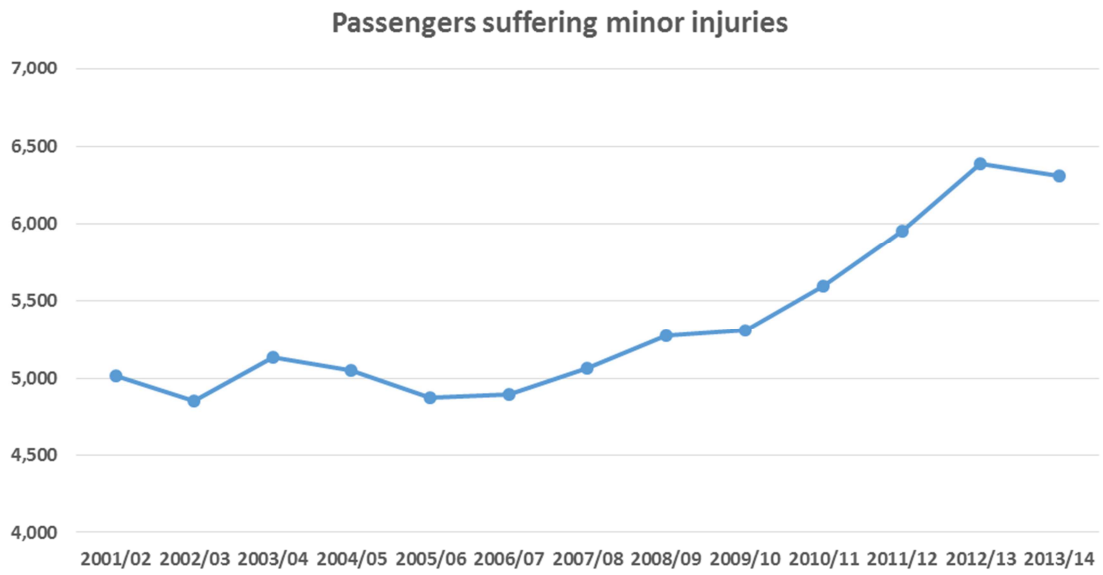

Figure 3: Number of minor injuries suffered by passengers during the period 2001 and 2014 [7].

To achieve improved passenger safety and reduce injuries and casualties from impact the rail industry continually strives to develop more crash-capable vehicles. Rail vehicle "crashworthiness" can be defined as the ability of a rail vehicle's structure to minimise the amount of injury-causing energies reaching the occupants. Applying this principle to the design of rolling stock can lead to a reduction in the severity of injuries received by the occupants, thereby increasing the survivability of impacts. All transport modes retain their own approach to crashworthiness which are dependent on a number of factors, including but not limited to: the most likely mode of impact, most effective means of energy absorption, passenger position, applicable safety standards, etc.

However, in all modes of transport the basic relationship between the passenger and vehicle remain largely the same during impact. In normal operation the relative velocity between vehicle and passenger should be kept to a minimum. In an impact the vehicle's velocity undergoes a sudden change (Figure 4 "A") but the passenger velocity remains, for a period, unchanged (Figure 4 "B"). It is this difference in the relative velocity between the vehicle and its passenger that leads to the passenger impacting the internal structure of the vehicle (Figure 4 "C"), until the passenger's velocity matches that of the vehicle (Figure 4 "D").

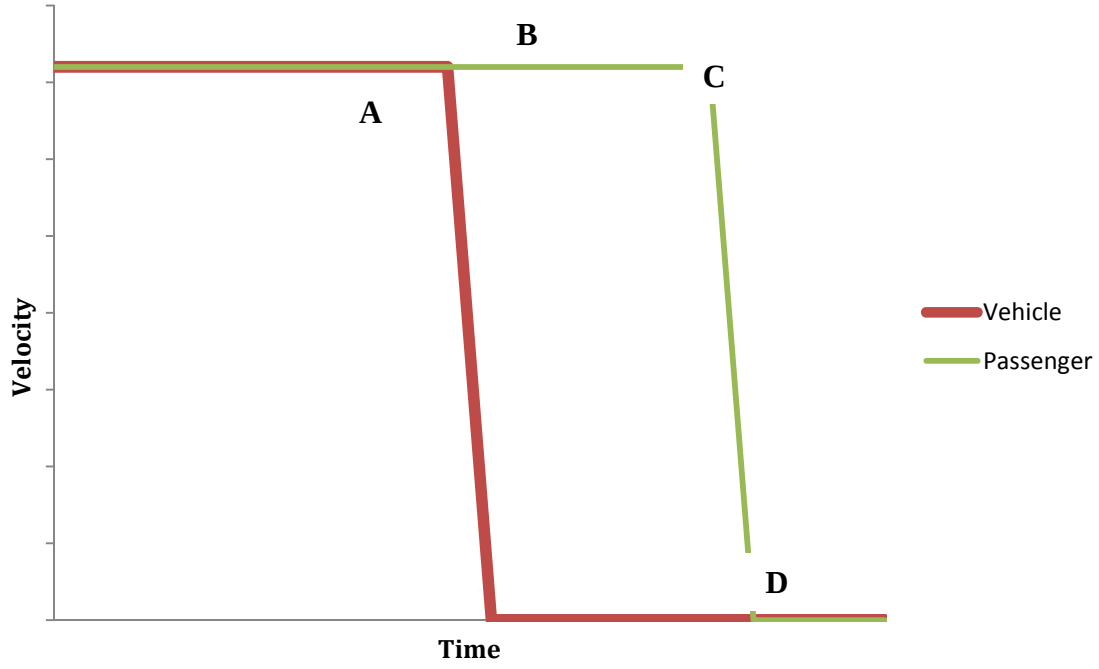

Figure 4: Graph of velocities of vehicle and passenger during a collision

As such, each collision can be considered as a series of two or more collisions [10]:

1. The impact of the **vehicle** with an **external object** leading to a rapid decrease in velocity.
2. The impact(s) of the **passenger(s)** with the **vehicle interior** leading to injury.

From a design perspective there are two approaches to improving the safety of vehicles based on these two collision scenarios:

a) Active Safety which addresses the preventative measures to avoid the accident and pre-impact preparation of the vehicle.
b) Passive Safety which addresses the impact of the vehicle and post-impact response.

1.1.1. *Active Safety*

Active Safety describes any method which assists in the prevention of collisions and the pre-impact preparation of the vehicle for potential impact, as shown in the rail collision process model in Figure 5.

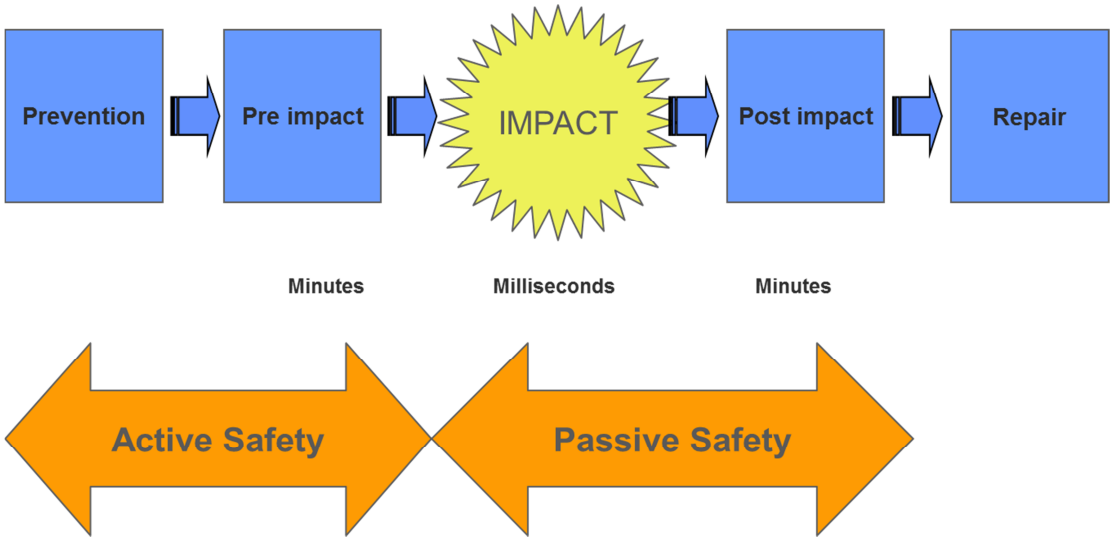

Figure 5: Rail collision process model [11]

In the rail industry active safety is embodied in the form of systems such as signalling, Automatic Train Protection systems (ATP) [12] or Rail Traffic Management Systems (RTMS).

As an example, ATP can activate the braking system of a piece of rolling stock if the driver fails to reduce the velocity of the train in a timely manner. A stop signal sends a transmission to the train, either via transmission rails or signal beacons, which is then processed on-board the train. If the velocity exceeds safe braking distance parameters the brakes are automatically engaged to ensure the train does not pass the stop signal (Figure 6). Technologies such as ATP seek to prevent the initial impact occurring thereby keeping the relative velocities between the passengers and surrounding vehicle low.

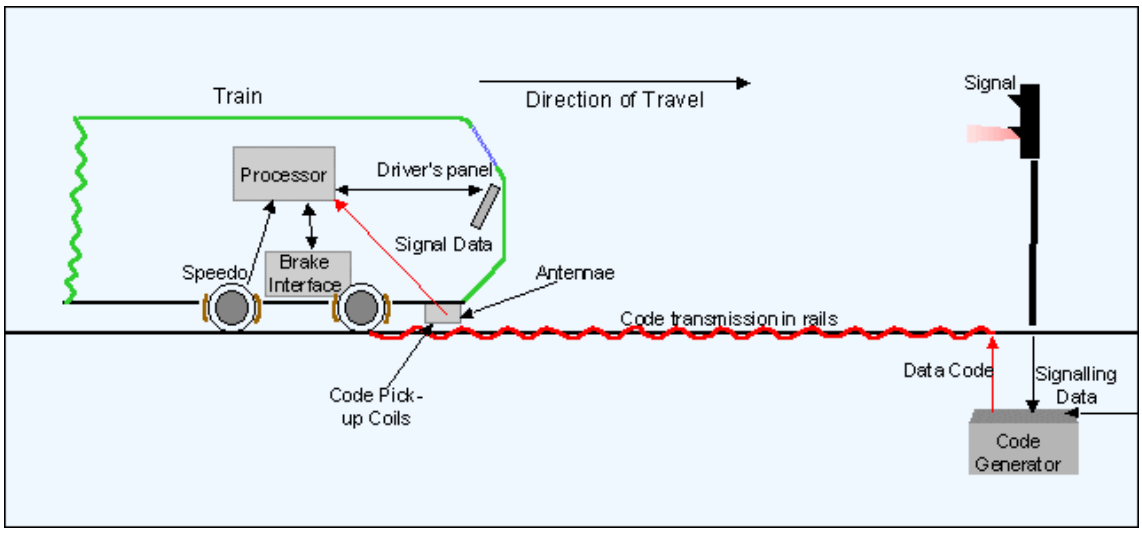

Figure 6: Principal of Automatic Train Protection system, a form of rail Active Safety [13]

Intelligent train control and monitoring systems can have a vital role in providing reliable, adaptable and flexible trains necessary to deliver reliable train services that meet the expectations of modern rolling stock operators and rail customers. When these systems or technologies prove insufficient to avoid impact, it is the function of Passive Safety to protect the driver and occupants.

1.1.2. *Passive safety*

Passive Safety refers to those parts of the vehicle which seek to protect the occupants during and post impact (Figure 5). In an article on passive safety of rail vehicle interiors [14] Palacin discusses primary and secondary impact, observing that "*Occupants can be injured as a result of two main events occurring in the immediate aftermath of a crash, namely the sudden acceleration/deceleration of the vehicle and/or mechanical damage to the vehicle structure*".

The structural design of a rail vehicle for crashworthiness is in itself a form of passive safety. By analysing how the vehicle structure reacts during collisions and improving the design such that the integrity of the passenger compartment is maintained the passive safety capability of the vehicle can be increased. In the rail industry this is embodied in the principle of Crash Energy Management (CEM) [15] which seeks to absorb impact energies in a controlled

manner to reduce the relative velocity between passengers and the surrounding coach whilst preserving the occupied volume.

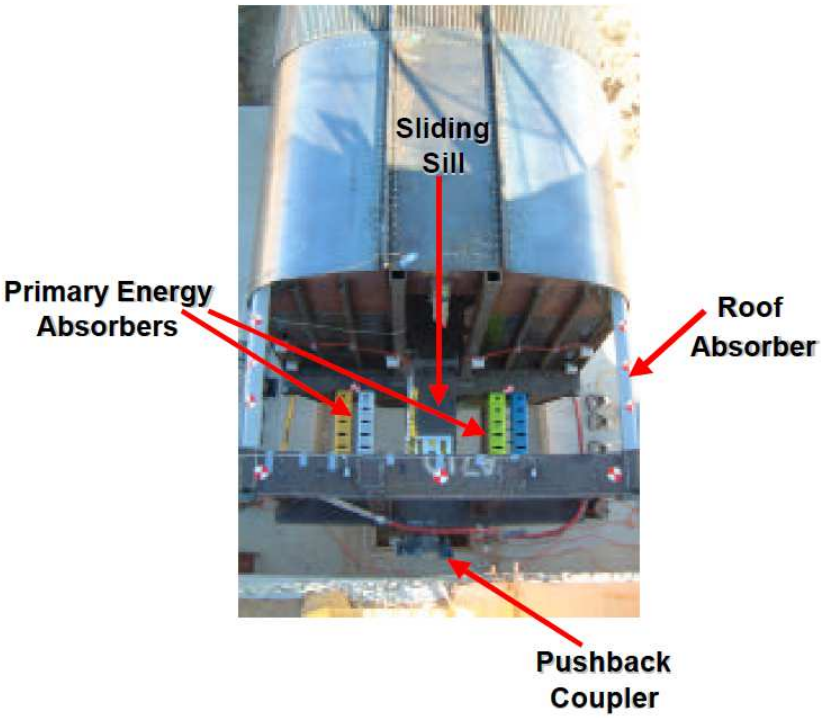

Figure 7: Rail vehicle car body with integrated Crash Energy Management elements [16]

This principle is described and applied by Tyrell et al. [16][17] who tested a CEM design for rail vehicles (Figure 7) which demonstrated a marked improvement in passenger safety for speeds of up to 38 mph.

1.2. Crashworthiness across transport modes

1.2.1. *Aerospace*

The aerospace industry primarily relies on the implementation of Active Safety systems to help protect passengers. Not specifically designed to absorb energy on collision, aircraft have a number of built-in levels of system redundancy (typically a triple redundancy system [18]) to reduce the likelihood of failure which may lead to a crash, as well as using collision avoidance systems to prevent in-air impacts. In the event of a ground impact, the aircraft systems attempt to reduce the likelihood of event escalation which may lead to passenger

injury. For example, fuel cut-off valves engage to prevent fire spread, whilst passenger restraint systems (seatbelts) are supplied to keep passengers in position until the crew can initiate the evacuation procedure.

Aircraft landing gear systems deploy a number of energy/shock absorption solutions, ranging from complex hydraulic oleo struts (Figure 8) to simpler bungee cord strapping which allows the whole strut assembly to flex (Figure 9).

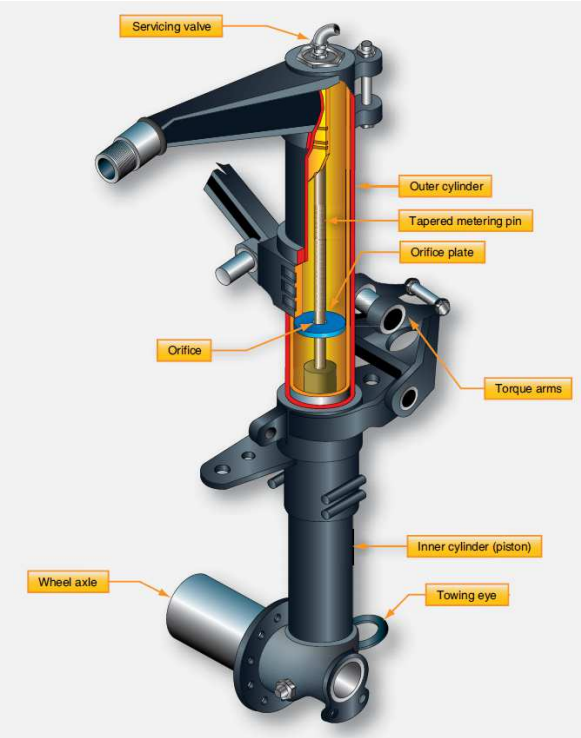

Figure 8: Typical energy absorbing aircraft landing gear oleo strut [19]

Figure 9: Bungee cord absorbers on an American Eagle A-101 biplane [20]

Passive absorbers have been investigated for use on Earth Entry Vehicles by NASA [21] to eliminate the requirement for active systems using absorber devices constructed from foam-filled composite cellular materials with additional requirements that the design be able to withstand not only omni-directional impact loads but also penetrative loads.

The application of crashworthiness principles on helicopter design has been intensively reviewed by Shanahan [22] with the author noting that implementing these principles will "*involve trade-offs between the perceived risk of a crash and increased cost*", adding that "*crashworthiness is not inherent in most aircraft designs since features that enhance crash performance do not usually improve operational performance or efficiency*". The author notes however that crashworthiness in helicopters could bring about two major benefits: a) a reduction in injury and b) a reduction in repair costs.

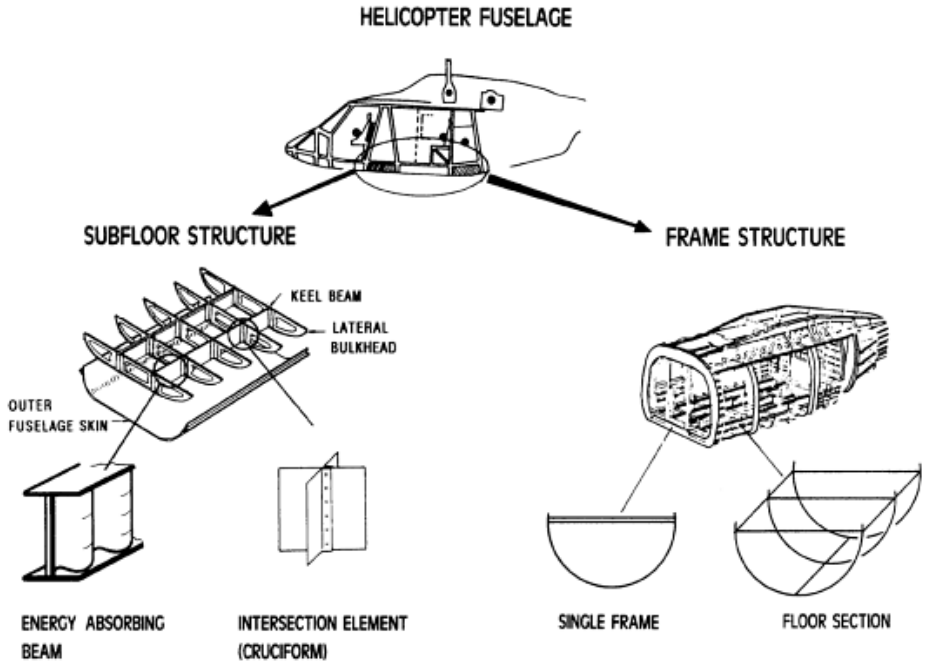

Figure 10: Energy absorbing elements in a helicopter subfloor [23]

Aspects of the performance characteristics of energy absorbing subfloor elements for helicopters is discussed by Kindervater et al. [23] where the authors note that energy absorbing keel beams have the capacity to limit the deceleration forces caused by impact, while the company "Bell Helicopters" have perceived the potential benefits of subfloor energy absorbers manufactured from composite materials as far back as 1983 when they filed

a patent to protect the concept for helicopters, a patent which was subsequently granted in 1986 [24].

1.2.2. *Automotive*

In order to implement crashworthiness into the design of road vehicles the automotive industry needs to consider impacts from all lateral directions. To achieve this they use both vehicle design and vehicle systems to protect the occupants, applying both passive and active safety technologies. Anti-lock braking, traction control, active suspensions etc. all contribute to the initial prevention of an accident. From a passive safety perspective crumple zones which are designed to crush on impact absorb energy thereby reducing the peak forces experienced by passengers, while seatbelts and airbags prevent further injury by reducing the likelihood of impact with internal fixings.

The Formula One industry not only uses composites for lightweight purposes but they also employ these materials to absorb impact energy through controlled crushing. To ensure the safety of the driver, the Formula One governing body, the FIA (Fédération Internationale de l'Automobile) enforce strict safety guidelines concerning the crashworthiness of Formula One racing cars. Each car must be designed to incorporate four impact structures: front, rear, side and steering column [25]. Current FIA test procedures require the energy absorbed by each of the four impactor segments to be between 15% and 35% of the total energy absorption. To achieve this composite energy absorbers are employed (Figure 11) to control the crush sequence, thus reducing the forces transmitted to the driver whilst containing the damage within the impact absorbing structure [26].

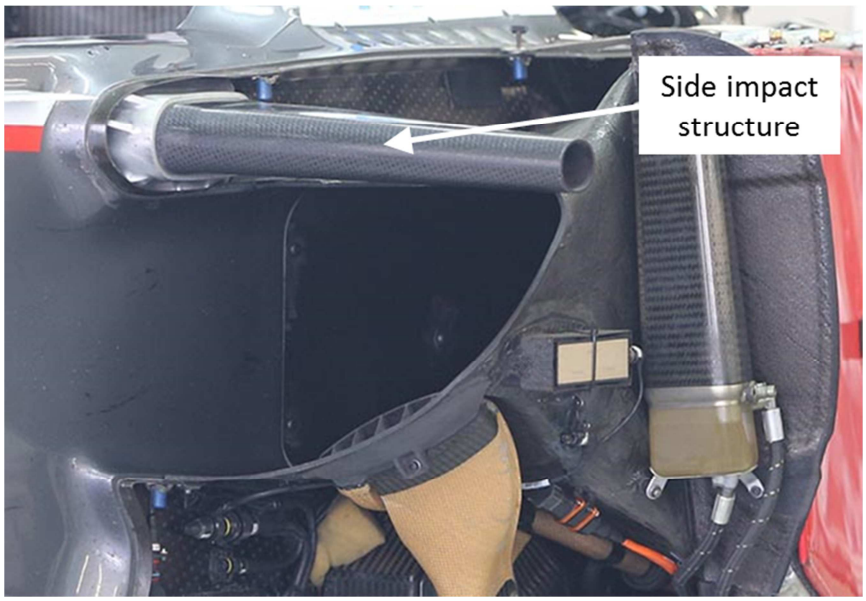

Figure 11: Side impact structure of the 2014 Sauber C33 Formula 1 car [27]

1.2.3. *Rail*

The rail industry focuses on linear impacts towards the front and rear of the train, with a suite of pre-defined collision scenarios being described in the European and British Crashworthiness Standard for rail vehicles [28] (further discuss in Section 1.3).

Protection is achieved primarily through structural design, catering for crumple zones throughout the entire train length, thereby absorbing large amounts of energy whilst reducing the forces experienced by the passengers. The primary energy absorbers located at the front of the driver's cab are designed to absorb the majority of the impact energy. These tend to be of a tubular design, with a controlled crumple pattern which absorbe energy to a specified depth into the front/rear end of the vehicles which reduces the likelihood of passengers experiencing excessive peak loads. Figure 12 depicts the result of a typical front-end impact, whilst the types of energy absorbers used within the rail industry are described in Section 2.1.

Figure 12: Front end collision between rail vehicles depicting cab crush and maintenance of driver's survival space (note undamaged driver's window) [29]

1.2.4. *Maritime*

The maritime industry considers the maintenance of hull integrity as their primary method of crash survival. In the event of an impact, minimising the effects of a hull breach will improve overall passenger survival rates. Double-skinned hulls and watertight bulkheads assist in containing the spread of water through the ship thereby maintaining buoyancy. Crashworthiness has not been readily adopted into commercial ship design due to the perception that the mass of the vessel will inevitably have to increase, thereby reducing its commercial competitiveness [30].

1.2.5. *Summary*

Due to the differing crashworthiness requirements for each of these transport modes, the implementation of crashworthiness within each vehicle design is specifically tailored to meet that transport sector's needs. This leads to the development of crashworthy technologies which meet functional requirements but do not make optimal use of the available design space. For example, tubular energy absorbers aligned longitudinally on a train will meet the

rail industry requirements but they do not take full advantage of the volume available within the front end of the driver's cab.

Treating the design of a rail vehicle and its energy absorbing elements separately can lead to a conflict between achieving the specified design and incorporating the crash requirements set by industry and standards. This in turn can lead to unnecessary design iterations in the development stage, or the implementation of more expensive energy absorber solutions to fit within an immovable design envelop. A more unified approach is required, one which incorporates energy absorbing elements into the design by maximising the energy capacity of the available space. It is this approach, in conjunction with lightweighting targets (as discussed in Section 1.5), which forms the core investigations of this thesis.

1.3. A Focus on Rail Vehicle Crashworthiness

1.3.1. *Crash Energy Management*

In a recent review of British, European and U.S. research, the UK Rail Safety & Standards Board (RSSB) [31] noted a common approach to achieving rail vehicle crashworthiness comprising:

1. Crashworthy design aimed at preserving occupant survival space and the maintenance of low deceleration levels.
2. Identification of a series of crash scenarios based on historical impacts.
3. Energy absorption criteria based on the crash scenarios.
4. Conceptual design and build of vehicle (proof-of-concept).
5. Crash performance validated through testing.
6. Development of design standards and requirements for industry-wide application.

Common conclusions from the studies reviewed within this report indicate that Crash Energy Management (CEM) is required in order to have distributed crush zones throughout the vehicle. Achieving this goal is dependent on a number of factors identified by Lim [32] such as: the gap between coaches, the effect of the couplers, the number of coaches in the

impacting trains. Lim concludes that while even distribution of energy along the rake is theoretically possible it is not achievable in practice.

Additionally, the effects of rail vehicle articulation cannot be ignored. Xue et al. [33] describe the differences between the support and coupling patterns in articulated and non-articulated vehicles and the effects it can have on the collision performance. The primary difference in construction and layout between articulated and non-articulated trains is as follows; a non-articulated train consists of a series of car-bodies, each of which is supported by two inboard bogies where the connection between vehicles is provided by a central coupler, whereas an articulated train will be semi-permanently coupled using shared bogies between each car (see Figure 13). Xue et al. conclude that due to the inherent stiffness of an articulated vehicle there is little scope for this to form part of a collapse structure without compromising the stability of the vehicle post-crash.

As a result of the articulated layout the ends of the train are required to absorb significantly more energy when compared with non-articulated vehicles, which can absorb energy throughout the rake.

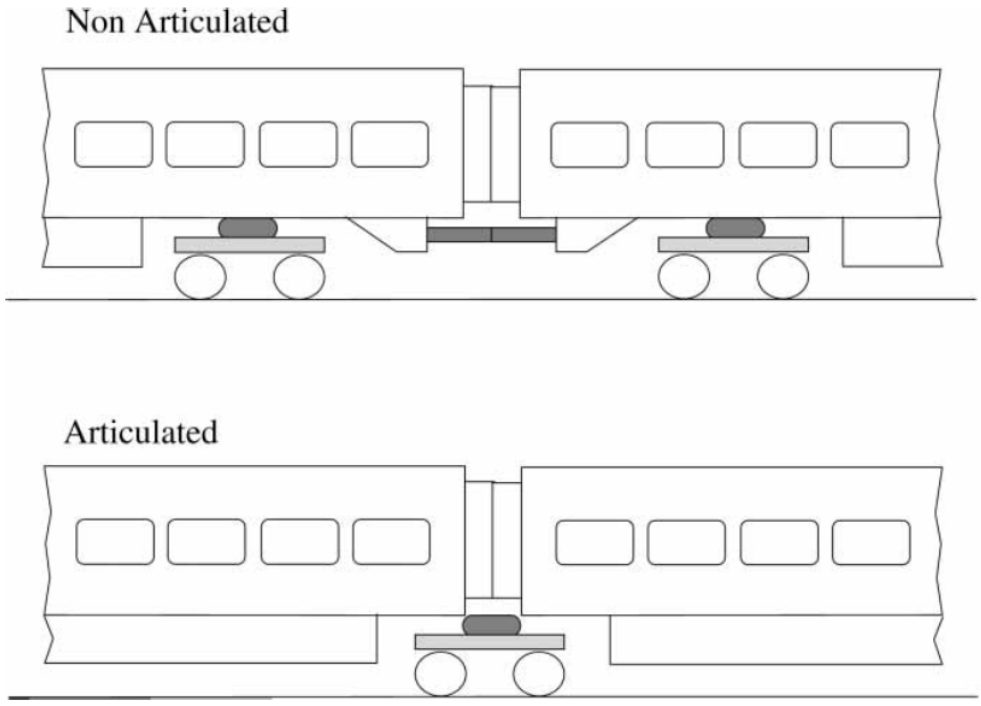

Figure 13: The difference between non-articulated (top) and articulated (bottom) train configuration [33].

As such, the cab ends of the vehicle should be designed to absorb higher levels of energy than the trailing coaches, this being especially relevant to articulated designs.

CEM is the principle of controlling the force-crush behaviour of a vehicle during high energy impact. For rail vehicles this involves developing specific areas of the vehicle which are intentionally designed to crush in a predictable and controlled manner. By distributing these areas along the entire vehicle rake (specifically at the ends of individual coaches) as recommended by Roberts et al. [11] more energy can be absorbed throughout the unoccupied areas of the train. The ultimate goal of CEM is to provide a dedicated survival volume for passengers whilst dissipating by plastic structural crushing and deformation of the vehicle carbody the energies involved in rail vehicle collisions.

Figure 14: US Federal Railway Authority crash tests using a conventional vehicle (showing significant loss of occupied space - top) and a CEM equipped vehicle (occupied space remains intact - bottom) [34]

The US Department of Transportation undertook a significant study into the design of CEM devices [16]. This study and subsequent full-scale tests [34] have shown that without CEM the impact can lead to the total destruction of the impacting coach as well as derailment of trailing coaches (Figure 14).

The impact scenarios governing the crashworthiness of rail vehicles are contained within EN 15227 *"Railway applications – Crashworthiness requirements for railway vehicle bodies"* [28]. According to the classification system of EN 15227 a vehicle operating on a regional network with level crossings (which forms the basis for this thesis, see Section 1.5) is a "Category C-I" vehicle for crashworthiness purposes. Category C-I vehicles must consider the following primary collision scenarios:

- **Collision Scenario 1:** a collision with an identical train unit at 36 km/h (Figure 15).

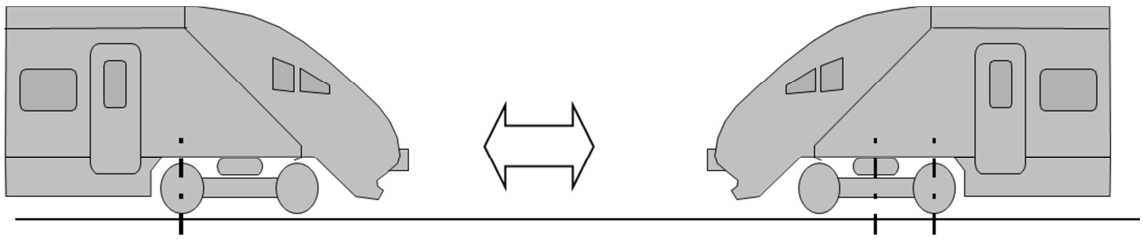

Figure 15: Collision Scenario 1 as defined by EN 15227 [28]

- **Collision Scenario 2:** a collision with an 80 tonnes wagon at 36 km/h (Figure 16).

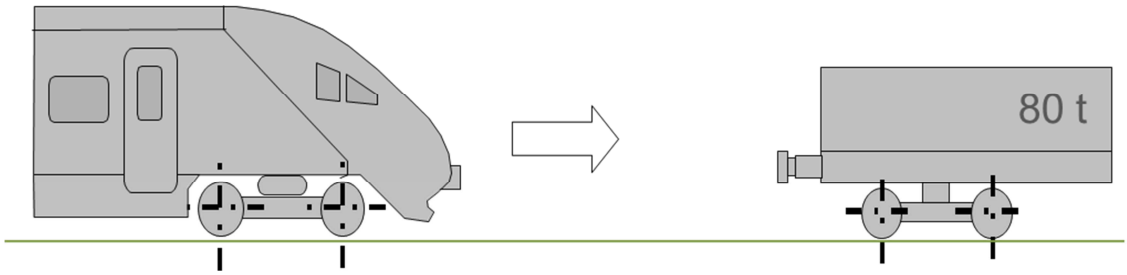

Figure 16: Collision Scenario 2 as defined by EN 15227 [28]

- **Collision Scenario 3:** a collision with a 15 tonnes deformable obstacle at a speed that is 50 km/h below the maximum operational speed of the vehicle (Figure 17).

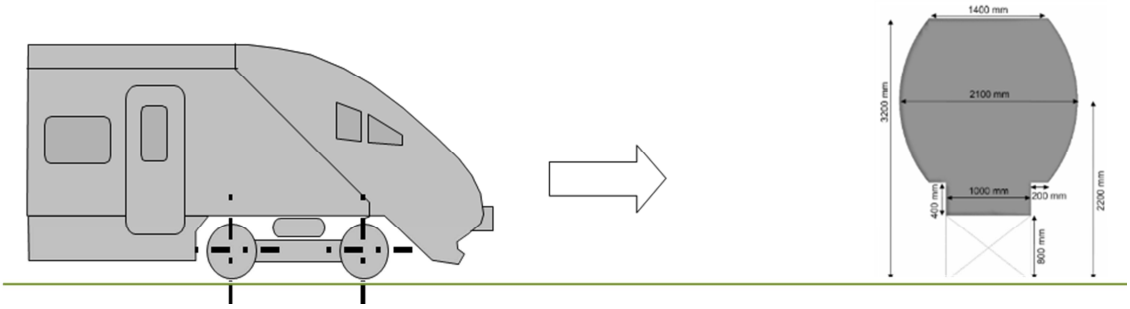

Figure 17: Collision Scenario 3 as defined by EN 15227 [28]

Under each of the collision scenarios outlined above, a rail vehicle's design for crashworthiness should seek to:

- Reduce the risk of overriding. This is simulated by ensuring that the criteria for deceleration and survival space (see below) are maintained when an initial **vertical offset of 40 mm** is employed between the two vehicles in Collision Scenario 1 (Figure 18).
- Absorb collision energy in a controlled manner.
- Maintain survival space and structural integrity of the occupied areas. For a cab this means that the driver's survival space should remain intact throughout the collision.

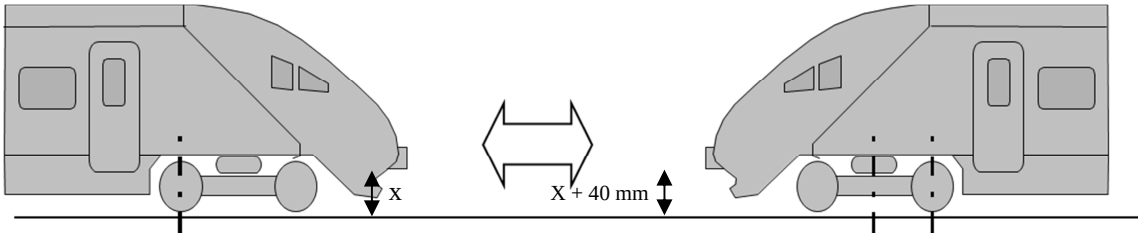

Figure 18: Collision Scenario 1 with 40 mm offset as defined by EN 15227 [28]

1.4. Rail vehicle structural load requirements

The initial design development phase of a rail vehicle will have the static structural requirements as defined in the EN 12663 standard *"Railway applications – Structural requirements of railway vehicle bodies"* [35] as one of its key design drivers. EN 12663 – "Structural requirements of railway vehicle bodies". This standard provides the minimum loading requirements which a vehicle must withstand to achieve certification.

According to the classification system of EN 12633, Bombardier's Spacium train (which forms the design basis for this work, see Section 1.6.1), as a passenger carrying fixed unit is classified as a "Category P-II" vehicle. The longitudinal static loads relevant to the cab of a Category P-II vehicle are summarised in Figure 19 where each load case has been assigned a number for reference (LS-1, LS-2, etc.) within the EN standard. It should be noted that the loads are applied individually, not collectively.

1.4.1. *Longitudinal loads*

Longitudinal forces defined in the EN 12663 ensure that there is sufficient structural rigidity along the length of the vehicle to ensure that damage is not caused to the structure as a result of operation loads (e.g. coupling, shunting, aerodynamic loading etc.).

In the event that these longitudinal loads are excessive, for instance during a high energy impact, the structure will suffer a rapid catastrophic failure and its ability to further sustain the longitudinal loads will be compromised. As the impact progresses the load required to buckle the structure decreases as the vehicle weakens, leading to further damage to the impacting coach. In a multi-coach train, should the lead coach perform in this manner it will absorb the majority of the impact energy, ultimately resulting in its total destruction.

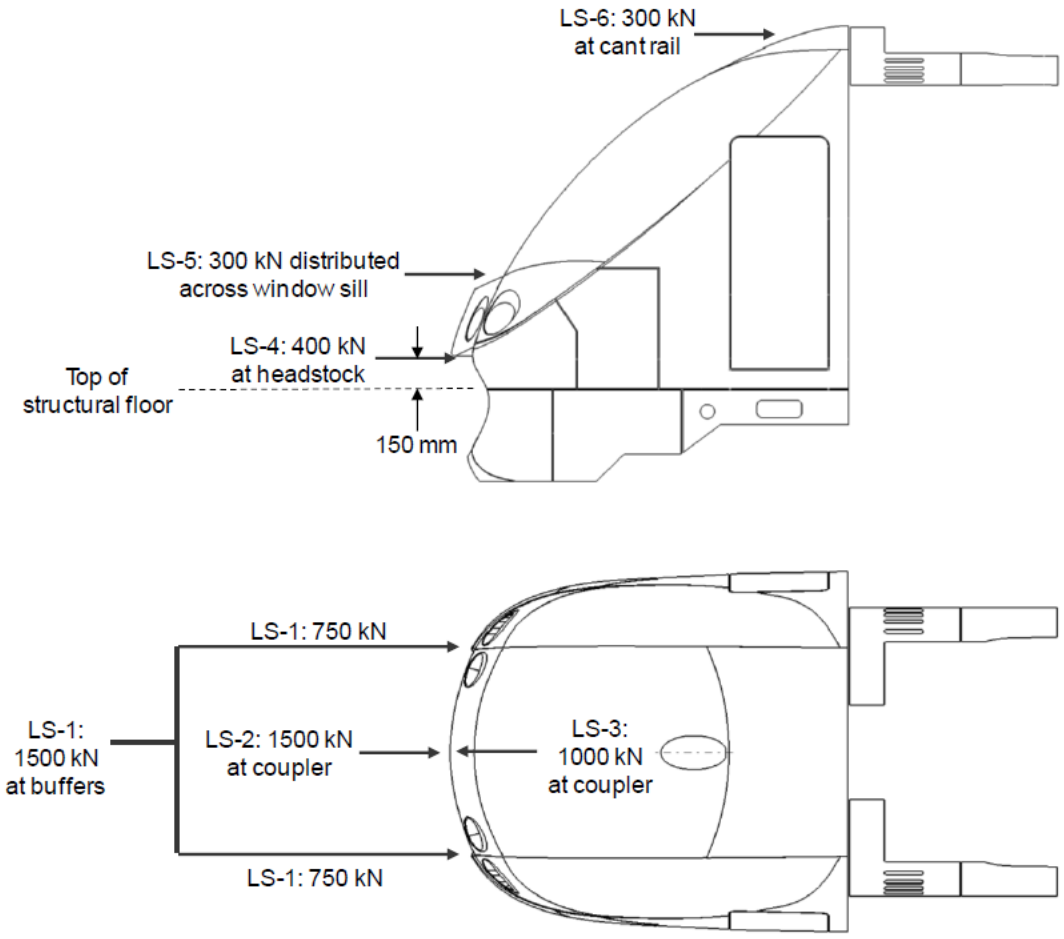

Figure 19: Longitudinal static loads superimposed on a rail vehicle driver's cab

1.4.2. *Vertical loads*

The vertical static loads due to both operating payload and lifting are also specified in EN 12663. Although such load cases generally apply to a complete vehicle there is the possibility that load introduction points (e.g. for lifting) could be located in the vicinity of the cab and may require the cab to transfer the applied loads accordingly. Therefore, such vertical loads cannot be neglected with respect to the cab. To determine the effect of such load cases an analysis of the full carbody (i.e. the entire drive-car) would be required which is beyond the scope of this thesis.

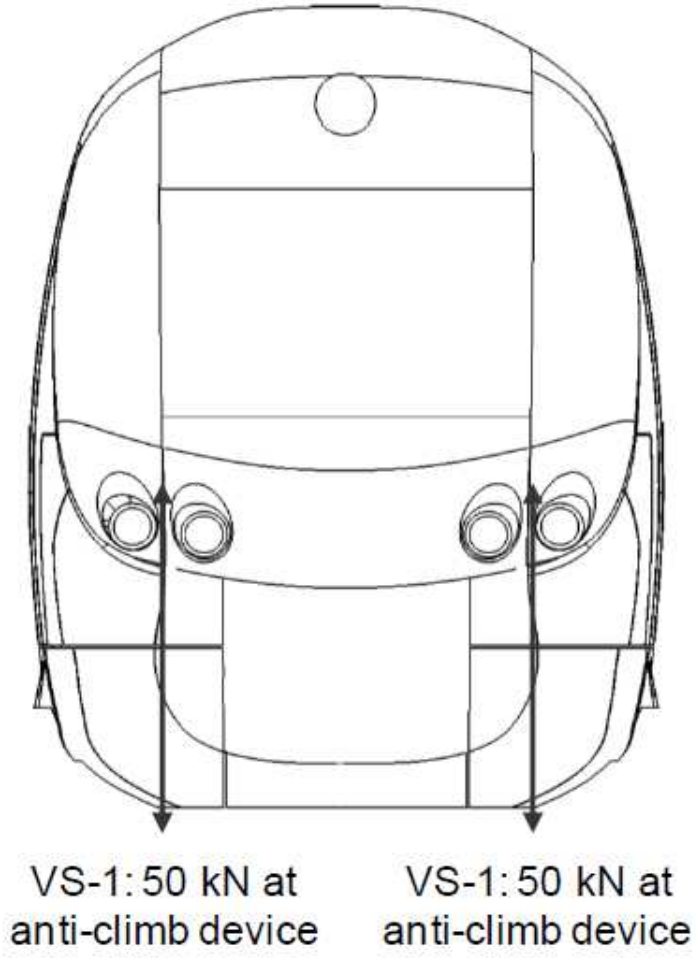

Figure 20: Vertical loads as defined in EN 12663 for the driver's cab.

EN 12663 defines a 100 kN vertical load which is divided equally between the two anti-climbers (Figure 20). The vertical load is applied in combination with a 1,000 kN longitudinal compressive load, 500 kN at each anti-climber.

1.5. Lightweighting of rail vehicles

While the solutions presented in the Section 1.3 may meet the requirements with respect to crashworthiness the current desire for low-cost energy efficient rail vehicles is driving the adoption of lightweight composite materials into more structural applications. With increased pressure being placed on the rail industry to reduce weight [36] an increasing number of rail vehicle manufacturers are looking to advanced composite materials to achieve significant weight reductions in their vehicle design.

Recent studies by Ford [37] have indicated that trains have generally become heavier over the last thirty years (Figure 21). Whilst these increases in vehicle mass can often be attributed to the provision of enhanced passenger environments (air-conditioning, improved accessibility, information systems, etc.) they clearly lead to the undesirable side-effect of heavier trains. Everything else being equal, a heavier vehicle will consume more energy/fuel in operation than a lighter one, thereby making it more costly to run.

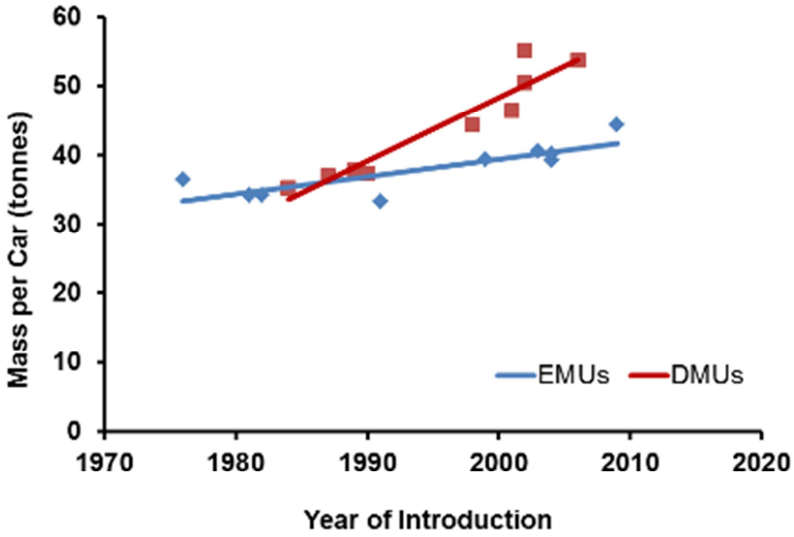

Figure 21: Increase in rolling stock mass 1975-2010 [37]

Increased energy/fuel consumption also implies a likelihood of higher CO_2 emissions within the energy supply chain. Furthermore, heavier trains are more likely to cause damage to the track, thereby resulting in higher costs for infrastructure maintenance and renewal.

The Office of Rail Regulation stated in a report [36] that the railway industry "*cannot afford to become complacent about its current environmental advantage*", adding that "*…in some respects, for instance the weight of trains…, the industry's performance is deteriorating*.". This sentiment is echoed in the UK's Rail Technical Strategy 2012 [38] which calls for lighter more efficient trains as part of its strategy to deliver improved rail capacity and performance. It identifies lightweight materials as being one of the key enablers in reducing energy consumption and thereby encourage the shift of passengers and freight from more energy-intensive modes.

A report produced by the International Union of Railways (UIC) and Fundación de los Ferrocarriles Españoles (FFE) [39] details the fundamental links between a train's mass and its energy consumption. The findings indicate a directly proportional relationship between the vehicle mass and the following aspects:

- Energy needed to overcome mechanical resistance on straight track.
- Energy needed to overcome mechanical resistance on curves.
- Kinetic energy dissipated in speed reductions.
- Manufacturing energy used in constructing the vehicle.

The primary recommendation of this report with respect to reducing energy consumption for rolling stock is to reduce the vehicle mass per seat. This can be achieved in potentially three ways:

1. **Capacity optimisation** - increasing the capacity by introducing more seats.
2. **Design optimisation** - increasing the capacity by increasing the size of the train to accommodate more seats.
3. **Mass optimisation** – using lighter materials to achieve a reduction in overall mass.

While these solutions can be readily applied to the passenger compartments of rail vehicles, the driver's cab presents unique challenges in achieving significant mass reductions due to its requirement to meet the EN standard for crashworthiness.

The benefits of reducing the mass of rolling stock are further investigated by Eickhoff et al. [40] where aspects such as energy savings and track wear were compared across routes and vehicle types. The paper estimates annual cost savings of between € 630 per tonne (for inner suburban routes) and € 2,440 per tonne (for inter-city routes).

In addition to the energy and cost savings which can be achieved by adopting a lightweighting strategy for rolling stock there is a CO_2 benefit which can further improve the environmental credentials of rail travel. In a report by the Association of Train Operating Companies (ATOC) [41] they noted that passenger rail accounts for 0.5% of the total UK CO_2 emissions and that in the period 1995/6 to 2007 there was a 22% decrease in the CO_2 emissions per

passenger kilometre, largely brought about by increases in passenger growth. Noting that newer rolling stock is more energy intensive it also states that achieving the optimum mass is under active consideration as a means of improving the overall energy efficiency of modern trains.

Key to achieving the safety, crashworthy and lightweighting targets in the rail industry is the development and application of composite structures capable of absorbing crash energies without compromising safety of the driver or passengers.

1.6. Scope and objectives of thesis

It is the achievement of rail vehicle crashworthiness through the use of a lightweight structural design philosophy that is the primary concern of this thesis. Of particular interest is the development and implementation of crashworthy design solutions to meet the stringent requirements of current European Standards for rail vehicle collisions.

The objective of this thesis is to merge and harmonise the requirement for crash energy management with the industry's desire to develop and produce lightweight and more efficient rolling stock by creating an innovative design solution for the driver's cab using composite materials.

1.6.1. *Extending current knowledge*

Conventional rail vehicle cab structures are typically based on welded steel assemblies, often with a thin non-structural fibreglass cover and are consequently relatively heavy. Furthermore, current cab designs tend to be very complex, having high part counts and assemblies with fragmented material usage. This is because they must meet a wide range of stringent industry demands relating to proof loading, crashworthiness, missile protection, aerodynamics and insulation. Assembly costs for existing cabs are high resulting from the manpower and time required to weld steel plate into the desired configuration and from a design perspective there is little in the way of functional integration.

By contrast, with the next generation cab described in this thesis the intention is to exploit the opportunities for design integration that are afforded by composite sandwich material technology in order to produce a lightweight construction in which the structural, crash, aerodynamic and insulative functionalities are realised in a single integrated package (Figure 22)

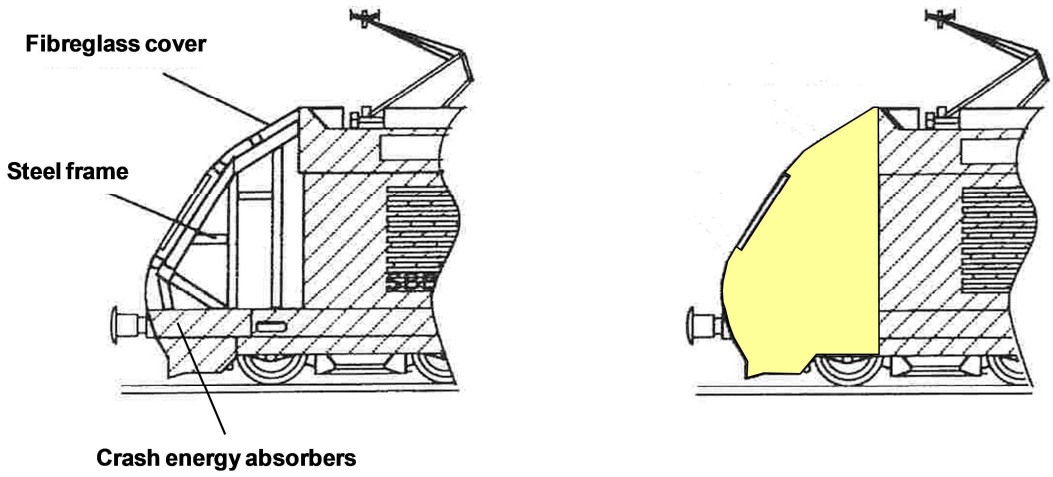

Figure 22: The contrast between a conventional cab structure (left) with fragmented components and materials, and the highly integrated composite sandwich solution developed by O'Neill (right). The figure is a modified version of that presented by Cortesi et al. 1991 [42].

The driver's cab provides a particular challenge to incorporating lightweight materials due to the structural and crashworthiness requirements placed on this area of the vehicle by European standards [28] [35].

Current energy absorber designs lend themselves to steel construction forming a tubular shape aligned axially with the direction of impact. An opportunity exists to employ the predictable crush characteristics of aluminium honeycomb to meet the crashworthiness requirements to produce a lightweight design to react-proof loads and absorb high energy impacts.

The basis for the lightweight cab design described in this thesis, named "D-CAB", was Bombardier's SPACIUM 3.O6 commuter train (see Figure 23). This currently features a conventional cab assembly consisting of a steel primary structure, steel energy absorbers and a thin non-structural fibreglass shell. One of the primary objectives for this thesis was to meet the existing requirements of the SPACIUM cab using composite sandwich materials so as to

realise significant savings in mass, cost and part count. With the principles of lightweighting and CEM in mind, this thesis details the design of a fully composite energy absorbing driver's cab based on Bombardier's SPACIUM vehicle [43] shown in Figure 23. With the aerodynamic outer skin and driver's survival space already pre-defined, the challenge addressed by this thesis was to integrate lightweight energy absorbing elements within the given volume without encroaching into or penetrating the existing design surfaces.

Figure 23: Bombardier's SPACIUM Vehicle – picture Bombardier [44]

This thesis addressed the issues surrounding the disparity between design space allowances and the implementation of crashworthiness requirements. Focussing on the rail industry, it investigated the reconfiguration of unused regions behind the aerodynamic shell of the driver's cab and developed a crashworthy design which made optimal use of the available space whilst reducing the overall mass of the design.

For example - typical steel tubular energy absorbers can weigh up to 900 kg [45] , but it is envisaged that significant weight can be removed through the use of volumetrically enhanced, lightweight, energy absorbing structures.

The objective of Chapters 2 & 3 of this thesis is to investigate the energy absorption properties for materials and various energy absorber designs, and develop a straightforward methodology for enhancing the available volume using these materials.

This encompasses:

- A review of the methods of energy absorption currently deployed in the rail and other industries, discussing the materials used and their implementation within the energy absorbing design.
- Enhancement of various 2-dimensional and 3-dimensional geometries to maximise their energy absorption potential constrained by the geometric properties of energy absorbing materials.

The objective of Chapters 4 - 7 of this thesis is to use the materials identified in Chapter 2 and the methodology derived in Chapter 3 to design, analyse and manufacture a rail vehicle driver's cab (based on Bombardier's SPACIUM design) such that it meets the industry's crash energy management and lightweighting requirements. This includes:

- The design of a rail vehicle driver's cab structure using composite materials to produce a lightweight crashworthy design.
- The maximised use of available space for a new lightweight upper energy absorber design.
- The maximisation of the space within the design envelope of a lower energy absorber to produce a unique and lightweight energy absorber.
- Compliance investigation of the design with European structural and crashworthiness standards.
- Details of the patents filed which protect the designs developed in this thesis.
- Realisation of the design through the manufacture of a full-scale prototype.
- Mass, part-count and cost reductions achievable through the discussed design.

1.7. Context of thesis:

1.7.1. *A note on rail industry fire requirements.*

The introduction of the European fire safety standard EN 45545 [46] has resulted in the rail industry needing to reassess existing materials as well as prompting the researching and validation of new materials, which are cost-effective, high-performance and lightweight. The EN 45545 standard outlines a holistic approach where the importance of the vehicle architecture and the interdependences of its constituent components are emphasised. The design, functional and material requirements in the standard efficiently support passengers and staff to evacuate the vehicle and to reach a place of safety, if an emergency event should occur.

As a result of the introduction and adoption of EN 45545 EU-funded projects such as Fire-Resist (co-ordinated by this author) [47] were established to undertake research specifically targeting the fire performance of novel materials and the achievement of complaint to EN 45545.

The scope of the De-Light project (on which this thesis is based) did not include fire testing or simulation to prove the fire performance of the materials developed although its importance for commercial application was recognised and acknowledged. Research in this field was carried out within the follow-on Fire-Resist project where a more focussed research approach to fire performance would be achieved through a dedicated project budget, partner capabilities and testing capacity.

Among the results achieved from this project was the design, development and prototyping of a rail vehicle interior which was fully compliant to EN 45545-2 Hazard Level 3 (HL3). This was achieved using fire-resistant cork and furan sandwich structures for the bulkheads, tables, wall panels, window pans, and luggage racks (Figure 24).

Figure 24: Fire-resistant rail vehicle interior developed from lightweight furan-based materials as part of the Fire-Resist project.

1.7.2. *Material choice*

Where possible the materials chosen for the manufacture of the cab were in keeping with the lightweighting philosophy discussed in Section 1.5. Market forces and project constraints had to also be considered in the material selection to ensure costs are kept low to achieve a solution that would fall within the affordability profile of the rail industry in order to increase its economic attractiveness. Off-the-shelf materials were chosen to avoid any requirement to develop new materials or processing methods which would have been beyond the scope and budget of the De-Light project.

The materials chosen for the construction of the cab by the project were:

1. **High density polyurethane foam (HD-PUR)** was chosen as the core for the primary load bearing structure of the driver's cab (i.e. non-energy absorbing elements).

   This material was chosen for its dimensional stability, easy of cutting and shaping by hand and machine and is compatible with a wide range of resin systems (epoxy, polyester and vinylester resin systems). Sourced from Easycomposites [48] by AP&M this material suits their primary production needs for the marine industry and is used to produce boat bulkheads. Table 1 below summarises the material properties for HD-PUR.

Table 1: HD-PUR properties extracted from material datasheet [49] .

Property	Units	HD-PUR	Notes
Nominal Density	kg/m^3	96	-
Upper temp. limit	°C	100	
Dimensional stability	%	< 0.5%, 70°C for 7 days < 0.5%, 50°C, 100% rh for 7 days < 0%, -20°C for 7 days	-
Compressive Strength	kPa	1050	(BS.4370 Pt.1 1968 Method 3) Normal to major plane
Tensile Strength	kPa	1060	(BS.4370 Pt.2 1973 Method 9) Parallel to major plane
Cross break strength	kPa	1600	(BS 4370 Pt.1 method 4) Perpendicular to major plane
Closed cells	%	> 95%	(BS4370 Prt. 2 Method 10)

2. The polyurethane foam was faced and encapsulated using **M705 chopped strand** mat supplied by Owens Corning [50]. M705 CSM is produced using medium fibre, multi length Advantex®[1] E-glass [51] which is bonded together using an emulsion binder.

   M705 CSM is well suited to the hand lay-up process which is the preferred manufacturing method of AP&M, the De-Light project's prototyping partner, due to its ease of handling and ability to conform to complex contours and moulds. Table 2 and Table 3 below contain a summary of the material properties for the M705 CSM and Advantex® glass.

Table 2: Summary of material data for M705 CSM [50]

Property	Units	M705 CSM
Nominal CSM weight	g/m^2	450
Procured roll width	cm	95

Table 3: Advantex® e-glass fibre properties [51]

Property	Units	Test Method	Advantex®
Single Filament Tensile Strength	MPa	ASTM D2101	3,100 - 3,800
Young's Modulous of Elasticity	GPa	Sonic	80 - 81
Fibre Density	g/cc	ASTM D1505	2.62

3. The preferred epoxy resin system used by AP&M and chosen for production of the cab prototype was **Sicomin SR1500** used in conjunction with **SD2507 hardener**. This epoxy system is used due to its low toxicity, good wet-out of fibres and excellent adhesion to glass, aramid, carbon and polyester fibres. The system was developed to meet the varying needs of the marine, aerospace and automotive industries, specifically for prototyping and tool making.

   The mechanical properties of the SR1500/SD2507 epoxy resin system are summarized in Table 4.

[1] Advantex® is a registered trademark of the Owens Corning company.

Table 4: Properties of the SR1500/SD2507 epoxy resin system. [52]

	Units	SR1500 / SD2507 epoxy resin system
Curing cycle		14 days @ 23 °C
Tension		
Modulus of elasticity	N/mm^2	3300
Maximum resistance	N/mm^2	80
Resistance at break	N/mm^2	74
Elongation at max. load	%	3.7
Elongation at break	%	4.5
Flexion		
Modulus of elasticity	N/mm^2	3450
Maximum resistance	N/mm^2	123
Elongation at max. load	%	4.8
Elongation at break	%	7.8
Charpy impact strength		
Resilience	kJ/m^2	19
Glass Transition		
T_g	°C	55

1.7.3. *Quasi-static testing limitations*

Due to financial constraints of the De-Light project and the in-house test capabilities of the project partners, the testing conducted within the scope of this thesis is quasi-static in nature. This author recognises the importance of undertaking dynamic testing of composite materials due to the magnification of properties that can occur when lower strain-rates are used.

The effects of strain-rate is discussed further in Section 1.7.6 and serves as a reminder that quasi-static limitations will mean that further analysis and investigation is required to fully determine the cab structure's dynamic energy absorption. For the purposes of preliminary design and for the scope of this body of work such an approach is deemed acceptable.

1.7.4. *Current dynamic and crash performance testing in the industry*

The development of a crashworthy rail vehicle begins with the establishment of a crash concept based on the vehicle specification, route, interfacing rail vehicles and applicable standards (Figure 25). Using this cash concept the vehicle manufacturer can produce a 1D analysis on the energy absorption profile for the vehicle and target performance for CEM devices. Once refined this leads to a detailed train architecture which forms the basis of the vehicle specification for the final tender document [53].

To perform the 1D analysis, the following key information is needed to proceed:

1. Conceptual crash performance for the train
2. 1D Analysis criteria – spring/mass/damper systems to represent the train
3. Construction – general construction parameters; geometry, material, joints, coupling.
4. Seat Layout – number and distribution of passengers, catering cars.
5. Seat Profiles – for preliminary passenger impact analysis
6. Drivers Desk - for preliminary driver impact analysis

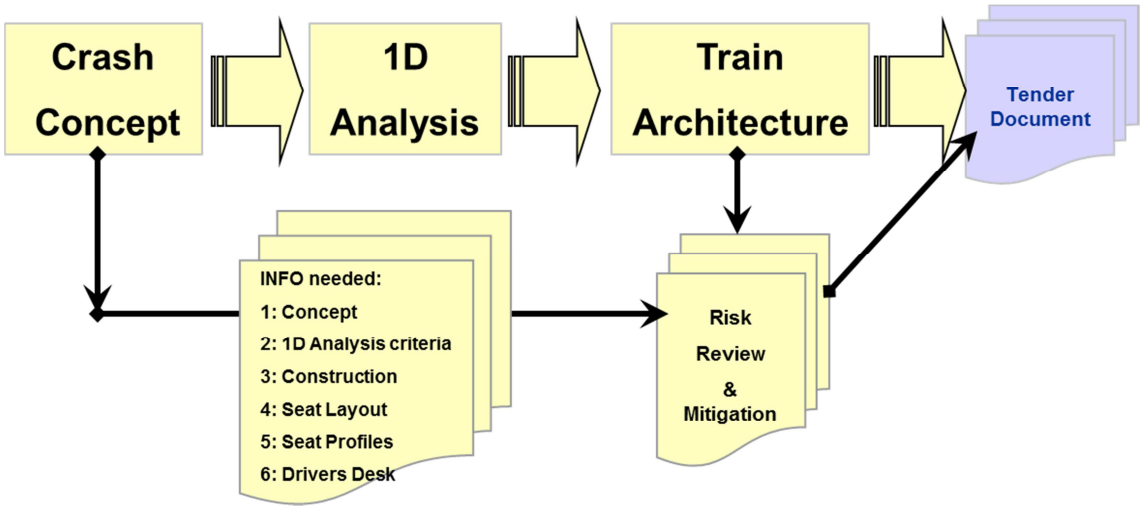

Figure 25: Development of crash performance and analysis (pre-tender submission)

Once Notification to Proceed (NTP) has been granted the rail vehicle manufacturer will begin a lengthy test and analysis programme to produce the required safety documentation for submission to the Notified Body (NoBo) who will certify the rolling stock as being fit for use on the rail network.

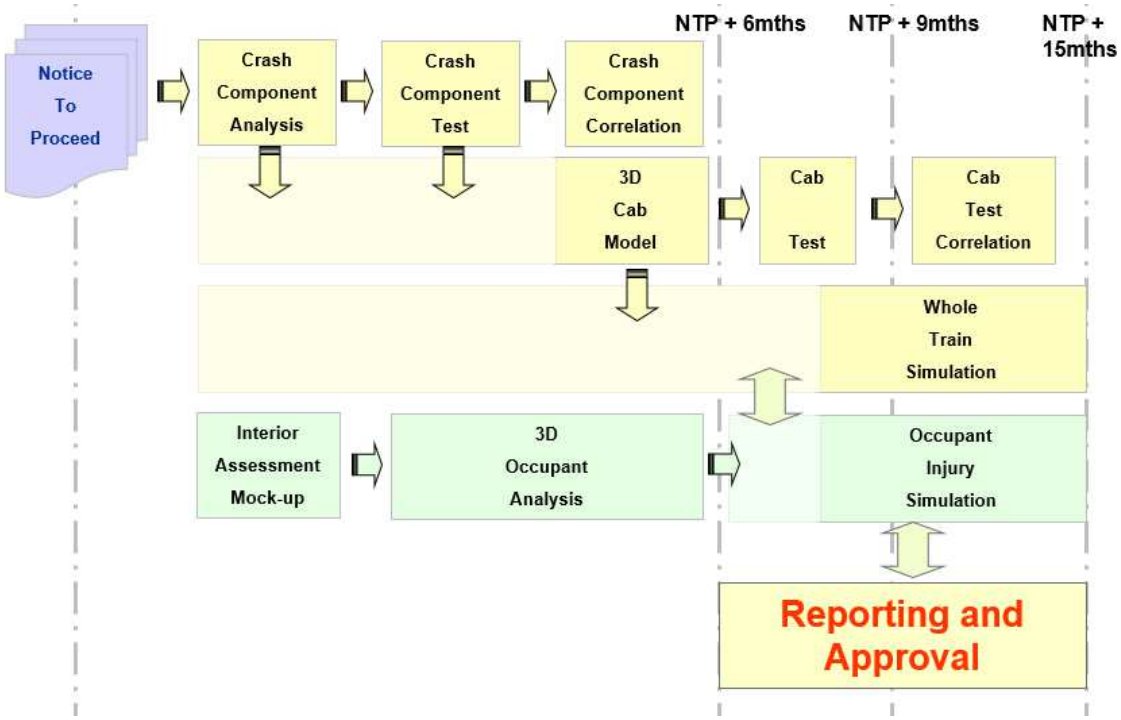

Figure 26: Test and analysis programme for a typical intercity train

Individual elements of the CEM system are assessed using finite element modelling supported by crash component testing (Figure 26). The component testing validates the finite element model which is transposed into a whole train simulation (the vehicle itself is not validated for crashworthiness by physical test).

Figure 27: Rail cab structure dynamic testing. Rolling incline test trolley (left) and just prior to impact (right). Images courtesy of Bombardier.

The driver's cab undergoes full static and dynamic testing (Figure 27) to ensure correlation is achieved between actual response and finite element modelling results.

Two levels of testing are adopted:

- **Component Level**
  - Coupler Criteria Modelling or Supplier report.
  - Energy absorbing devices.
- **Vehicle level**
  - Cab assembly as tested.

The simulation outputs (verified by testing), in addition to the occupant injury simulation deliver the required NoBo reports to achieve safety approval for network running.

1.7.5. *Dynamic modelling of composites for the rail industry*

Performing sequences of large scale series of dynamic tests can quickly become financially inhibitive and for the rail industry the preferred approach to validating rail vehicle performance is through simulation rather than full-scale testing. The industry is of the approach that validation is through simulation, with the simulation being verified by smaller scale (i.e. component level) testing.

Listed in Table 5 is a selection of finite element software available to the rail engineer to determine material static & dynamic performance, as well as vehicular performance in static and dynamic running modes.

Table 5: A selection of finite element software available to the rail industry.

Software Package	**Notes:**
ABAQUS	FEA software with emphasis on linear and nonlinear and heat transfer applications.
ANSYS/LS-DYNA	Nonlinear structural dynamics specialism (impact, large deformation, nonlinear materials, etc.)
ANSYS/MECHANICAL	Complete structures/thermal/acoustics modelling.
GENESIS	Integrated finite element analysis and numerical optimization software for structural analysis.
LUSAS	Structural analysis software
MSC NASTRAN	Structural analysis software for static, dynamic, and thermal analysis (linear and nonlinear)
PAM suite	FEM software optimized to study restraint systems (PAM-SAFE), impacts (PAM-SHOCK) and crash analysis (PAM-CRASH)
RADIOSS	Structural analysis solver for highly non-linear problems under dynamic loadings
STARDYNE	The world's first commercially available Finite Element Analysis software.
STRUDL	Structural Analysis and structural engineering software
VAMPIRE	Rail vehicle dynamics modelling software

Composite materials introduce significant complexities to computational analysis relating to:

- Modelling of constituent parts (resin, fibres, etc.) through a micromechanical approach.
- Anisotropic properties of components (e.g. fibre direction) modelled through a macromechanical approach using lamina.
- Non-homogenous composition (e.g. foam cores with irregular microstructures).
- Crack propagation across material boundaries.
- High strain rate performance (ballistics).

Tools such as LS Prepost and ANSYS Composite PrePost have assisted in the creation and evaluation of complex finite element models where multi-laminate build-ups can be quickly generated to represent complex composite structures [54].

In order to generate the finite element models used for rail vehicles the software requires a Property Card and a Material Card which are numerically associated to describe its characteristics (geometric for the property, mechanical characteristics for the material).

For the material cards, it data required depends on the chosen material which is being modelled: Metallic materials are usually modelled using parameters which are representative in all directions (isotropic). Composite materials require more parameters due to differing characteristics in each direction (anisotropic). Properties include:

- Young's Modulus (E_x, E_y, E_z)
- Poisson's Ratio (ν_{xy}, ν_{yz}, ν_{xz})
- Shear Modulus (G_{xy}, G_{yz}, G_{xz})
- Tensile Strength
- Compressive Strength
- Shear Strength

Within LS DYNA the material cards for composites can be categorised into four families [55]:

- Long fibre reinforced plastics
- Short fibre reinforced plastics
- Cores and foams
- Adhesives and matrix.

The following is the list of the material cards available in LS-DYNA, classified per family:

1. Long (Continuum) Fibre Reinforced Plastics.
    - MAT_22 (*MAT_COMPOSITE)
    - MAT_54/55 (*MAT_ENHAMCED_COMPOSITE_DAMAGE)
    - MAT_58 (*MAT_LAMINATED_COMPOSITE_FABRIC)
    - MAT_59 (*MAT_COMPOSITE_FAILURE_option_MODEL)
    - MAT_116 (*MAT_COMPOSITE_LAYUP)
    - MAT_117 (*MAT_COMPOSITE_MATRIX)
    - MAT_118 (*MAT_COMPOSITE_DIRECT)
    - MAT_158 (*MAT_RATE_SENSITIVE_COMPOSITE_FABRIC)
    - MAT_161 (*MAT_COMPOSITE_MSC)
    - MAT_162 (*MAT_COMPOSITE_MSC_DMG)
    - MAT_261 (*MAT_LAMINATED_FRACTURE_DAIMLER_PINHO)

- MAT_262 (*MAT_LAMINATED_FRACTURA_DAIMLER_CAMANHO)

2. Short Fibre Reinforced Plastics
   - MAT_187 (*MAT_SAMP-1)

3. Cores and Foams
   - MAT_26 (*MAT_HONEYCOMB)
   - MAT_126 (* MAT_MODIFIED_HONEYCOMB)
   - MAT_77 (*MAT_OGDEN_RUBBER)
   - MAT _181 (*MAT_SIMPLIFIED_RUBBER/FOAM)
   - MAT _183 (**MAT_SIMPLIFIED_RUBBER_WITH_DAMAGE)

4. Adhesives and Matrix
   - MAT_138 (*MAT_COHESIVE_MIXED_MODE)
   - MAT_184 (*MAT_COHESIVE_ELASTIC)
   - MAT_185 (*MAT_COHESIVE_TH)
   - MAT_186 (*MAT_COHESIVE_GENERAL)

Each material card has two types of parameters:

- Numerical parameters: used for a purely numerical purpose or within post-processing. It often influences the quality of the results and based on recommended practices.

- Physical parameters: parameters that characterize the physical material. These parameters are characterized using sample tests or assumptions (external references/sources).

Within the rail industry there is currently a focus on the analysis of composite materials relating to their capability to withstand high velocity localised impacts. Flying ballast as a result of passing trains, projectiles such as rocks, bottles etc. intentionally thrown from bridges and impact strike with tree branches or animals has generated a greater research interest in the performance of composites under high strain rate conditions.

Hague et al. [56] studied the creation of validated model parameters to predict the performance of unidirectional and plane weave composite structures and used these to assess the resistance behaviour of the material to crush, ballistic and blast-loading conditions. This work was built upon by Onder et al. [57] who assessed the validity of using quasi-static punch tests to mimic the performance of E-Glass fibre/polyester resin plates under high velocity impacts (V>50m/s). The complexities of modelling composite materials under high strain rate conditions and deriving definitive conclusions on the finite element results are discussed in Section 1.7.6.

1.7.6. *Effects of strain rate*

Conclusions concerning the effect of strain rate on the energy absorption capacity of fibre reinforced plastics is divided across authors, with some reporting increases in energy absorption with loading rate and others describing notable decreases.

A literature study into the effects of strain rate on the mechanical properties of composite structures conducted by Barré et al [58] highlights the discrepancies in research data in this matter. The author's compiled data, reproduced here as Table 6, demonstrate contradictory findings for a variety of materials. For example, the data shows a decrease of the ultimate stress (σ^u) for unidirectional glass/epoxy specimens (REF line 22) but a contradictory increase in the ultimate stress from other authors (REF lines 2&3). For UD carbon/epoxy systems, the longitudinal elastic modulus (E_{11}) was found to have demonstrated a 20% increase (REF line 23) yet remain unchanged elsewhere (REF line 6).

Table 6: Strain-rate observations for carbon-, glass-, and Kevlar-epoxy systems [58]

REF	Material	Test	Strain rate (s^{-1})	Observations
1	UD carbon/epoxy	Tensile	Static - 5	Decrease of E and σ^u
2	UD glass/epoxy	Tensile	Static - 5	Increase of E and σ^u
3	UD glass/epoxy	Tensile	Static - 30	E increased 50%, σ^u multiplied by 3
4	Dry glass fibre	Tensile	Static - 30	σ^u multiplied by 3
5	Angle-ply glass/epoxy	Tensile	Static - 30	E unchanged, σ^u increase of 20-30%
6	UD carbon/epoxy	Tensile	Static - 27	E_{11} and σ_{11} unchanged; E_{22}, G_{12} (off-axis), σ_{22}, τ_{12} increase of 40-60%
7	UD S-glass/epoxy	Tensile	Static - 27	E_{11} and σ_{11} unchanged; E_{22}, G_{12} (off-axis), σ_{22}, τ_{12} increase of 40-60%
8	UD boron/epoxy	Tensile	Static - 27	E_{11} and σ_{11} unchanged; E_{22}, G_{12} (off-axis), σ_{22}, τ_{12} increase of 40-60%
9	UD Kevlar 49/epoxy	Tensile	Static - 27	E_{11} and σ_{11} increase of 20%; E_{22}, $G12$ (off-axis), σ_{22}, τ_{12} increase of 40-60%
10	UD steel/epoxy	Compression	Static - 10^3	E unchanged, σ^u increase of 100%
11	UD carbon/epoxy	Tensile	10^{-4} - 10^3	E_{11} and σ_{11} unchanged
12	Plain glass/epoxy	Tensile	10^{-4} - 10^3	E and σ^u increased by 2.5 and 1.7 times (resp) in the 0 and 45 directions
13	Satin Kevlar/polyester	Tensile	10^{-4} - 10^3	E increased 100%, σ^u increase of 50-70%
14	Satin carbon/polyester	Tensile	10^{-4} - 10^3	E increased 100%, σ^u increase of 50-70%
15	Satin glass/polyester	Tensile	10^{-4} - 10^3	E increased 100%, σ^u unchanged
16	Plain,satin, UD, glass polyester, glass epoxy	Tensile	10^{-3} - $2x10^3$	σ^u increase of 100%
17	Plain carbon/epoxy	Tensile	10^{-3} - $2x10^3$	σ^u unchanged
18	UD carbon/epoxy	Compression	10^{-3} - $6x10^2$	σ_{11} increase of 50%, σ_{22} increase of 30%
19	Plain UD glass/polyester	Compression	Static - 600	Increase of σ^u more for woven material than for UD
20	Plain glass/epoxy	Compression	10^{-4} - 10^3	Increase of E and σ^u
21	Laminates cardon/epoxy	Interlaminar shear	10^{-4} - 10^3	τ_{13} increase of 20-30%
22	UD glass/epoxy	Tensile	Static - 500	Increase of E, decrease of σ^u and ε^u
23	UD carbon/epoxy	Tensile ring	500	σ_{11} unchanged, E_{11} increased 20%, G_{12} increased 30%, E_{22} and σ_{22} multiplied by 2-4
24	Dry Glass fibre	Tensile	$2x10^{-4}$ - $2x10^{-1}$	Increase of σ^u

Barré et al. [58] surmise that no general rule can be proposed for the influence of strain rate, a caution also reflected by Carruthers [59] who suggests that under different strain rates the energy absorption capability is likely to be a function of material, fibre orientation and geometry.

Farley [60] undertook a number of crush tests on carbon-epoxy, kevlar-epoxy and glass-epoxy tubes to determine the mechanisms which control the crushing process under static and dynamic loads. In comparing the energy absorbed the author concludes that the test specimens exhibited essentially the same energy absorption, failure modes and post crushing integrity across the static and dynamically loaded specimens. However Mamalis et al. [61] reported that geometry can have a significant influence over a material's high strain-rate performance, noting that conical specimens produced from glass fibre chopped strand mat exhibited a decrease of 35% in specific energy absorption.

Schmueser & Wickcliffe [62] also reported that energy absorption was lower in dynamic tests than that observed in static tests. For carbon-epoxy, glass-epoxy and aramid-epoxy tubes they surmise that static testing may over-estimate the specific energy absorption by up to 30%. Mamalis did however state that there was no definitive evidence of a decrease in the specific energy absorption for thin-walled tubes (< 4 mm) under high speed crushing (up to 24 m/s).

For very high rate of strain Hague et al. [56] suggest that the energy absorbing capabilities of the fibres in conjunction with the geometrical configuration is less important, as the structure responds in a local buckling crushing mode, with the authors preferring to focus on the magnitude of the dissipated energy through mechanisms such as delamination, debonding and fibre pull-out.

Current literature on the matter of the effect of strain-rate on composite material energy absorption remains undecided, however it is recognised that material choice and structural configuration can play a major role in improving performance in this respect. Additionally, Carruthers [59] reports that composite sandwich structures can exhibit a magnification of dynamic properties where the yield strength and collapse plateau can both increase with strain rate. As such, caution should be used in drawing direct comparisons between quasi-static and

dynamic crush performance, with a dedicated suite of dynamic crush tests being the preferred option to accurately determine the energy absorption capabilities of composite structures.

Chapter 2: Review of energy absorbing structures and materials for crashworthy design

2.1. Crashworthy Design & Energy Absorbers

A major part of CEM is the deployment of energy absorbers in the driver's cab located at the front and rear of trains which have the capacity to absorb significantly higher amounts of energy when compared with passenger coach ends. The mechanics by which these devices absorb energy fall into the following categories:

- Deformation Tubes
- Crumple Columns
- Guided Crumple Columns
- Tube Inversion
- Expansion Tubes
- Metal Splitting
- Peeling Technology
- Recoverable energy absorption – pistons

2.1.1. *Deformation Tubes*

Deformation tubes represent the simplest form of energy absorption. The process involves the progressive axisymmetric folding of the walls of a circular tube undergoing axial (longitudinal) loading. The folding mechanisms and material plastic deformation which underlie their energy absorption properties are well understood: Bardi et al. have performed an experimental analytical study of the onset of collapse of steel tubes under crush loads, as well as modelling to a significant degree of accuracy the geometric characteristic of folding under such loads [63]. Reid focuses on thin walled steel tubes to compare this buckling mode with external inversion (Section 2.1.4) and axial splitting (Section 2.1.6), noting that the non-fracture modes exhibit high mean load profiles with effective strokes of approximately 70%, whilst the fracture mode compensates for its lower mean load profile by having effective strokes approaching 95% [64]. The manner and modes of early stage folding were further investigated by Bardi et al. in a series of experiments on stainless steel tubes, which identified uniform axial wrinkling as the first instability encountered under constant displacement loading [65].

Alghamdi noted in a review of energy absorber characteristics that a reasonably constant operating force is one of the key reasons why metallic tubes prove to be a popular energy absorber solution [66]. This paper also noted that theoretical studies usually ignore dynamic (inertia) effects and treat the problem as a quasi-static case, which is acceptable at low impact velocities.

Deformation tubes can be prone to Euler buckling which greatly reduces their energy absorption capabilities. To better understand the criteria and set-up that influences the onset of Euler buckling, I undertook a series of quasi-static compression tests on steel tubes to determine the material's failure mode under axial loading.

These compression tests were performed at the Mechanical Engineering laboratories of the University of Gdansk in Poland.

Six 350 mm mild steel tubes, diameter 50 mm with 4 mm wall thickness were tested. Three of the specimens have trigger holes which were designed to promote the onset of local buckling and folding (#4, #5 & #6), see Figure 28.

Figure 28: Steel tube test specimens.

Each specimen was axially crushed to determine the mode of failure and susceptibility to Euler buckling.

Test preparation:

- Each specimen was mounted vertically on a flat surface within the machine.
- Each specimen was loaded axially using a flat surface at the maximum displacement rate allowed by the machine (5mm/sec).
- The load variation with respect to displacement was captured.
- 3 specimens with trigger holes were tested first followed by remaining specimens.

Measurement system consisted of data acquisition Peekel Autolog 2180 system (2000 measurements/sec. at 16 bits) and connected laptop as user interface device and data recorder.

Three values were measured and registered during the test: time, load and displacement of the load application plane. Measurement of the load was carried out by Hottinger HBM C1/250 load transducer (SN 50453, range: 2500 kN, class of accuracy: 0,1). Measurement of displacement was done by Hottinger 1-WA/500 MM-L displacement transducer (SN 121110070, range: 500mm, class of accuracy: 0,1). Time was recorded as output from internal clock of Autolog 2180 system.

The location of transducers is presented in Figure 29 and actual view Figure 30.

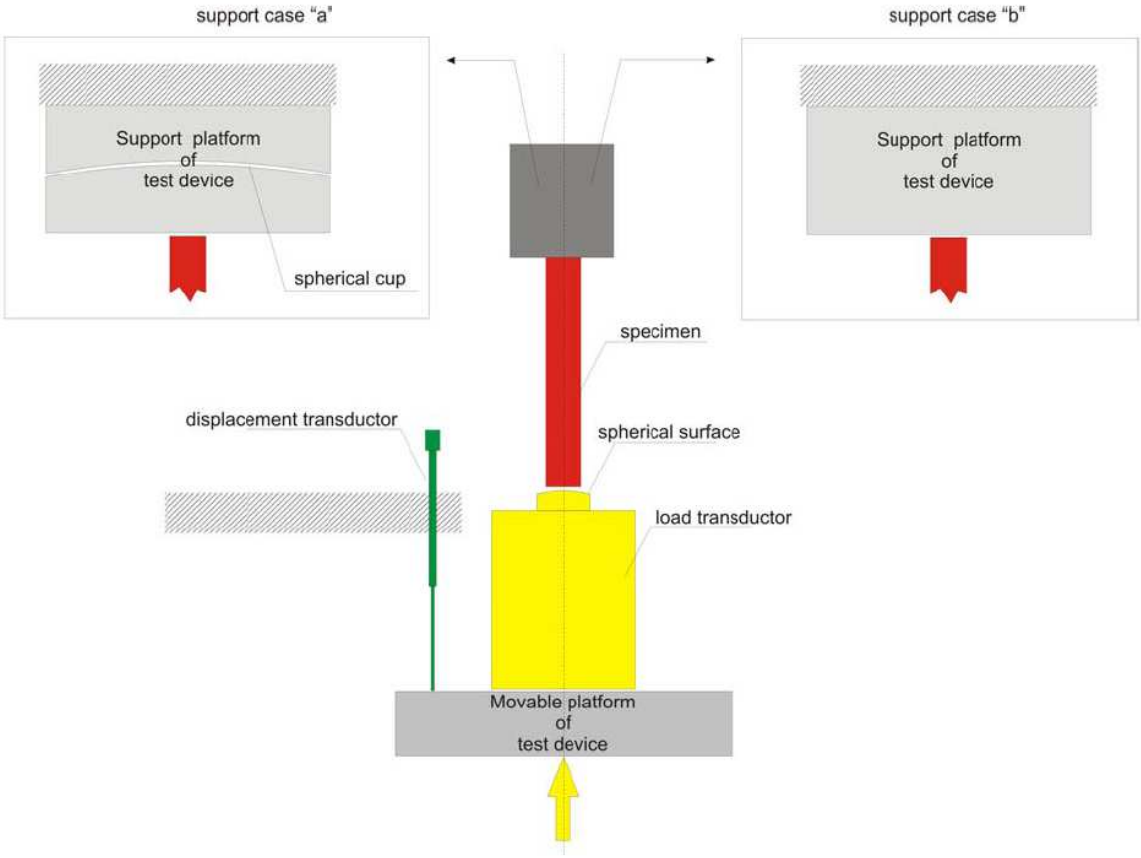

Figure 29: Specimen support cases.

Figure 30: Test machine set-up in case "a".

After preliminary tests of specimen #1 and #4 which exhibited Euler buckling (not the desired crush mode), it was decided to reduce length of some of rest specimens as follows:

- Specimen #2 was cut into two subparts: #2a length of 200 mm (without trigger holes) and #2b (without trigger holes) with length as result of cutting of 97.3 mm.
- Specimen #3 was cut into two subparts: #3a length of 150 mm (without trigger holes) and #3b (without trigger holes) with length as result of cutting of 148 mm.
- Specimen #5 (with trigger holes) was leave and tested with preliminary length 300 mm.
- Specimen #6 was cut into two subparts: #6a length of 200 mm (with trigger holes) and #6b (without trigger holes) with length as result of cutting of 97 mm.

RESULTS & DATA

Test configuration “a”

Specimens #1, #2a, #3a, #3b, and #4 were all tested in test configuration “a”. The results obtained are shown in Figure 31, Figure 32, Figure 33, Figure 34 and Figure 35 respectively.

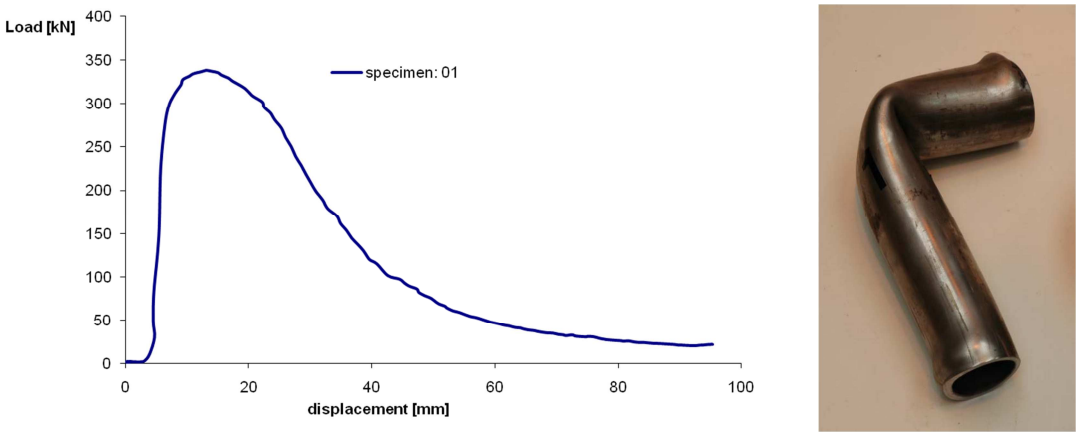

Figure 31: Results obtained with specimen # 1.

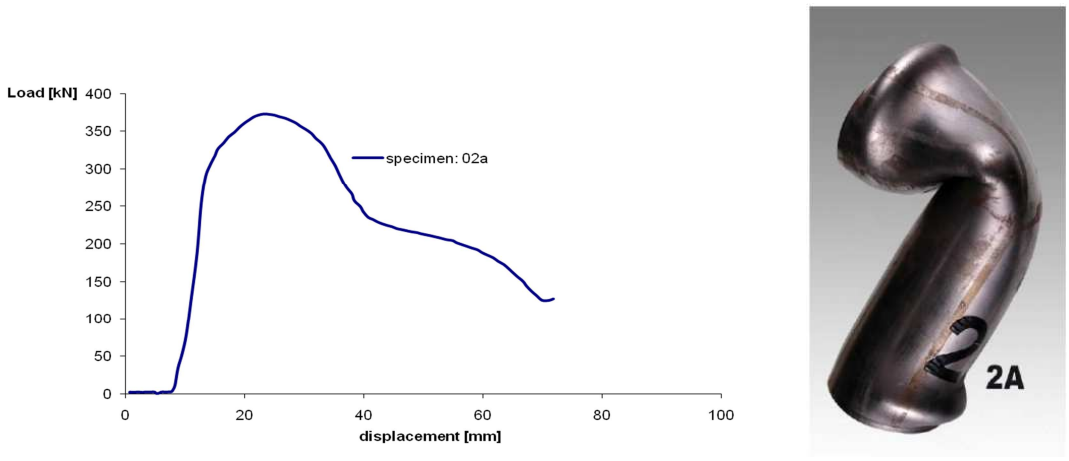

Figure 32: Results obtained with specimen #2a.

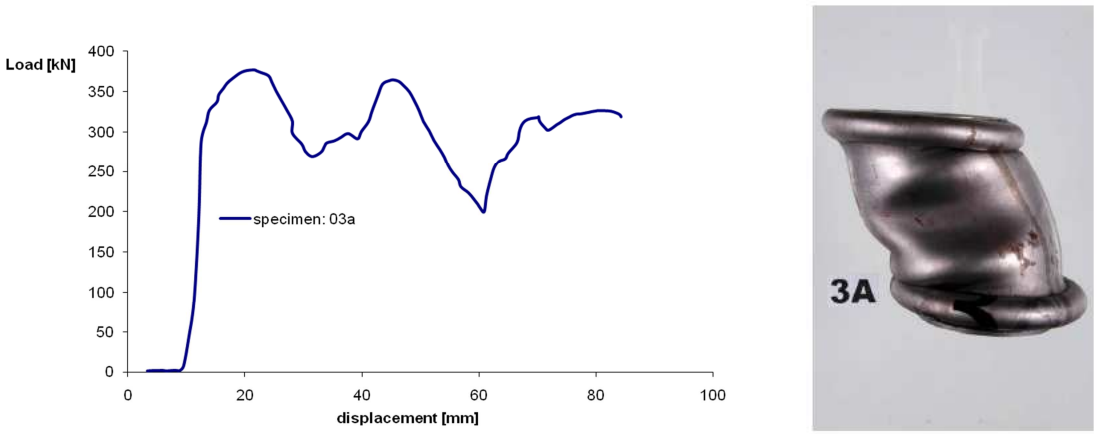

Figure 33: Results obtained with specimen #3a.

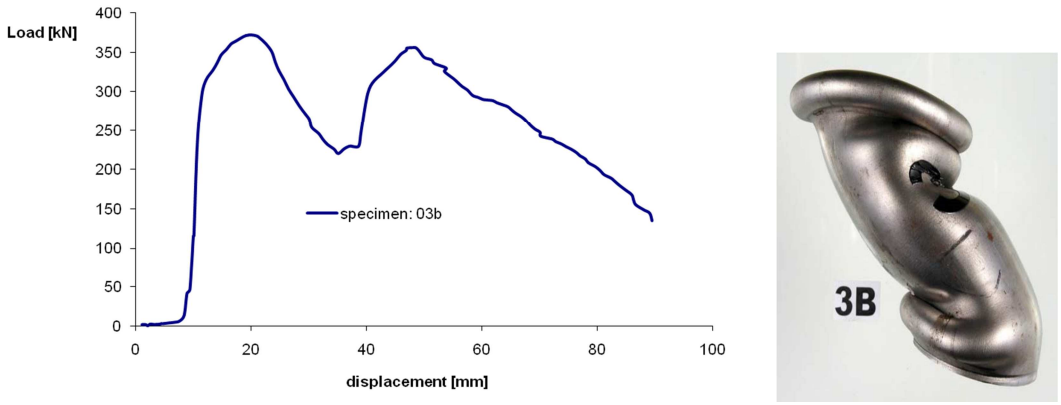

Figure 34: Results obtained with specimen #3b.

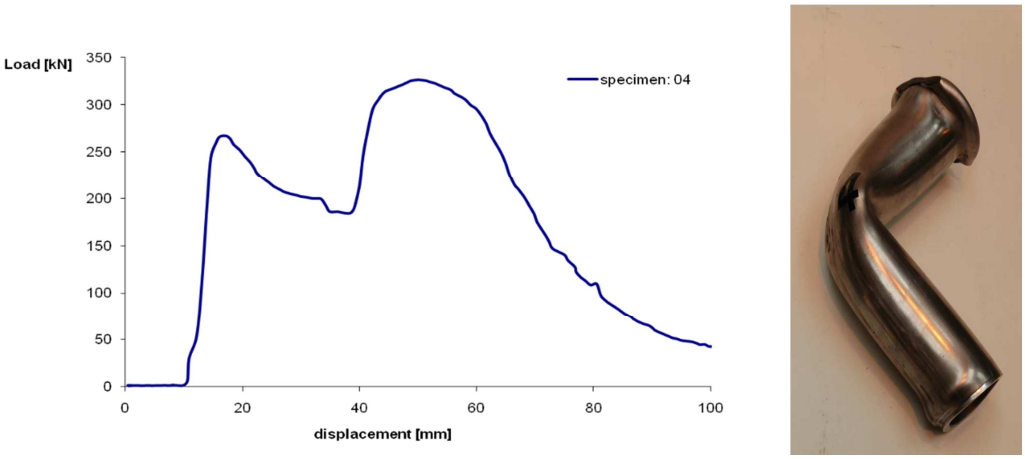

Figure 35: Results obtained with specimen # 4.

Test configuration “b”

Specimens #2b, #5, #6a, and #6b, were all tested in test configuration “b”. The results obtained are shown in Figure 36, Figure 37, Figure 38 and Figure 39 respectively.

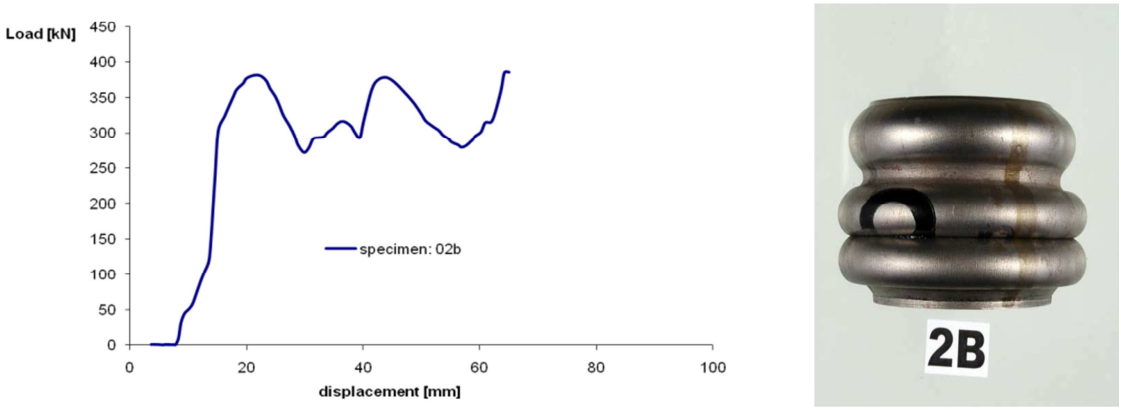

Figure 36: Results obtained with specimen # 2b.

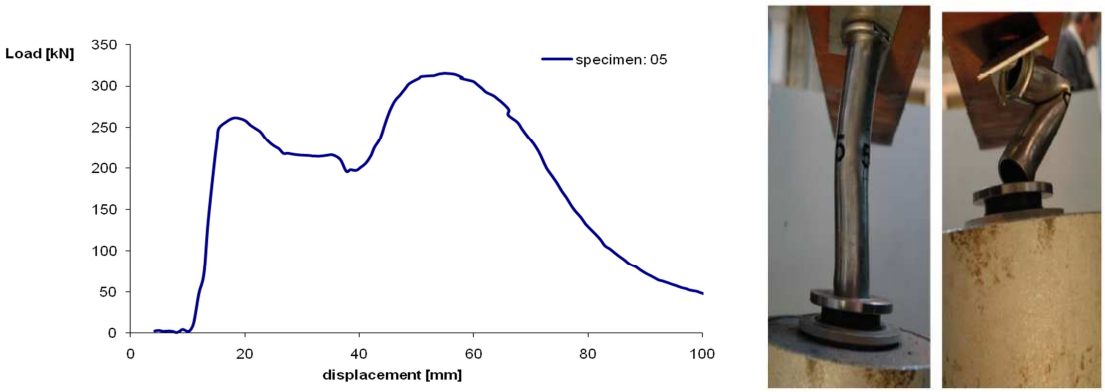

Figure 37: Results obtained with specimen # 5.

Figure 38: Results obtained with specimen # 6a.

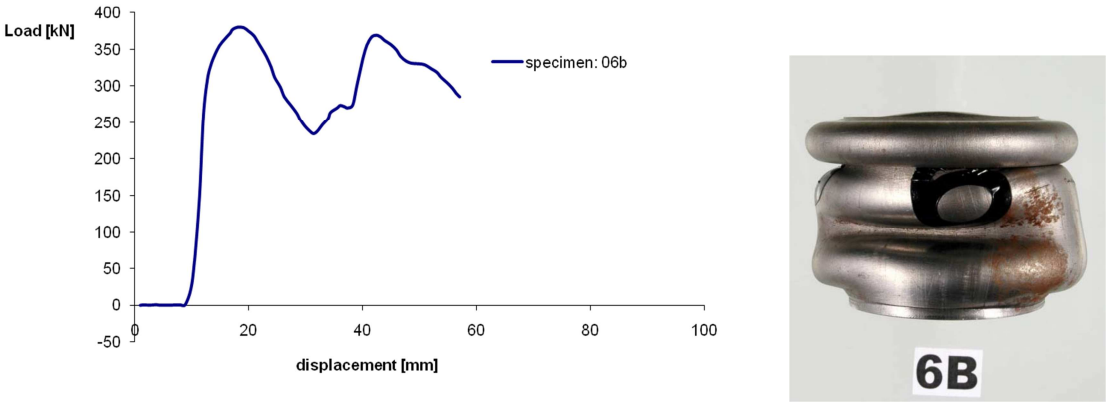

Figure 39: Results obtained with specimen # 6b.

Table 7: Failure modes of steel tube specimens under axial compressive load.

	TEST CONFIGURATION	FAILURE MODE	PEAK FAILURE LOAD (kN)
SPECIMEN #1	a	Euler Buckling	347
SPECIMEN #2A	a	Euler Buckling	371
SPECIMEN #3A	a	Axisymmetric folding followed by Euler buckling	375
SPECIMEN #3B	a	Axisymmetric folding followed by Euler buckling	369
SPECIMEN #4	a	Axisymmetric folding followed by Euler buckling	332
SPECIMEN #2B	b	Axisymmetric folding	390
SPECIMEN #5	b	Axisymmetric folding followed by Euler buckling	331
SPECIMEN #6A	b	Non-axisymmetric mode with 2 circumferential waves	352
SPECIMEN #6B	b	Axisymmetric folding followed by non-axisymmetric mode with 1 circumferential wave	381

Table 7 describes the different failures mode of each specimen. All specimens which underwent loading using support case “a” exhibited Euler buckling due to the movement of the support platform during loading. However, with support case “b” specimens, local buckling was dominant due to the perfectly (and continually) aligned compressive load throughout the test.

The average peak load for the specimens is 361 kN, with maximum of 390 kN and minimum of 331 kN. These values fall short of the LS-1 750 kN static load requirement specified in Figure 19. In applications where true axial alignment cannot be guaranteed this test demonstrates the sensitivity with which the buckling mode can be affected and it is clear that the effectiveness of steel tubes as energy absorbers cannot be fully realised. Improvements can be achieved by modifying the design to include groups of tubes, and varying the wall thickness or material to manage the peak load and crush strength. However, these modifications come with an associated increase in production and design costs due to increased complexity.

2.1.2. *Crumple Columns*

Crumple columns are an extension of the deformation tubes as described in Section 2.1.1 in that their energy absorption mode is through folding and plastic deformation of the material. The primary difference between crumple column and deformation tubes is that the cross-section of the absorber is non-circular. Examples are: square/rectangular tubes (Figure 40), truncated cones (Figure 41) [67] [68], truncated pyramid (Figure 42) and hexagonal tubes [69]. The benefit of these structures is that they are tailored to meet specific design and capability requirements; for example the truncated cone being more suitable for racing car nose cones [70] due to aerodynamic requirements. As such they seek to make optimal use of the available space by employing non-circular and tapered volumes, often using composite materials to achieve the required geometry [26][71]. This however requires considerable design and manufacturing effort to achieve stable crush performance making them less suitable for cost-sensitive applications. `

Figure 40: Square cross-section steel crumple column post-impact [72]

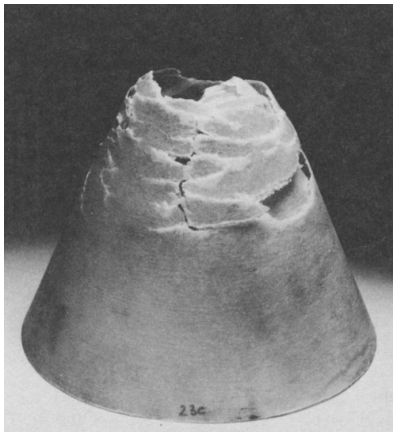

Figure 41: Axially crushed composite cone [71]

Figure 42: Truncated pyramid energy absorber for Formula 3 car [70]

2.1.3. *Guided Crumple Columns*

Guided crumple columns are a derivative of crumple columns which are specifically designed to improve the functionality of the device in the event of an off-axis loading. This is typically achieved through the use of guide pins attached to the impact head, which pass through a series of guide holes to keep the folding of the crumple column aligned with the direction of impact. In the design depicted in Figure 43 the guide pins ensure the anti-climber remains in a vertical plane to guarantee the folding mechanism of the steel casing (crumple tube) remains effective for the full stroke of the absorber.

Whilst this solution functions well it is achieved at the expense of weight, with energy absorbers for the rail industry having a mass of approximately 200 kg per absorber [45]. The pins and plates add significant mass to the final design without specifically adding to the absorption capacity of the device.

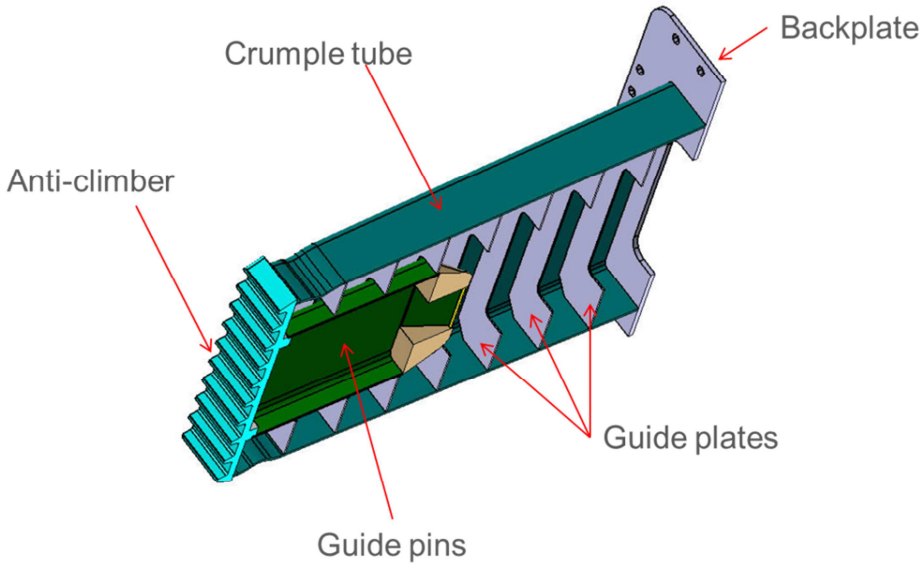

Figure 43: Cross-section of a guided crumple column energy absorber (for rail vehicles) [45]

2.1.4. *Tube Inversion*

This type of energy absorber functions by the turning inside-out or outside-in of a thin-walled ductile tube (Figure 44) with energy being absorbed as a result of the plastic deformation of the metal. This system was introduced and deployed by General Motors in their steering columns in 1969 [73].

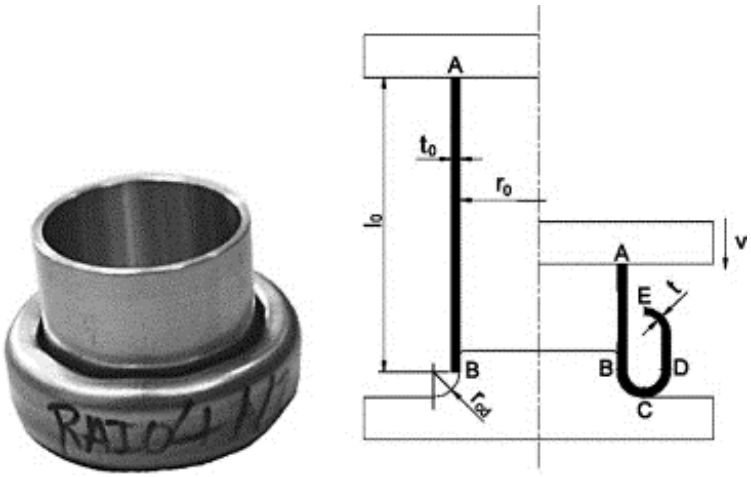

Figure 44: The inversion of a thin-walled metallic tube [74]

The energy absorbing efficiency of these structures was investigated by Guist et al. who determined that the inversion load was directly proportional to the wall thickness and inversely proportional to the tube diameter [75]. The work concluded that greater energy absorption efficiencies are achieved as the wall thickness is increased. In many cases a die is used to encourage and progress the inversion process, with the geometry of the die being critical to achieving the inversion without undesired buckling occurring [66][74]. However, the inversion process is highly prone to cracking and buckling of the tube due to its sensitivity to the ratio of die fillet radius to tube inner radius, r_{cd}/r_o (Figure 44).

2.1.5. *Expansion Tubes*

Expansion tube energy absorbers consist of a cylindrical metal deformable tube (primary) within which fits a secondary rigid tube which acts as a die to expand the primary tube (Figure 45). Asymmetrically aligned, the secondary tube is forced into the primary tube on impact and through this mechanism the crash energy is converted into plastic deformation energy by circumferential expansion [76]. This solution however can have a significant weight penalty due to the weight of the punch [77].

Figure 45: Expansion tube energy absorber before impact (left) and after impact (right) [78]

Individually these mechanisms do not absorb large amounts of energy (typically 1 MJ) primarily due to the effective stroke of the absorber being 50% of the total length. However, they can be arranged to function in parallel to absorb larger collision energies [78]. This type of absorber is dependent on the punch geometry as investigated by Kim et al. where an optimum angle of 30° on the punch head achieved the maximum energy absorption, with no discernible increase in energy absorbed above this angle [79].

2.1.6. *Metal Splitting*

Metal splitting can be considered a progression of tube inversion as described in Section 2.1.4 but where the die is designed to encourage the splitting of the material, thereby absorbing energy through bending, tearing and friction [80]. This mechanism is more suited to geometries with corners (e.g. square tubes) where stress concentrations at the corners propagate the failure mode linearly and in parallel with the loading direction (Figure 46).

Figure 46: Metallic tube of square cross section demonstrating metal splitting [80]

The experiments conducted by Huang et al. indicate that this process is relatively efficient at absorbing energy, with 15 kJ of energy being absorbed per kilogram of mild steel [81]. However, the thin-walled nature of the absorber necessitates a long crush stroke to achieve high levels of energy absorption. In their work, a 200 mm long mild steel specimen of 3 mm wall thickness and 50 mm^2 section could only absorb 3 kJ of energy. The requirement for the SPACIUM vehicle is 1,100 kJ per absorber (see Section 6.2). This makes it prohibitive for rail applications due to space constraints.

In addition, this type of absorber is very dependent on geometry to provide the stress concentrations and on the manufacturing quality of the specimen, with imperfections and voids reducing the overall effectiveness of the device.

2.1.7. *Peeling Technology*

Peeling technology absorbs impact energy through permanent deformation of a strip of steel cut from the shaft (usually cylindrical) onto which the buffer or anti-climber is mounted. Also, by converting mechanical energy into thermal energy additional impact energies can be absorbed. The mechanism by which this is achieved takes the form of a cutting knife which engages with the surface of a steel shaft and as the shaft passes over the cutter a strip of metal is removed (see Figure 47). The level of absorbed energy depends on the section size of the cut strip, giving a broad range of adjustment depending on the needs of a specific application.

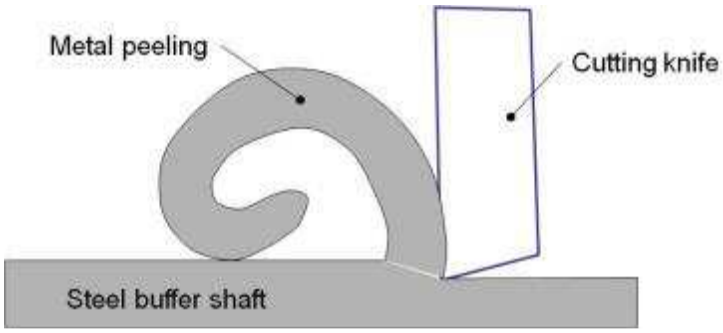

Figure 47: Energy absorption through metal peeling

Energy absorbers based on this technology are available to the rail sector through products by Axtone Group who have developed a number of solutions to meet the needs of passenger and freight vehicles [82].

The problem with this solution lies in the space required to achieve energy absorption. As demonstrated in Figure 48 the buffer shaft must penetrate through the driver's bulkhead in order to achieve full deployment of the absorber. This requires significant space behind the bulkhead as well as the requirement to introduce holes into the highly-loaded bulkhead to receive the buffer shaft.

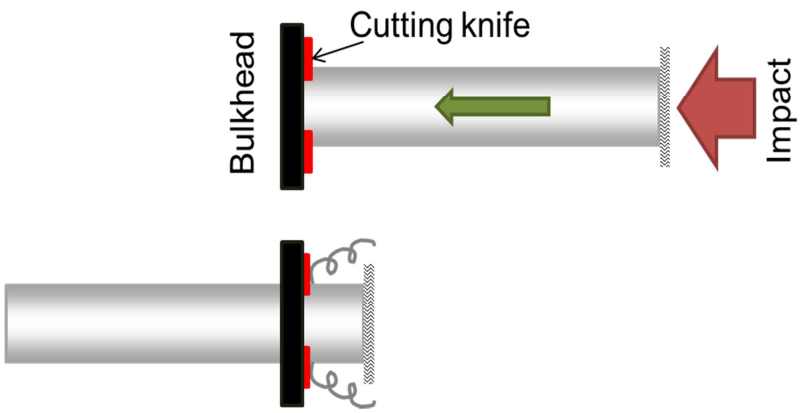

Figure 48: Single stroke peeling technology energy absorber detailing bulkhead through-penetration

To overcome this bulkhead penetration problem, it is possible to introduce a “receiving” shaft on which the cutting knife is mounted. However, this effectively reduces the stroke (and therefore the energy absorption capacity) by half.

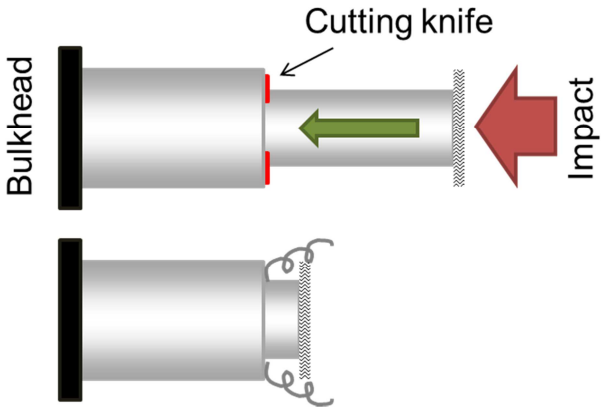

Figure 49: Single stroke half-length energy absorber using peeling technology

Neither of these peeling technology solutions offer a volumetrically considerate energy absorbing capability, with the space requirement to accommodate the length of the absorber heavily impacting the overall rail vehicle design.

2.1.8. *Recoverable energy absorption – pistons*

Typically classified as shock absorbers, these gas or fluid filled devices absorb energy by forcing high pressure gasses or fluids through an orifice. These systems are generally recoverable through the deployment of a return spring which will return the absorber to its original state.

Figure 50 details the internal structure of a fixed orifice energy absorber. As the impact is received by the piston rod it forces the piston head into the cylinder. The fluid in the cylinder is thereby pressurised and forced through the orifice in the piston head, providing a resisting force in the piston rod. The displacement accumulator compensates the system for the rapid displacement of the piston head.

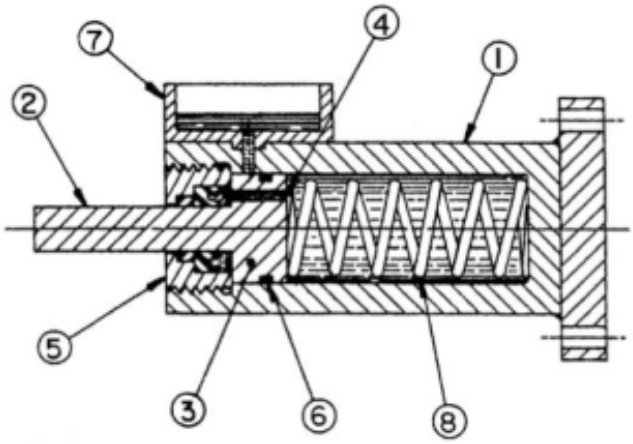

Figure 50: Fixed orifice shock absorber [83]

① Cylinder ② Piston rod ③ Piston head ④ Orifice hole ⑤ End cap and seal assembly (low pressure) ⑥ Piston head seal (high pressure) ⑦ Piston rod displacement accumulator ⑧ Return spring

Whilst a number of variants of this system exist to improve the efficiency of the basic design (such as metering tube and metering pin designs) the complexity of the design increases as efforts to reduce the peak force are embodied [83].

Ultimately these systems are design and manufacturing intensive and are best suited to low energy, repetitive impacts as opposed to high energy collisions as defined by the crashworthiness standards for rail vehicles. Absorbers based on this technology are available

to the rail market through the product range of Oleo International [84]. However the maximum energy absorption level achievable is 70 kJ reversible and 420 kJ non-reversible [85], making them more suited as low-impact buffers as opposed to crash energy absorbers.

2.1.9. *Summary of energy absorber designs*

The type of structure used to absorb impact energies will be dependent on the nature/magnitude of the expected impact and the space available to incorporate the absorber into the final design. As such, absorbers tend to be tailored to meet the specific requirements of the final industrial application. It is useful therefore to review the capabilities of the energy absorbers described in Sections 2.1.1 to 2.1.8 against criteria specific to the rail industry. The following assessment categories were chosen:

- **Design Complexity** – This refers to the level of development and design effort required to create an energy absorbing solution which meets the rail industry's requirements. *Range: Low – Medium - High*
- **Geometric sensitivity** – This criterion assesses whether minor changes in the geometry of the device, either at the design stage or via manufacturing tolerances, can have a large impact on the effectiveness of the energy absorber. *Range: Low – Medium – High*
- **Off-axis functionality** – This aspect is in direct relation to the offset case in the EN15227 standard which stipulates that absorbers must function as desired under a vertical offset of 40mm (see Section 1.3). *Range: Poor – Average – Good.*
- **Material quality dependency –** Some energy absorbers are highly sensitive to the quality of the materials employed to absorb energy. This category assesses whether material imperfections can have an exaggerated impact on the capability of the device to absorb energy. *Range: Low – Medium - High*
- **Manufacturing quality dependency** – Quality in the manufacturing processes used to produce the absorber can have an impact on its capability to function correctly. This criterion assesses the dependency between manufacturing quality and absorber functionality. *Range: Low – Medium – High*
- **Penetration through bulkhead** – If a portion of an energy absorber is designed to penetrate the bulkhead on which it is mounted then the space in that area must be left

clear to ensure full and complete functionality of the device. This design is not particularly advantageous in space-constrained rail vehicle designs such as trams. *Range: Yes - No*

- **Effective stroke –** For each design only a percentage of the mechanism's length will actually perform the energy absorption. The remaining length is often occupied by the residual material, or where by design the absorber has reached the limit of its capable stroke. *Range: 0-100%*

Table 8: Assessment of energy absorber systems

	Deformation Tubes	Crumple Columns	Guided Crumple Columns	Tube Inversion	Expansion Tubes	Metal Splitting	Peeling Technology	Recoverable energy absorption
Design complexity	Low	Medium	High	High	High	Medium	Low	High
Geometric sensitivity	Medium	Medium	High	High	High	Medium	High	High
Off-axis functionality	Poor	Poor	Good	Poor	Poor	Average	Good	Average
Material quality dependency	Low	Low	Low	Low	Medium	High	High	Low
Manufacturing quality dependency	Low	Low	Low	Low	High	High	Medium	High
Penetration through bulkhead	No	No	Yes	No	Yes	No	Yes	No
Effective stroke (%)	70-80	70-80	70-80	70-90	50	70-90	50-75%	70-80

Of the eight technologies assessed in Table 8 the **deformation tubes** have the best overall capability for meeting the rail industry's requirements.

Whilst these may seem to be a viable solution for energy absorption due to their predictable folding mechanism my research and testing has shown that their performance is greatly dependent on the loading mechanism and direction, otherwise they can be prone to Euler buckling, which greatly reduces their energy absorption capabilities. It is this poor off-axis performance that makes them unsuitable for deployment on trains.

As a result, vehicle manufacturers invest heavily in the design of technologies such as guided crumple columns or peeling technology to meet the EN standards and in particular to achieve the 40 mm offset impact requirement. Significant drawbacks of these two methodologies are

the weight penalty incurred by the interior structure of guided crumple columns and the bulkhead penetration caused by the peeling technologies.

Therefore a design solution which can utilise the predictable crush of deformation tubes, coupled with a simple and effective off-axis solution would be of significant benefit to the rail industry.

2.2. Composite Materials as an Energy Absorber

In instances where structural crashworthiness plays a key role in energy absorption, the choice of materials for use within these areas is critical. For crumple zones it is necessary to use materials which can withstand the expected static loads whilst at the same time being deformable under high impact loadings to allow for the absorption of energy.

While metals such as steel and aluminium dominate the rail energy absorber market, considerable work has been undertaken to determine the performance of composite materials under crash loads to assess their energy absorption properties. Carruthers performed an in-depth analysis of these materials noting that fibre reinforced plastics (FRPs) have demonstrated excellent energy absorption potential [59]. His approach also considered wider issues relating to composite materials, such as their structural capability and manufacturing issues, which could be potential barriers to industrial uptake.

2.2.1. *Energy absorbing composite tubes*

Fibre-reinforced energy absorbing tubes have been investigated in numerous bodies of work which study the effect of composition variations on crush performance:

Ramakrisna et al investigated the effect of fibre architecture on the load/displacement response, crush morphology and energy-absorption capability of carbon fibre tubes under axial load [86]. The authors conclude that the specific energy-absorption capability increased with fibre content, noting that tubes with less than 15% fibre content crushed irregularly.

Hull investigated the micro-mechanisms which underlie the progressive crushing of composite tubes [87]. The author determined that two mechanisms come into play during crush: fragmentation and splaying. Hull surmised that the transition between fragmentation and splaying can be constrained by the orientation of fibres in the hoop direction, thus decreasing the likelihood of shear fracture across the tube wall under load. The progressive crush mechanisms he observed over a broad range of crush speeds suggest that the energy absorption of the studied tubes is not strain rate dependent.

A study into the effect of braided fabrics was conducted by Karbhari et al [88] who produced test specimens using a resin transfer moulding (RTM) process with braided biaxial preforms of Tex glass and triaxial hybrids of glass/Kevlar/carbon fibres. The author surmises that the triaxial hybrid delivers enhanced specific energy absorption level and that the bucking modes, based on the rate of crush, appear to be dependent on the strain rate sensitivity of the constituent fibre tows.

Pitarresi et al describe an experimental evaluation of tied-core sandwich structure for the rail sector [89]. The author investigate the performance of sandwich structures which use internal corrugations, webs and tubes as stiffeners between the sandwich facings. These were designed to improve the crush performance by increasing the overall stiffness of the foam-core sandwich panels, and promote stable high energy failure by inhibiting de-bonding. Tubular test specimens were produced using a variety of cores wrapped in glass fibre mats and impregnated with epoxy resin using vacuum assisted resin transfer moulding (VARTM). The author concludes that such structures are a cost-effective means of achieving energy absorption, and that higher energy absorption capabilities can be achieved through thicker sandwich facings, optimised trigger mechanisms and reinforcement in the hoop direction, commensurate with the findings of Hull above [87].

The restriction of the approaches described in these works lies in the design of the energy absorbing element, which tend toward a tubular design based on composite materials, rather than fully using the volume occupied by the absorbing element. This places the solution into the “black metal” category which substitutes existing designs with composite materials rather than reviewing the design approach and utilising the available volume to achieve maximum energy absorption.

The following sections will explore some of the bulk material[2] options available in order to exploit the available space within a given volume, with the objective of applying these materials to achieve significant energy absorption without compromising the lightweighting objectives discussed in Section 1.5. Therefore foams and honeycomb materials will be investigated due to their relatively low density and their ability to undergo large deformation whilst maintaining a near constant stress value.

2.2.2. *Foams*

2.2.2.1. Rigid Polyurethane Foams (PUR/PIR)

Rigid polyurethane (PUR) is made by reacting a liquid polyol (long-chain alcohols derived from vegetable sources) with a liquid polymeric isocyanate in the presence of a blowing agent [90]. The mixed components then react exothermally to form a rigid thermosetting polymer and since the blowing agent evaporates during this exothermic reaction a rigid closed cell low density insulation product is created (Figure 51). PUR has a very low thermal conductivity due to the gasses trapped in its closed cell structure and is often used as an insulator for building applications.

Figure 51: Sheets of PUR foam [91]

Rigid polyisocyanurate (PIR) is produced using an excess of isocyanate. In the presence of a catalyst the isocyanate reacts with itself to form isocyanurate. PIR is characterised by greater

[2] Bulk materials in this context relates to low-density composite or metallic materials which have the capacity to readily occupy large volumes.

heat stability delivering higher working temperature limits making it suitable for applications which demand a higher fire performance [92].

Figure 52: PIR foam block with aluminium facings [93]

The material can be manufactured in a wide range of densities ranging from 30-700 kg/m^3 [94]. It is considered a non-structural material due to its poor load bearing capacities, and its energy absorption efficiency[3] is only 50% when compressed statically [95]. It is therefore more generally used in composite sandwich structures where the material which encapsulates it forms the load bearing element (Figure 52). The energy absorption of such structures was extensively investigated by Pitarresi et al. [89] where polyurethane foam was used as a lightweight filler material to produce the final form and shape of the energy absorber test specimens.

2.2.2.2. Aluminium Foams

Aluminium foam is a rigid cellular structure produced from molten aluminium that contains a large volume fraction of gas-filled pores (Figure 53). The material is manufactured by introducing gas bubbles or additives (such as hollow glass spheres) into the molten metal matrix creating a product that is similar to a hard metallic sponge. It is worth noting that gas-filled structures tend to be irregular, with pore sizes of between 10 μm to 10 mm and exhibit non-uniform distribution of pores due to growth and coalescence of bubbles [96].

The potential use of this material in transport industries was investigated by Baumeister et al. who concluded that the material itself does not represent an optimum energy absorbing

[3] Defined as the ratio of the absorbed energy up to a selected stress level divided by the stress itself [95]

element [97]. He argues, however, that the material could efficiently dissipate energy if it is integrated into the whole body structure.

Figure 53: A block of aluminium foam. Note irregular pore sizes.

Under compressive loading its mechanical response is typical of highly porous cellular solids with an initial linear elastic region followed by a stress plateau, leading to densification and a corresponding marked increase in stress-strain curve (Figure 54). Energy absorption is achieved through the deformation of the aluminium foam structure via the progressive collapse of the cells under load. The cellular nature of the material means that it can exhibit collapse strains of approximately 80% [98].

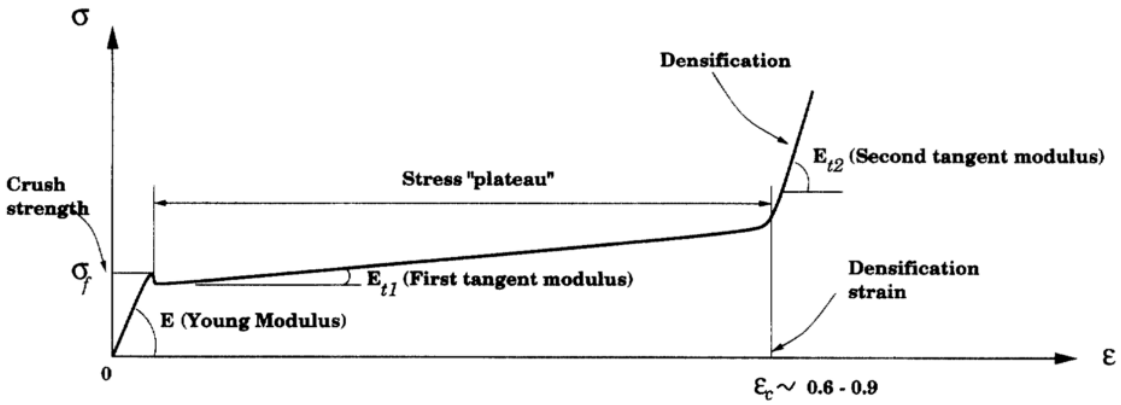

Figure 54: Mechanical response of aluminium foam under compressive load [98]

It is this property which makes aluminium foam a suitable candidate for use in energy absorber designs. The response of the material on a cellular level has been investigated by Cheon et al. [99] with particular reference to the potential use of the material in the automotive sector.

2.2.2.3. Steel Foams

Steel foams can be manufactured in a similar manner to aluminium foams (introduction of compressed gas or additives) or through powder-metallurgy in which hollow steel spheres are compacted with steel power and sintered together [100] (Figure 55). The suitability of this material as an energy absorber was investigated by Cardoso et al. [101] for racing car applications, concluding that the best performance was achieved by the lightest and most expensive of the steel foams investigated. This cost barrier to the use of metal foams was analysed by Maine et al. [102] citing that when compared to the solid metals from which they derive, the production processes are time and labour intensive leading to a more expensive end product. Additionally, the impetus for commercialisation is not currently strong and as such steel foams remain a highly specialised material for advanced applications only [103].

Figure 55: Steel foam manufactured from hollow steel spheres [104]

2.2.3. *Honeycombs*

Honeycomb materials have been widely used by the aerospace industry to provide flat or slightly curved panels exhibiting excellent strength-to-weight ratios. A cellular material, it is primarily manufactured using expansion or corrugation techniques (Figure 56). Its principle properties are governed by: cell size; cell wall thickness; cell wall material.

The expansion method lends itself to lower density honeycombs (up to 160 kg/m^3) whereas the corrugation method is mainly used for higher density honeycombs or materials that cannot be formed using the expansion process. Honeycomb materials fall into two main categories: metallic and non-metallic.

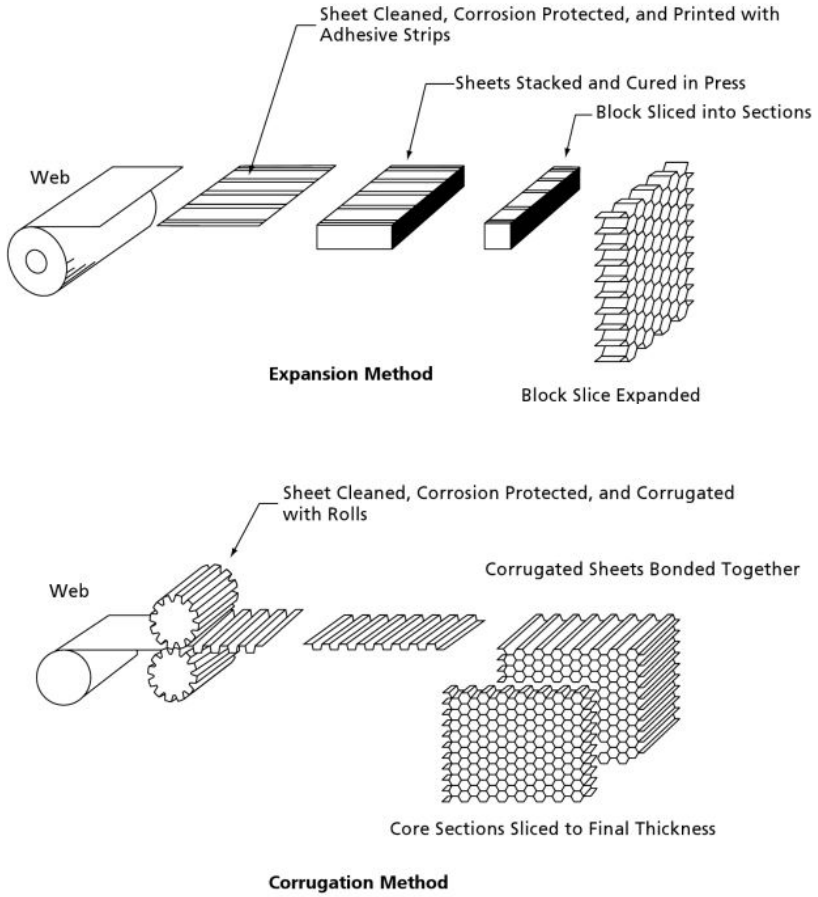

Figure 56: Manufacturing methods for honeycomb materials [105]

2.2.3.1. Metallic Honeycombs

The more common metallic honeycombs on the market are produced from aluminium, stainless steel and in some cases titanium. The stainless steel and titanium varieties have been developed to meet specific applications, but the aluminium honeycomb (Figure 57) comes in a commercial grade (3003) as well as specification grades such as 2024, 5052, and 5056 [106]. Widely used in the aerospace and defence industries [107], these materials are now becoming a regular feature of designs for the marine, rail and automotive industries.

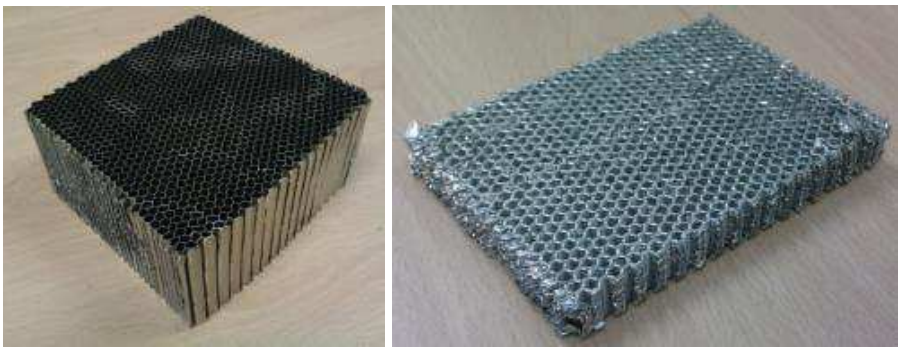

Figure 57: Sample of aluminium honeycomb before (left) and after (right) axial compressive loading [108]

One of the unique properties of aluminium honeycomb is the predictable and uniform manner in which axial crush loads are absorbed. Each cell in the honeycomb acts as a tube progressively folding under load until the sample is completely crushed.

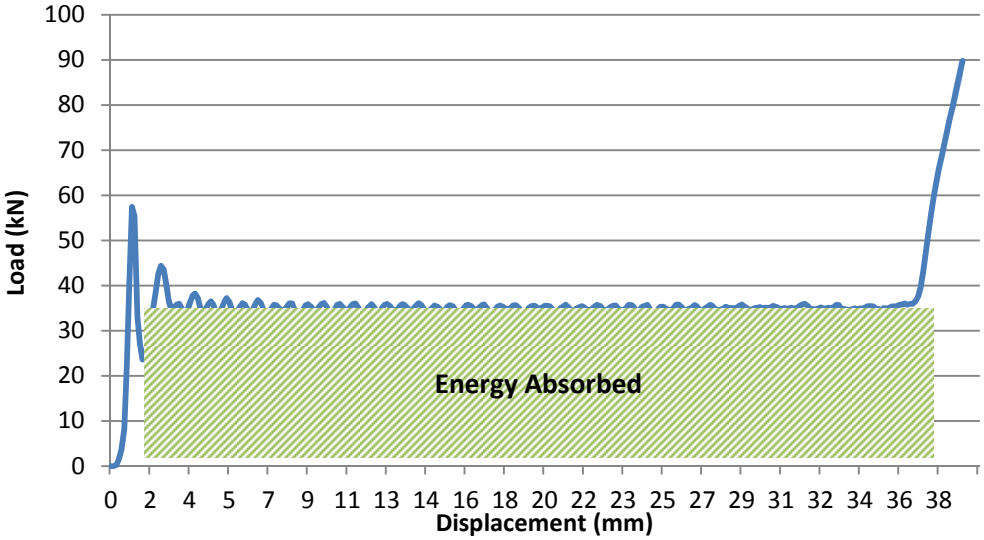

Figure 58: Load-displacement profile of aluminium honeycomb under axial compressive crush loading [108]

The load-displacement curve generated is linearly stable/constant (Figure 58), which allows for the rapid calculation of the total energy absorbed (the hatched area in Figure 58). The load value at which this "plateau" forms is known as the crush strength. This value varies depending on the aluminium type, wall thickness and cell size. It is generally accepted that the crush strength of honeycomb in the orthogonal directions to the cell axis is 10 times less than the axial crush strength [109]. Knowing the axial crush strength value can allow the designer to quickly determine the material density to use to absorb a given amount of energy – see Section 5.1.2 for a worked example.

2.2.3.2. Non-metallic Honeycombs

Whilst honeycomb structures can be manufactured from almost any thin sheet, the most commonly used non-metallic honeycombs are Nomex (aramid fiber paper coated with phenolic resin - Figure 59) and Kraft paper (a paper-board or cardboard shaped into hexagonal cells - Figure 60). The cores, when formed, are often dipped in phenolic, epoxy and thermoplastic resins to improve high-temperature performance and toughness.

These materials are highly customisable, being easily cut, shaped and draped into complex curvatures. However, the manufacturing process of cutting the blocks to size and shape exposes the edges of the material along the sawn surfaces [106]. Left untreated these can quickly absorb moisture which considerably reduces the strength of the core.

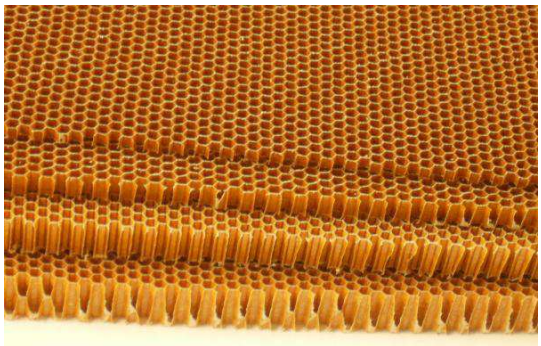

Figure 59: Nomex honeycomb cores of various thicknesses [110]

Figure 60: Sandwich boards with Kraft paper honeycomb core [111]

Under crush loads their behaviour is relatively unpredictable. Initially, in the elastic phase of the force-displacement curve, the phenolic resin breaks throughout the height of the honeycomb followed by an initial folding of the structure. Thereafter the failure mode becomes more complex, with tearing and de-bonding dominating the crush response [112].

Table 9: Comparison of Aramid and Aluminium honeycombs (Data source: Hexcel [113])

Aramid Honeycomb (HRH-10)	Density (kg/m^3)	Compressive			
		Bare	Stabilised		Normalised
		Strength (MPa)	Strength (MPa)	Modulus (MPa)	Modulus (MPa)
HRH-10-1/8-1.8	28.8	0.72	0.79	55.16	1.92
HRH-10-1/8-3	48.1	1.99	2.24	137.90	2.87
HRH-10-1/8-4	64.1	3.58	3.96	193.05	3.01
HRH-10-1/8-5	80.1	4.82	5.31	255.10	3.18
HRH-10-1/8-6	96.1	7.24	7.76	413.69	4.30
HRH-10-1/8-8	128.1	11.55	12.62	537.79	4.20
HRH-10-1/8-9	144.2	13.79	14.48	620.53	4.30

5052 Alloy Aluminium Honeycomb	Density (kg/m^3)	Compressive			
		Bare	Stabilised		Normalised
		Strength (MPa)	Strength (MPa)	Modulus (MPa)	Modulus (MPa)
1/8-5052-.0007	28.8	1.97	2.07	517.11	17.96
1/8-5052-.001	48.1	3.79	3.93	1034.21	21.50
1/8-5052-.0015	64.1	6.76	7.03	1654.74	25.82
1/8-5052-.002	80.1	10.34	10.76	2413.17	30.13
1/8-5052-.0025	96.1	14.48	15.51	3447.38	35.87
1/8-5052-.003	128.1	18.62	19.99	6205.28	48.44

Table 9 gives a comparison of the compressive modulus of a selection of aramid and aluminium honeycombs. To account for differing densities, the modulus is normalised with respect to the material density, allowing a realistic comparison to be made. As can be seen from the data the aramid honeycomb has a normalised compressive modulus range of between 1.9 and 4.3 MPa/kg/m^3, whereas the aluminium has a range of 17.96 to 48.44 MPa/kg/m^3.

Coupled with the unpredictable response under crush loading, it is evident from these figures that aramid/paper honeycombs are unsuitable for absorbing energies of the scale required by the rail industry. See Section 5.1.2 which defines the criteria for the down-selection of aluminium honeycomb materials for rail vehicle absorber applications.

2.2.4. *Summary of energy absorbing materials*

The properties of a selection of lightweight materials have been discussed and their application to the rail industry as energy absorbers can now be explored. While each of these materials have the capability of making optimal use a given space, not all have the energy absorbing capabilities required to offset the impact of a rail vehicle, or are too expensive to produce in sufficiently large quantities for the rail industry. In addition, the properties of these materials (especially the foams) can be highly dependent on the manufacturing process, with their inherent properties being heavily affected by the quality and process of manufacture. These irregularities make it difficult to predict the response of the material under crush load, and as such will be dismissed from consideration for use as an energy absorber.

Of the bulk materials investigated, aluminium honeycomb offers the best solution in fully utilising the space available while still offering a high degree of predictable crush behaviour. Its predictable crush profile, availability in a range of densities and a proven track record in other industries makes it the ideal candidate to take forward for use as an energy absorber for rail crashworthy applications.

Aluminium honeycomb is produced for the market in rectangular blocks and can be machined to size using high speed steel or carbide-tipped cutters [114]. Shaping the honeycomb to fit more complex geometries could weaken the sidewalls of the honeycomb, causing non-axial crushing and thus reducing the energy absorption capacity. To minimise the cutting operations and potential damage to the honeycomb sidewall structure Chapter 3 will seek to capitalise on the unused volumes available within rail vehicles by means of strategically introducing aluminium honeycomb rectangular blocks.

Chapter 3: The Deployment of Energy Absorbing Materials and Structures within Fixed Space Envelopes

3.1. Introduction

As discussed in Section 1.2.3 the majority of impact scenarios for the rail industry are linear in nature and occur along the longitudinal axis of the train. Xue et al. provide further insight into the mechanics of rail collisions and surmise that in order to minimise or prevent irregular structural weaknesses during impact that symmetric and large cross-section structures should be favoured by design engineers [33]. Material choice to fulfil the energy absorption requirements must also act along the same axis, making foams and honeycombs the primary lightweight material solutions. However from the material properties discussed in Section 2.2, foams do not adequately meet rail industry requirements. As such, aluminium honeycomb when axially aligned with the direction of travel offers the best solution for the development of a lightweight energy absorbing structure.

This material however has its limitations, one of them being the machinability of the honeycomb. Aluminium honeycomb is usually supplied commercially in rectangular blocks and subsequent shaping (either through cutting or grinding) may weaken the structure and reduce its capacity to absorb energy. As each cell acts as a tube which folds under loading, any off-axis cut will reduce the effective length of the tube, thus reducing the stroke over which it can absorb energy.

While a number of Computer Aided Design (CAD) packages can readily determine the total volume occupied by a particular 3D geometry, the insertion of linearly aligned block elements into such geometries is not a standard CAD capability. This chapter investigates methodologies to rapidly determine the "block volume" of a given space, thus maximising the amount of honeycomb material that can be placed within a fixed volume. This will allow the designer to rapidly and cost-effectively develop realistic design solutions based on the shape and nature of the material as supplied.

Additionally, CAD packages can be prohibitively expensive for small enterprises and SMEs who may wish to become involved in the rail industry supply chain. This chapter delivers an approach to producing design solutions without the need for, or reliance upon, CAD packages or the numerical methods contained therein.

Three cross-sections are investigated which form the closest approximation for the front end of rail vehicles: triangular, circular and elliptical. These sections are then mapped into 3D geometries, bearing in mind the directionality of maximum crush strength of aluminium honeycomb.

3.2. Maximising Triangular Cross-sections

To determine the maximum rectangular area that can be inscribed inside triangle OAB as in Figure 61, the slopes m_1 and m_2 of lines OB and AB respectively must be expressed in terms of *x*.

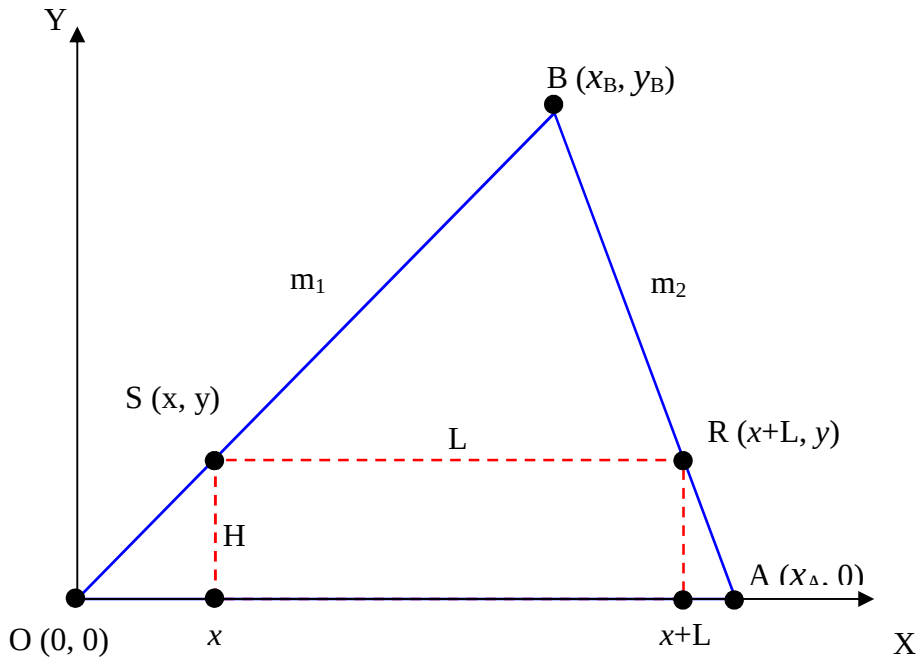

Figure 61: Maximum rectangular area inscribed in a given triangle

At point *S* on line OB, the distance *H* is equal to the y co-ordinate (*y*). The slope at this point can be expressed as follows:

$$m_1 = \frac{y}{x} = \frac{y_B}{x_B}$$

$$\therefore y = \frac{xy_B}{x_B} = H \qquad (1)$$

At point *R* on line AB, the distance *H* is equal to the y co-ordinate (*y*). The slope at this point can be expressed as follows:

$$m_2 = \frac{-y_B}{x_A - x_B} = \frac{-y}{x_A - x - L}$$

$$\therefore y = \frac{y_B(x_A - x - L)}{x_A - x_B} \tag{2}$$

Equating (1) with (2) and expressing in terms of *L* gives:

$$L = x_A - \frac{x_A x}{x_B} \tag{3}$$

The area of the rectangle is:

$$A = HL \tag{4}$$

Substituting (1) and (3) into (4) and simplifying gives:

$$A(x) = -x^2\left(\frac{x_A y_B}{{x_B}^2}\right) + x\left(\frac{x_A y_B}{x_B}\right), \qquad 0 \le x \le x_A \tag{5}$$

(5) is a polynomial equation with a negative leading coefficient. It has a maximum value when the slope of the curve is equal to zero.

Differentiating (5) and equating it to zero gives:

$$\frac{d(A)}{dx} = -2x\left(\frac{x_A y_B}{{x_B}^2}\right) + \left(\frac{x_A y_B}{x_B}\right) = 0 \tag{6}$$

Simplifying for *x* gives:

$$x = \frac{x_B}{2} \tag{7}$$

Substituting (7) into (1) and (3) gives expressions for H and L respectively.

$$H = \frac{y_B}{2} \tag{8}$$

$$L = \frac{x_A}{2} \tag{9}$$

Therefore, the rectangle with maximum area that fits within triangle OAB has a length (L) of half the base of the triangle (OA) and height (H) of half the perpendicular height.[4]

This result however does not take into account certain geometric constraints in the manufacturing of energy absorbing materials such as honeycomb which may not be manufacturable to the height recommended by this approach. As such, this methodology needs to take into account possible material manufacturing boundaries with respect to the overall height of the triangular cross-section, as well as a minimum base size for each rectangle to make energy absorption viable.

Using the similar triangles method described by Lange [115] it is possible to develop a simplified approach to maximising the area of a triangle based on restricted parameters.

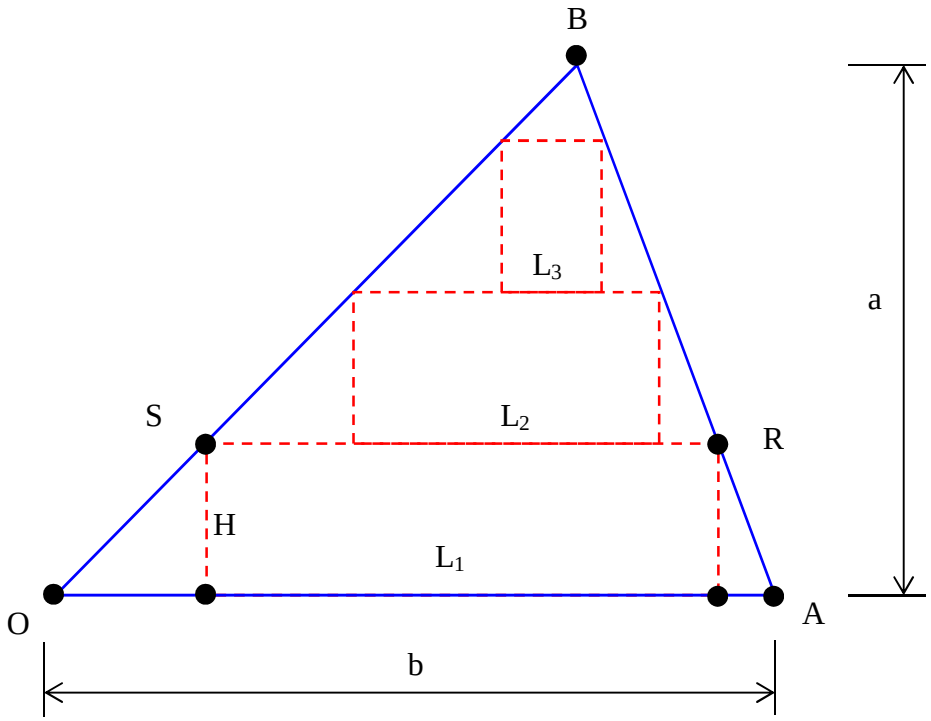

Figure 62: Maximising the area of a triangle with rectangles of given parameters

Where the height (H) of the rectangle is known, the length of the first rectangle (L_1) can be determined by cross-multiplying the ratios of the vertical heights of triangles OBA and SBR to their respective bases.

[4] This can also be established using the similar triangles methodology outlined in [115].

$$\begin{matrix} a : b \\ (a - H) : L_1 \end{matrix} \quad (10)$$

Rearranging for L_1 gives:

$$L_1 = \frac{b(a - H)}{a} \quad (11)$$

Similarly:

$$L_2 = \frac{b(a - 2H)}{a}$$

$$L_3 = \frac{b(a - 3H)}{a} \quad (12)$$

The sequence can be expressed as:

$$L_i = \frac{b(a - iH)}{a} \quad (13)$$

for $i = 1 \cdots n$ where $n < \frac{a}{H}$

Determining the total area covered by the honeycomb within this 2-dimensional space is simply a matter of multiplying (13) by *H*.

$$A_{tot} = HL_i \quad (14)$$

3.2.1. *Mapping Triangular Sections to 3D*

Mapping these 2D areas into 3D space will be dependent on the final desired shape and on the design into which the honeycomb blocks will be incorporated. A simple linear extrusion of the shape in Figure 62 could represent the front of a wide automotive vehicle. As such, the volume which could be occupied by the honeycomb can be determined by multiplying (14) by the width (W) of the vehicle.

For the rail industry where the nose cone of (for example) high speed vehicles is more akin to that shown in Figure 63, the 3D volume can be approximated as a square pyramid.

Figure 63: Nose detail of the high speed Shinkansen JR500 (Japan) [116]

This means that equation (13) needs to also be applied across the width of the vehicle, yielding:

$$W_i = \frac{b_W(a_W - iH)}{a_W} \tag{15}$$

for $i = 1 \cdots n$ where $n < \frac{a_W}{H}$

The total area formed is:

$$A_{tot} = L_i W_i \tag{16}$$

The total volume of the space occupied by honeycomb material is:

$$V_{tot} = L_i W_i H \tag{17}$$

3.3. Maximising Semi-circular Cross Sections

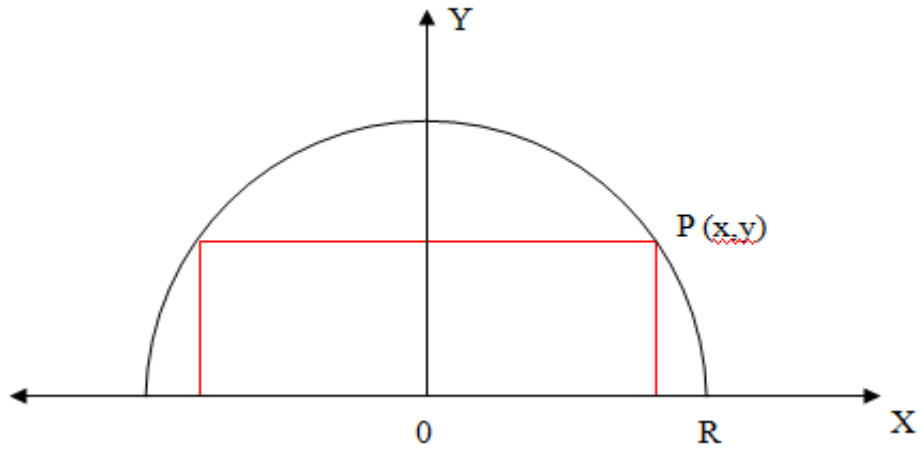

Figure 64: Maximum area of a rectangle inscribed in a semi-circle

The area of the rectangle shown in Figure 64 can be expressed as:

$$A = 2xy \tag{18}$$

And the equation of the circle can be expressed as:

$$x^2 + y^2 = R^2 \tag{19}$$

Rearranging (19) for *y* gives:

$$y = \sqrt{R^2 - x^2} \tag{20}$$

Substituting (20) into (18) gives:

$$A(x) = 2x\sqrt{R^2 - x^2} \tag{21}$$

To get the maximum area of rectangle, the derivative of (21) is found and set to zero.

$$A^{'}(x) = \frac{2(R^2 - 2x^2)}{\sqrt{R^2 - x^2}}$$

$$\frac{2(R^2 - 2x^2)}{\sqrt{R^2 - x^2}} = 0$$

$$x = \frac{R}{\sqrt{2}} \tag{22}$$

Substituting

(22) into (20) gives:

$$y = \frac{R}{\sqrt{2}} \tag{23}$$

Therefore the dimensions of the largest rectangle are:

$$L = R\sqrt{2}$$
$$H = \frac{R}{\sqrt{2}}$$

This is the maximum single rectangular area that can be inscribed in a semi-circle. As before, manufacturing constraints will determine the maximum height (H) of the rectangle that can be placed within the semi-circle. Subsequent rectangle sizes can be determined as follows:

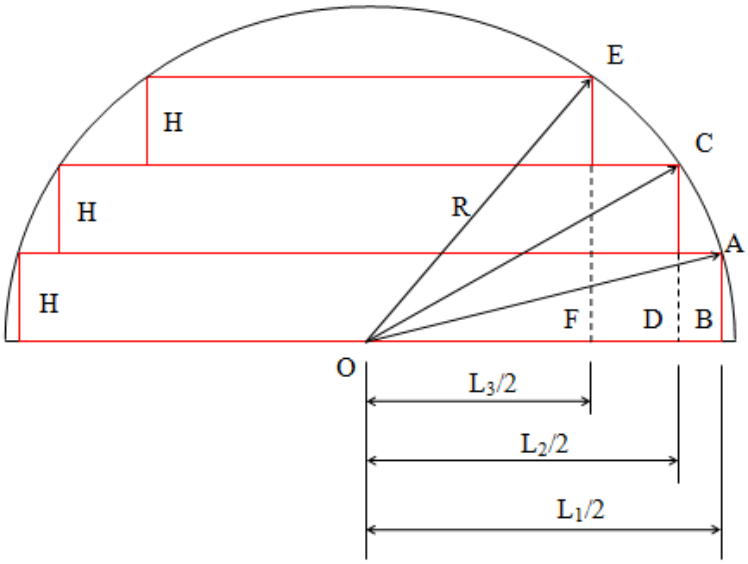

Figure 65: Optimising rectangles to fit in a semi-circle

Applying Pythagoras's theorem to triangle OAB in Figure 65 gives:

$$R^2 = H^2 + \left(\frac{L_1}{2}\right)^2$$
$$\therefore L_1 = 2\sqrt{R^2 - H^2} \quad (24)$$

For triangles OCD and OEF this gives respectively:

$$L_2 = 2\sqrt{R^2 - (2H)^2}$$

(25)

$$L_3 = 2\sqrt{R^2 - (3H)^2}$$

Where L_1, L_2, and L_3 are the bases of the inscribed rectangles.

Continuing the sequence until the area is filled yields:

$$L_i = 2\sqrt{R^2 - (iH)^2} \quad (26)$$

for $i = 1 \cdots n$ where $n < \frac{R}{H}$

3.3.1. *Mapping Semi-circular Sections to 3D*

The 350 high speed vehicle manufactured by Talgo (Figure 66) is an example of how a semi-circular cross-section can be extruded linearly across the width of a vehicle to approximate the existing structure. For such a design equation (26) can be multiplied by the width (W) of the vehicle to rapidly determine the volume occupied by honeycomb.

Figure 66: Talgo's 350 high speed train [117]

For a train which has a more bulbous or hemispherical front, the design in Figure 65 can be rotated through 180° to best represent the design. As such, equation (26) can be multiplied by itself to give the area:

$$A_{tot} = 4(R^2 - (iH)^2) \tag{27}$$

The volume is therefore:

$$V_{tot} = 4\mathrm{H}(R^2 - (iH)^2) \tag{28}$$

for $i = 1 \cdots n$ where $n < \frac{R}{H}$

3.4. Maximising Semi-elliptical Cross-sections

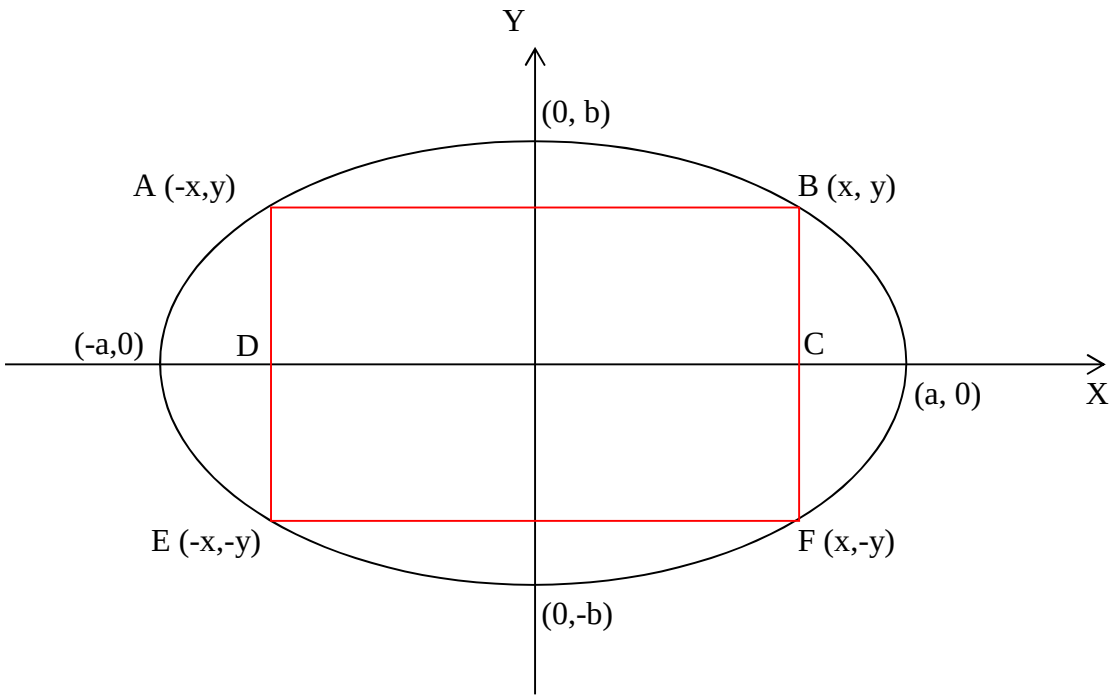

Figure 67: Maximum rectangular area inscribed in an ellipse

To determine the maximum area of the rectangle ABCD in Figure 67, the maximum area of rectangle ABFE must first be determined.

The equation for an ellipse is:

$$\frac{x^2}{a^2} + \frac{y^2}{b^2} = 1 \tag{29}$$

Rearranging for y gives:

$$y = \frac{b}{a}\sqrt{a^2 - x^2} \tag{30}$$

The area (A) of rectangle ABFE is defined as:

$$A = (2x)(2y) = 4xy \tag{31}$$

Substituting (30) into (31) gives:

$$A(x) = 4x\frac{b}{a}\sqrt{a^2 - x^2}\,, \qquad 0 \le x \le a \tag{32}$$

This equation has a maximum between 0 and *a* when the slope is equal to 0.

Differentiating gives:

$$A'(x) = \frac{d}{dx}\left[\frac{4b}{a}x\left(a^2 - x^2\right)^{½}\right]$$

$$= \frac{4b}{a}\left[(a^2 - x^2)^{½} + \frac{1}{2}x(a^2 - x^2)^{-½}(-2x)\right]$$

$$= \frac{4b}{a}(a^2 - x^2)^{-½}(a^2 - 2x^2), \qquad 0 \le x \le a \tag{33}$$

Setting (33) equal to 0, and simplifying for x:

$$A'(x) = 0 \leftrightarrow x^2 = \frac{a^2}{2}$$

$$\therefore x = \frac{a}{\sqrt{2}} \tag{34}$$

The base of the rectangle, DC, is twice the value of x:

$$2x = \frac{2a}{\sqrt{2}} = a\sqrt{2} \tag{35}$$

To determine the height, *y*, of the rectangle, the area of the maximum rectangle must be determined. Substituting (34) into (32) gives:

$$A\left(\frac{a}{\sqrt{2}}\right) = 2ab \tag{36}$$

Substituting (34) (35) and (36) into (31) yields:

$$2ab = 4\left(\frac{a}{\sqrt{2}}\right)y$$

$$\therefore y = \frac{b}{\sqrt{2}} \tag{37}$$

While this solution will maximise the volume that can be occupied by a block of honeycomb, manufacturing constraints will again predetermine the height (H) of the block. As such, equation (29) needs to be resolved in terms of H with respect to x.

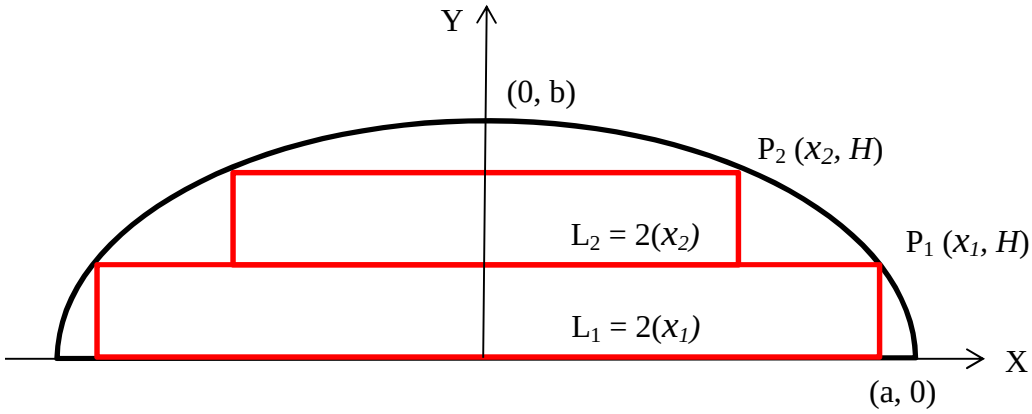

Figure 68: Optimising a semi-ellipse for honeycomb of defined thickness (H)

Substituting H for y in equation (29) and rearranging for x at point P_1 gives:

$$x_1 = a\sqrt{\left(1 - \frac{H^2}{b^2}\right)} \tag{38}$$

And at point P_2 this gives:

$$x_2 = a\sqrt{\left(1 - \frac{(2H)^2}{b^2}\right)} \tag{39}$$

Continuing the sequence until the area is maximised yields:

$$L_i = 2x_1 = 2a\sqrt{\left(1 - \frac{(iH)^2}{b^2}\right)} \tag{40}$$

for $i = 1 \cdots n$ where $n < \frac{b}{H}$

with the total area being calculated as:

$$A_{tot} = HL_i = 2Ha\sqrt{\left(1 - \frac{(iH)^2}{b^2}\right)} \tag{41}$$

3.4.1. *Mapping Semi-elliptical Sections to 3D*

Elliptical areas can be mapped or extruded linearly or rotationally. As with the other sections explored in this chapter, defining the volume for a linearly extruded shape can be achieved simply by multiplying equation (41) by the desired width (W).

Rotating and mapping the shape in Figure 68 through 180° about the y-axis yields a 3D compressed hemisphere, a shape often used in the nosecones of high speed trains such as the E6 series from Hitachi (Figure 69).

Figure 69: Elliptical nose on Hitachi's E6 series Shinkansen high-speed train [118]

The area defined for each honeycomb block as a result of this rotational sweep is:

$$A_i = {L_i}^2 = 4a^2\left(1 - \frac{(iH)^2}{b^2}\right) \tag{42}$$

With the total volume occupied by the honeycomb material being defined as:

$$V_{tot} = 4Ha^2\left(1 - \frac{(iH)^2}{b^2}\right) \tag{43}$$

for $i = 1 \cdots n$ where $n < \frac{b}{H}$

3.5. Summary of Fixed-space Mapping

This chapter has presented some of the preliminary equations which can be used to fill a specific volume using blocks of aluminium honeycomb. The ease of application of these equations is demonstrated in Section 5.1.1 to deliver energy absorbing capabilities which meet the demand of the rail industry.

From an engineering perspective, these equations have the capability to dramatically reduce the amount of time taken to develop an energy absorber design which needs to fit within a fixed volume. By varying the densities of the aluminium honeycomb greater or lesser amounts of energy can be absorbed within that same volume. This makes the design and manufacture of absorbers which are capable of absorbing significant impact energies a cost effective solution. This will better enable the rail industry supply chain to deliver low-cost mass-produced absorbers to meet the wide and varied needs of the rail industry.

Chapters 5 and 6 further develop this methodology for implementing the materials discussed in Section 2.2 in an existing driver's cab design and define the energy absorption capabilities realised through the methodologies set out in this chapter.

Chapter 4: Design of a lightweight rail vehicle cab for energy absorption and load transfer

4.1. Crashworthiness Requirements

European rail vehicle crash requirements are specified in EN 15227 which sets out three major collision scenarios for rail driver's cab:

- A collision with an identical train at 36 km/h.
- A collision with an 80 tonnes buffered wagon at 36 km/h.
- A collision with a 15 tonnes Large Deformable Obstacle (LDO) at V_{lc} - 50 km/h. The maximum operational speed of the SPACIUM vehicle is 140 km/h. Therefore a collision speed of 90 km/h will be employed in this case.

The first two crash scenarios are reacted primarily by the lower buffer-level energy absorbers (Figure 70) and will be discussed in Chapter 6. The third scenario must be reacted at a higher location in the cab leading to the introduction of two additional energy absorbers located above the buffer-level absorbers as shown in Figure 70. Here there is an opportunity to reduce weight by utilizing the available volume in this area and introducing lightweight structures in an energy absorbing role (See Chapter 5).

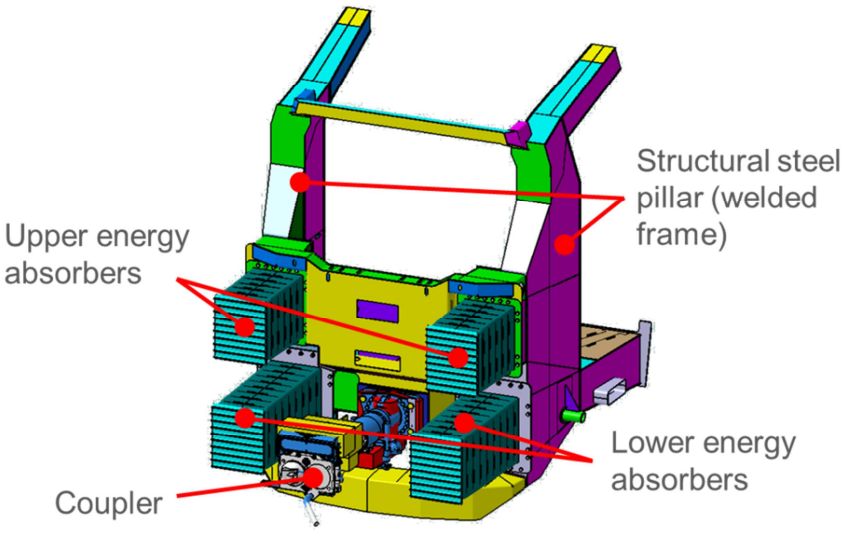

Figure 70: Typical embodiment of energy absorbers in a rail vehicle drivers cab (image courtesy of Bombardier)

The energy absorption capabilities of the various devices as shown in Figure 70 can be superimposed to generate the overall load-displacement characteristic for the SPACIUM cab. This is shown in Figure 71 for the first 1 m of collapse. The total energy absorption capacity of the complete system is approximately 3.3 MJ [119].

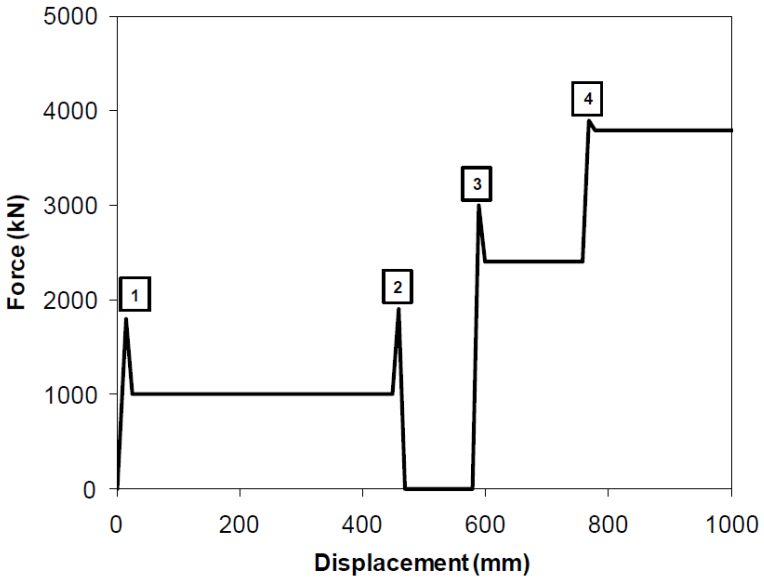

Figure 71: Load-Displacement profile for existing SPACIUM design by Bombardier [119]

Explanation of marked points:
1 = engagement of coupler; 2 = exhaustion of coupler; 3= engagement of buffer-level energy absorbers; 4 = engagement of upper energy absorbers.

The high energy absorption requirement for the cab of the SPACIUM vehicle can be attributed to the train's articulated design. This means that adjacent carriages in the train share a common bogie, rather than having their own unique bogie sets. Whilst there are benefits to reducing the overall number of bogies in a rake through articulation (reduced weight, reduced cost, reduced rolling resistance, etc.), articulation does make crash energy absorption through the deformation of intermediate carriage ends more problematic, as discussed in Section 1.3. This therefore places an increased energy absorption requirement on the front of the vehicle.

4.2. Designing within Existing Volumes to achieve Crashworthiness

To achieve the goal of a lightweight volumetrically enhanced cab for crashworthiness the structure is divided into discrete sections from fore to aft which allows for the stepwise absorption and reaction of crash energies imparted to the cab during collision.
Figure 72 shows the zones as identified for the SPACIUM design to define distinct areas, each with their own energy absorption or loading requirements.

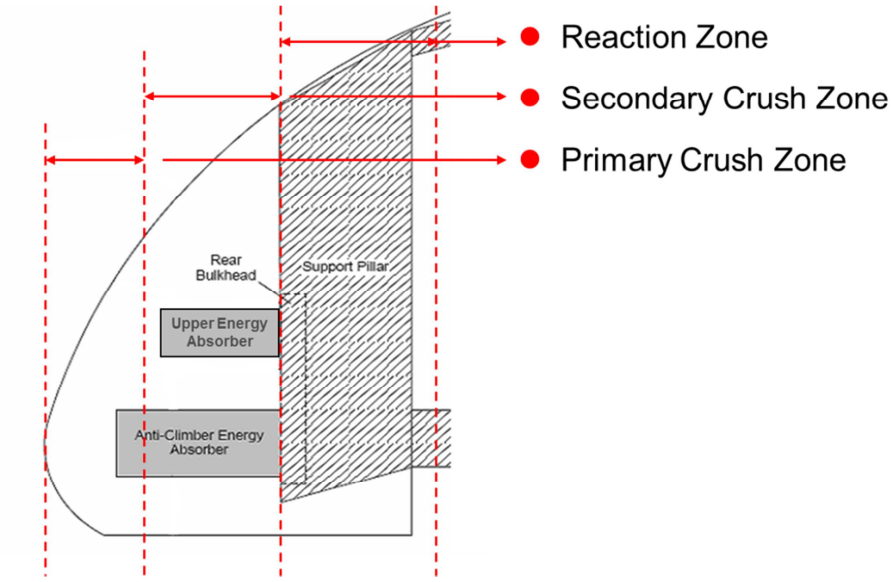

Figure 72: Energy absorption zones of the innovative energy absorbing driver's cab

4.2.1. *Primary Crush Zone*

The purpose of this zone is to:

- React small impacts (such as with buffer stops) with impact energy of less than 0.2 MJ
- Be aligned with the secondary crush zone so in the event of larger impacts it will function in unison with the lower absorbers.

Uniquely, for the first time in cab design, this is achieved through the introduction of a detachable composite nosecone. The frontal nose section which is the area most likely to suffer incidental in-service damage was designed to be easily removed for repair or

replacement. Removing the nose also provided easy access to the primary energy absorbing devices for inspection or replacement purposes.

Figure 73 shows the typical reaction of a rail cab in a low energy buffer-stop impact. In this scenario the cab skirt, valances and shell provide little energy absorption and as a result the main energy absorbers get partially utilised or damaged as they absorb the loads from the impact. In Figure 74 however, the cab's composite nose cone begins absorbing energy on impact, crushing in a controlled manner and thus dissipating the impact energy and reducing the forward momentum of the train, leaving the main energy absorbers undamaged.

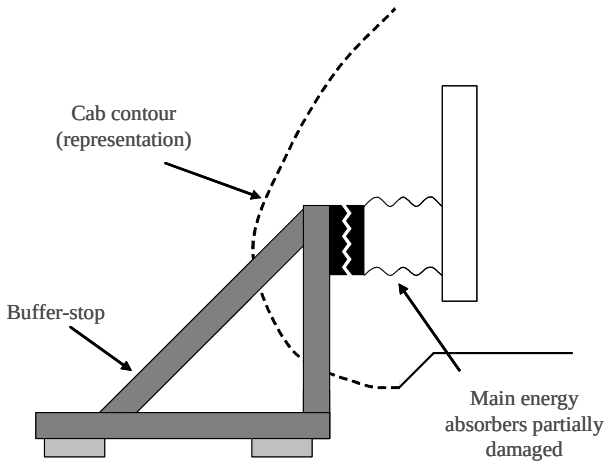

Figure 73: Typical result of low energy buffer-stop collision

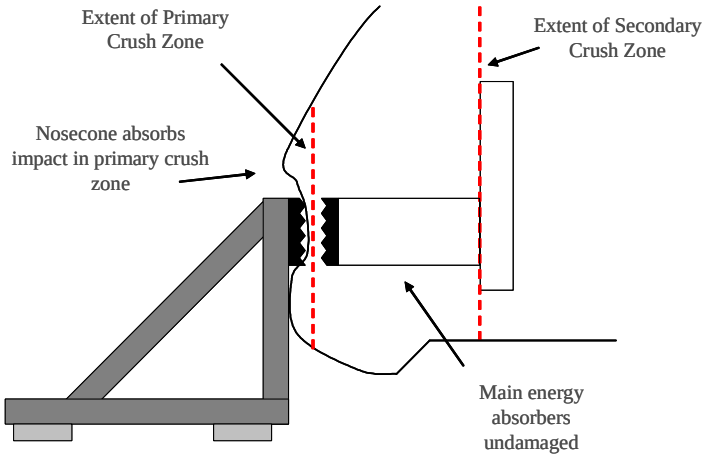

Figure 74: Low energy buffer-stop collision absorbed by nose cone alone, without damage to the main energy absorber (secondary crush zone)

For high energy impacts (collisions where the main energy absorbers would be expected to be fully utilised) the nose cone serves a secondary purpose: to react and transfer a proportion of the crash loads, as well as initiating a staged and controlled crush sequence from the primary crush zone through to the secondary crush zone. This extension of its primary functionality means that the rail cab as a whole can absorb collision energy more efficiently than through using the main energy absorbers alone.

4.2.2. *Secondary Crush Zone*

This zone houses the primary upper and lower energy absorbers and is designed to react the three crash scenarios defined in Section 4.1. The design of the Secondary Crush Zone elements is described in detail in Chapters 5 & 6.

4.2.3. *Reaction Zone*

The Reaction Zone is specifically designed to withstand the loads imparted on the structure as a result of a collision, thus protecting the driver. To react the loads introduced as a result of the crash scenarios whilst still achieving a significant reduction in mass, a step-change was required in the design and manufacture of rail vehicle cabs.

A major innovation in cab design was achieved through the replacement of the main structural members and fibre-glass cover of existing cabs with an integrated composite sandwich structure. This brings a range of potential benefits including reduced mass, reduced part count, reduced assembly costs, and opportunities for functional integration such as:

- The use of the sandwich core material as a thermal insulator.
- The use of the inner sandwich facing as cosmetic panelling for the interior of the cab.
- The incorporation of ducting for electrical wiring, air conditioning, etc. within the core of the sandwich.

In the existing SPACIUM cab construction steel pillars (formed from welded plate) located behind the energy absorbers perform the load reaction and distribution activities. The "D-CAB" solution developed and described by this thesis makes optimal use of this volume by replacing the hollow steel pillars with a foam -filled composite sandwich construction. This involved replacing the existing two steel pillars and separate outer fibreglass cover with a fully integrated composite sandwich structure, forming composite pillars and reactors (see Figure 75).

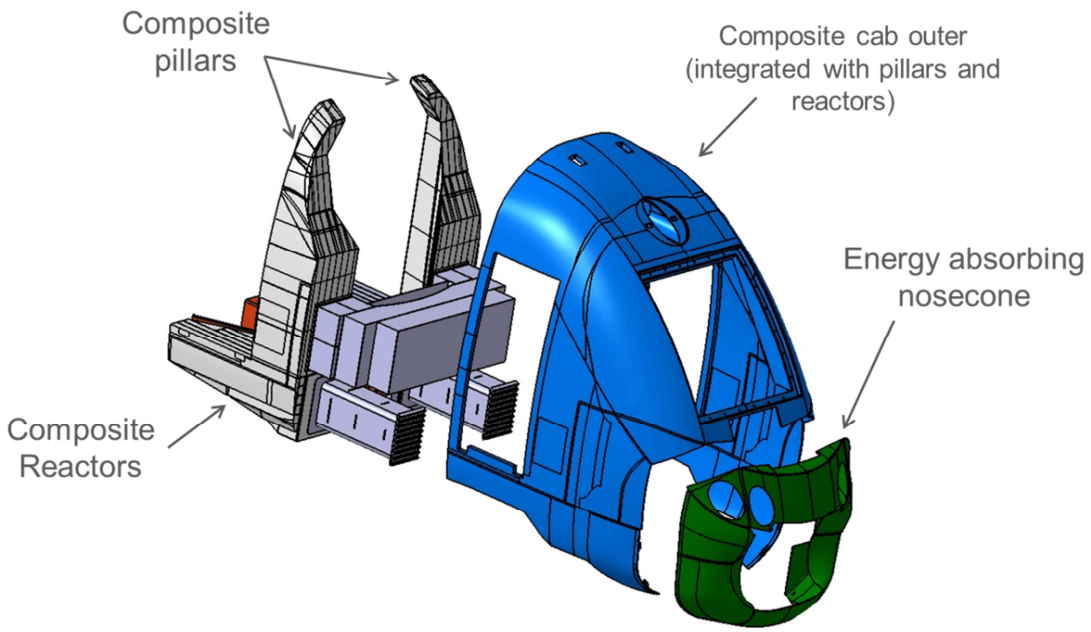

Figure 75: Exploded view of D-CAB components

This sandwich construction is produced from glass fibre reinforced polymer (GFRP) composite layers and polymer foam cores. The sandwich is significantly reinforced in the "pillar" region (where the upper energy absorber attaches) and the lower "reactor" region (where the buffer level energy absorbers attach) in order to provide the necessary stiffness and strength for resisting the energy absorber collapse forces without permanent deformation or damage (Figure 76). The pillars are comprised of blocks of foam core with layers of glass-fibre either side, while the reactors are glass-fibre tubes formed around a foam core.

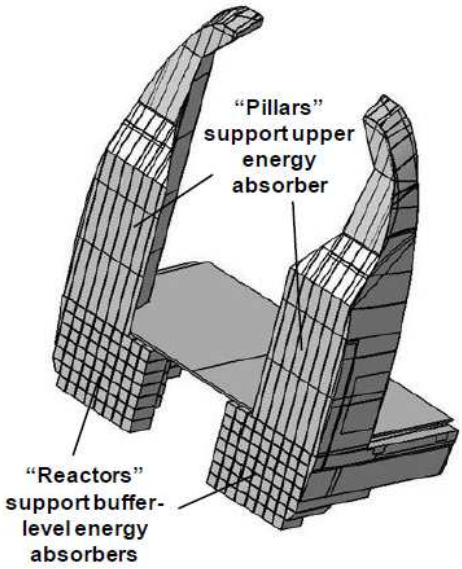

Figure 76: Detailed view of the pillars and reactors

Figure 77 shows the primary load paths within the D-CAB structure under crash loading. The load inputs to the structure are shown as orange arrows, whilst the green arrows show the subsequent load paths into the main vehicle bodyshell. The pillars and reactors function as one unit with the outer cab shell, transferring the load upwards and rearwards, and downwards and rearwards. It is this unique monocoque structure that ultimately delivers the structural strength required to meet the static and crash loads as defined by the rail standards.

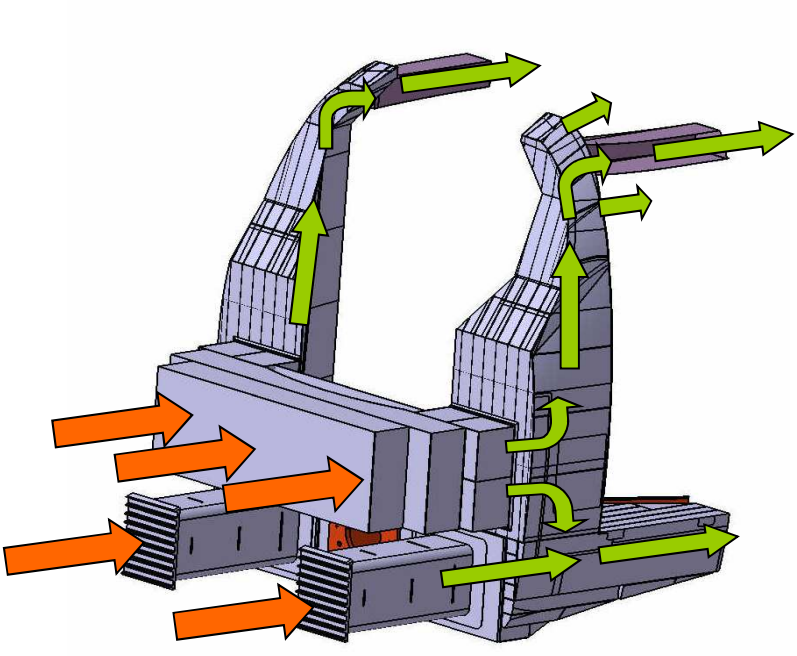

Figure 77: Load paths through upper and lower energy absorbers (orange) into composite pillars and reactors (green)

The joint between the pillars and the reactors was designed to accommodate the shear forces experienced in this area, as well as to provide a means of transferring some of the loads from the upper absorber down into the reactors.

To realise this joint the width of the individual foam columns in the pillars was specified to match the width of the individual reactor tubes. This allowed the insertion of a series of 5 mm thick continuous GFRP layers that extend from the pillars down through the floor level and into the base of the reactors (Figure 78). In this way, the whole pillar-reactor assembly became an integrated multi-layer GFRP-foam sandwich construction.

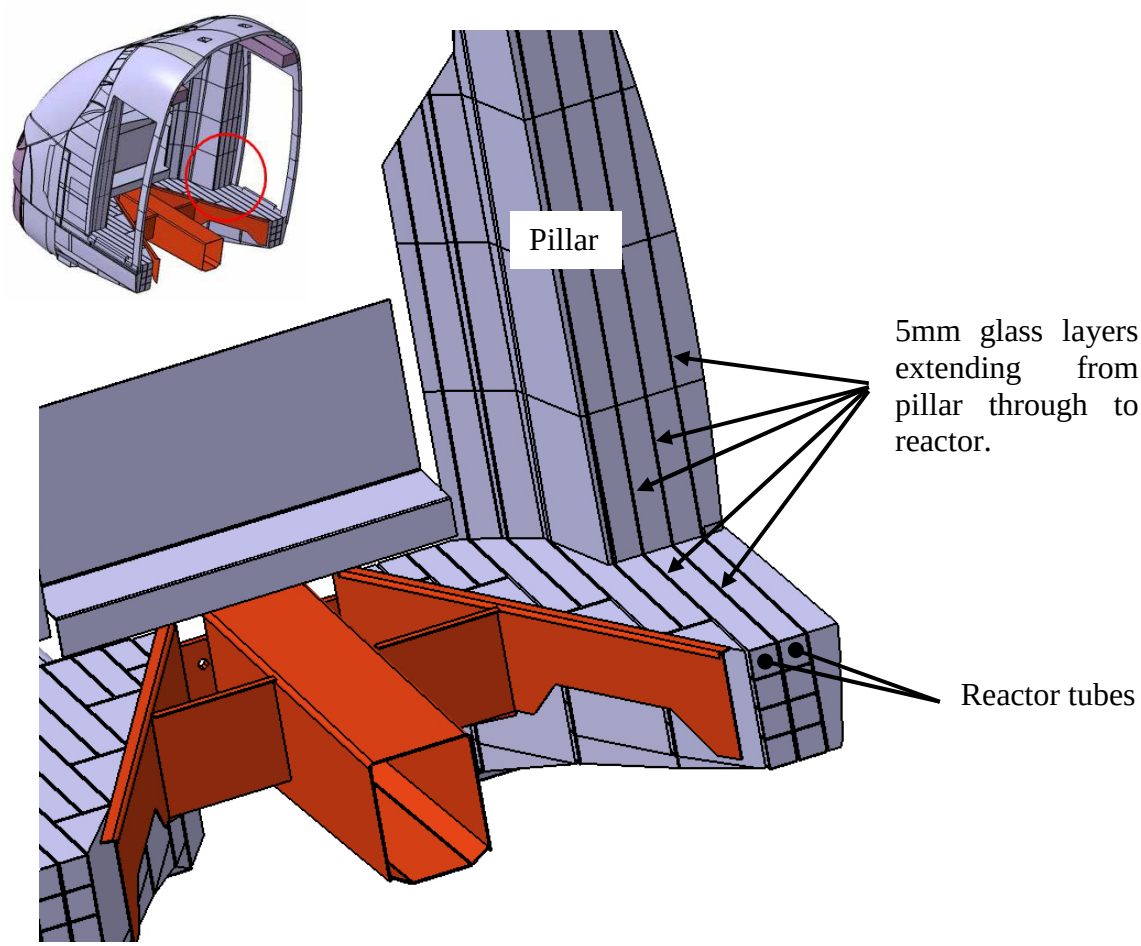

Figure 78: Details of the pillar-reactor joint

4.3. Testing of Lightweight Reaction Zone Design

In order to determine the strength of the reactor elements, a number of test specimens were manufactured and subjected to compressive load tests. Two solutions were evaluated:

A. Square arrays of high density polyurethane foam cores hand wrapped in M705 e-glass with SR1500/SD2507 epoxy resin system (Figure 79). Detailed specifications for these materials are given in Section 1.7.2.

B. Extruded glass reinforced plastic (GRP) (Figure 80). This material was a trial material produced by Exel Composites and due to disclosure restrictions I am unable to disclose specific material properties and configurations at this juncture.

4.3.1. *Test Specimen Specification*

Specimens “A”

These test specimens were manufactured at AP&M, Lagos, Portugal, using a hand-layup process of M705 E-glass in chopped strand mat form and SR1500/SD2507 epoxy resin system (full details in Section 1.7.2). These comprised of foam cores of square cross-section, wrapped in 2.5mm of glass reinforced epoxy then arranged in a 2x2 array and the entire block wrapped in another layer of 2.5 mm glass reinforced epoxy.

Figure 79: Glass-fibre wrapped tubes, specimens “A”

For ease of manufacture it was agreed that the edges along the length of the foam cores could be rounded-off to allow for easier layup of the glass fibre over the cores. The dimensions of the specimens are given in Table 10.

Specimens “B”

These were manufactured be Exel Composites, Runcorn, England, using continuous fibre s-glass and polyurethane resin in a pultrusion process to form a box-section which is then cut to length. The tubes are the same cross-sectional dimensions of the individual glass epoxy tubes prior to assembly. The concept is to use these tubes as a cheaper and less time consuming method of manufacture when compared with the hand layup of glass epoxy tubes. The dimensions of the specimens are given in Table 10.

Table 10: Reactor test specimen dimensions

Specimen Type	Length (mm)	Width (mm)	Depth (mm)	Wall thickness (mm)
"A"	300	215	215	5
"B"	200	100	100	4

Figure 80: GRP extruded tubes, specimens "B"

Target performance

The target load for each of the "A" test specimens can be determined from the load-displacement curve for the existing Bombardier lower absorbers (see Figure 112, Section 6.4). Each individual absorber has a load plateau of 1,200 kN, reacted over an area of 0.277 m2 (derived from Bombardier CAD models).

As the area of the test specimens was 0.046 m^2, this gives a target load of 200 kN for each specimen. Each of the "B" test specimens was 50 kN (being a quarter the area of specimens "A"). This was equivalent to the strength required to resist the peak buffer-level energy absorber collapse load of 1,500 kN (see Figure 112 in Section 6.2) in the full cab.

4.3.2. *Test Set-up*

Due to the limitations of the test equipment with the faculty, it was not possible to undertake large scale dynamic testing which would have been desirable for such test specimens, therefore quasi-static testing was used. As discussed in Section 1.7.6 caution should be used when determining the energy absorption properties under quasi-static load conditions where a magnification of properties can be expected depending on material choice and specimen geometry. Consequently this structure underwent static and dynamic finite element analysis by Grasso which assessed its performance under high velocity impact [120].

Target performance

These specimens reside in the reaction zone, therefore the test specimens needed to demonstrate that they were capable of reacting a load of 200 kN (derived from the crash scenarios in EN 15227 [28]) without damage to the structure. Additionally, it was important to establish that quasi-static testing at varying load-rates would not induce failure in the specimen up to 200 kN loading.

Specimens “A” were tested on the university’s Avery-Denison 5000 kN compression loading machine (Figure 81). Load rates of 40 kN/min, 120 kN/min, 240 kN/min and 1,000 kN/min were applied to the test specimens up to a load of 200 kN. This was undertaken to investigate whether the dynamic toughness and failure of the specimens could be induced using higher loadings rates. Due to the limitations of the machine is was not possible to get a continuous data readout during the experiment, however after each test the specimens were inspected to identify if cracks of failure had occurred. After successfully reaching this load target and determining that failure was not evident, each specimen was subsequently loaded at a rate of 1,000 kN/min to failure.

Figure 81: Reactor test specimen loaded in Avery-Denison 5000 kN compression loading machine

Specimens “B” were initially tested on the university’s DARTEC Universal Test Machine (±100 kN), see Figure 82, however the compression strength of the specimens was found to be greater than the machine’s capacity, so the test specimens were subsequently transferred to the university’s Avery-Denison 250kN compression loading machine where they were subsequently loaded to failure at a load-rate of 1,000 kN/min.

Figure 82: DARTEC Universal Test Machine

4.3.3. *Results*

Table 11: Results summary for Specimens "A"

Specimens	Mass (kg)	Density[1] (kg/m^3)	Load rate (to 200kN) (kN/min)	Failure load (kN)
A-01	3.7	266.8	40	592
A-02	3.6	259.6	120	488
A-03	3.7	266.8	240	546

[1] Density calculated for entire test specimen, not for individual glass fibre or foam parts.

Table 11 summarises the results obtained from the glass-wrapped test specimens. It was noted during testing that all specimens initially failed in the bond between the tubes, followed by catastrophic failure of the external glass wrapping (see Figure 83).

Figure 83: Failure mode of Specimens "A"

The average density of the specimens was 264.4 kg/m^3 with an average compressive failure load of 542 kN. The broad variation in the failure load of the specimens can be attributed to variations in the manual manufacturing process (hand lay-up) used to produce the test specimens. The average failure load of 542 kN delivers a Factor of Safety[1] of 2.7 for this design solution.

Table 12 summarises the results obtained from the GRP test specimens. It was noted during testing that all specimens failed at the corners (see Figure 84). This was as a result of failure in the matrix caused by localised stress concentrations derived from compression induced (Euler) buckling.

[1] Actual load bearing capacity versus design load capacity.

Table 12: Results summary for Specimens “B”

Specimens	Mass (kg)	Density[1] (kg/m^3)	Load rate (to failure) (kN/min)	Failure load (kN)
	(kg)	-	(kN/min)	(kN)
B-01	0.530	1725.3	1000	165.0
B-02	0.531	1728.5	1000	164.8
B-03	0.530	1725.3	1000	157.1
B-04	0.542	1764.3	1000	161.6

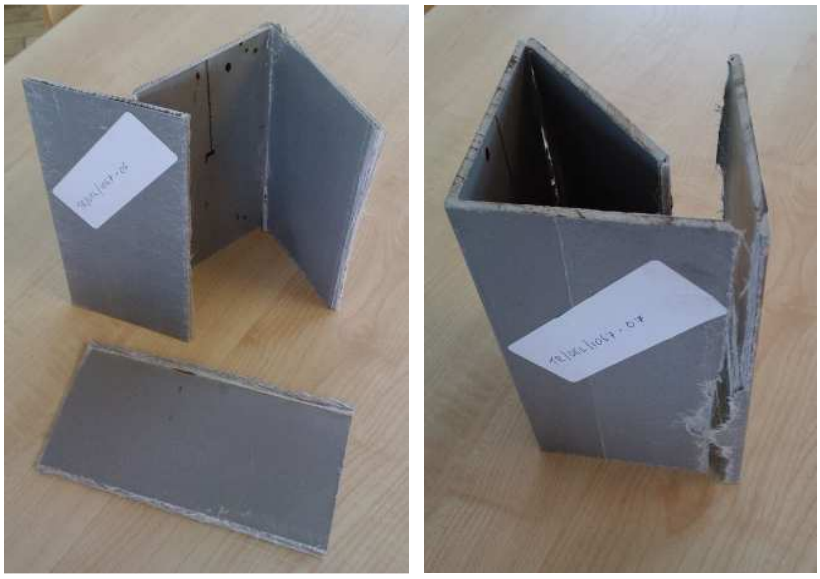

Figure 84: Failure mode of specimens B-03 & B-04 respectively

Figure 85 shows the load-displacement curve for specimens B-01 to B-04. The blue portion of the line represents the load-displacement curve generated by the DARTEC controller. The red portion of the line is the projected linear extrapolation of the graph to the failure load as determined by the Avery-Denison test machine.

[1] Density calculated for entire test specimen, not for individual glass fibre or foam parts.

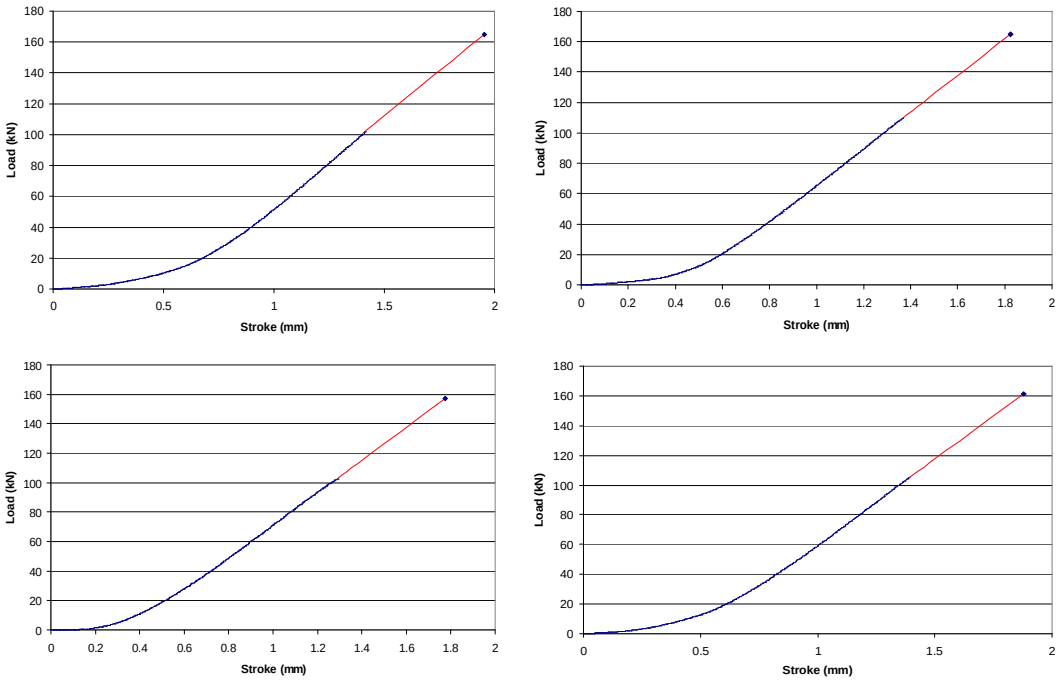

Figure 85: Load-displacement curve for Specimens B-01 to B-04

There is good consistency in the failure load for the "B" specimens which can be attributed to the automated process by which they are manufactured (extrusion). The average density of the specimens was 1735.8 kg/m^3 with an average compressive failure load of 162.1 kN. The average failure load of 162.1 kN gives a Factor of Safety of 3.2 for this design solution.

Using the data from the above results and the material date in Section 1.7.2, calibration models were prepared in ANSYS to calibrate the material parameters used by Grasso [120] in his simulations.

4.3.4. *Conclusions & Recommendations*

Specimens "A"

In all three test specimens the compressive failure load exceeded the design requirement. Based on the average failure load of 542 kN against the required design load of 200 kN, the glass-wrapped foam solution provides a design Factor of Safety of approximately 2.7.

All three specimens failed in the following manner:

- Longitudinally in the bond between the tubes,
- Complete catastrophic failure of the outer glass layer (crack propagated around the circumference of the specimen)

The variation in load rate did not affect the overall response of the specimens.

Specimens "B"

In all four test specimens the compressive failure load exceeded the design requirement. Based on the average failure load of 162.1 kN against the required design load of 50 kN, the extruded GRP solution provides a design safety factor of approximately 3.2.

Using these results Grasso [120] could generate representative finite element models and validate the simulation activity in LS-Dyna (Figure 86). To populate the material card, the data in Table 13 was used.

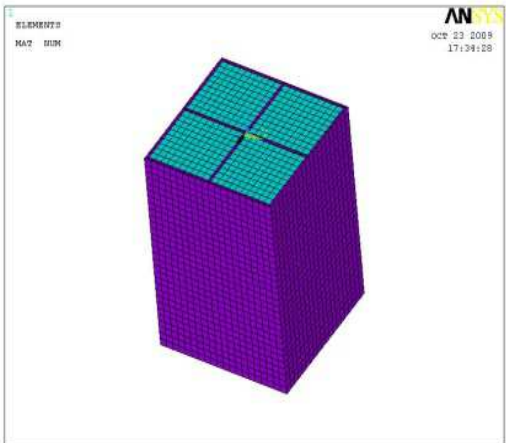

Figure 86: LS-dyna model created to validate the outputs of the finite element modelling [120]

Based on these results it has been shown that the design concept of using composite tubes to react the loads from the lower energy absorbers is successful. Each of the two types of tubes exceeded the desired design load criteria with safety factors in excess of 2.5.

Table 13: Material properties used in the LS-Dyna validation models.

Mechanical properties of M705 CSM with SR1500/SD2507 epoxy resin system	Value
E_x	16000 MPa
E_y	16000 MPa
E_z	17000MPa
ν_{xy}	0.132
ν_{yz}	0.132
ν_{xz}	0.33
G_{xy}	3500 MPa
G_{yz}	4000 MPa
G_{xz}	4000 MPa
PUR	**Value**
E	56 MPa
v	0.33

The complete finite element model of the cab was dynamically modelled in LS Dyna by Bombardier and statically modelled by Grasso [120], an extract of which is shown in Figure 87, who's analysis concluded that there was acceptable stress distribution throughout the reactor tubes for the LS-1 load case (see Figure 19).

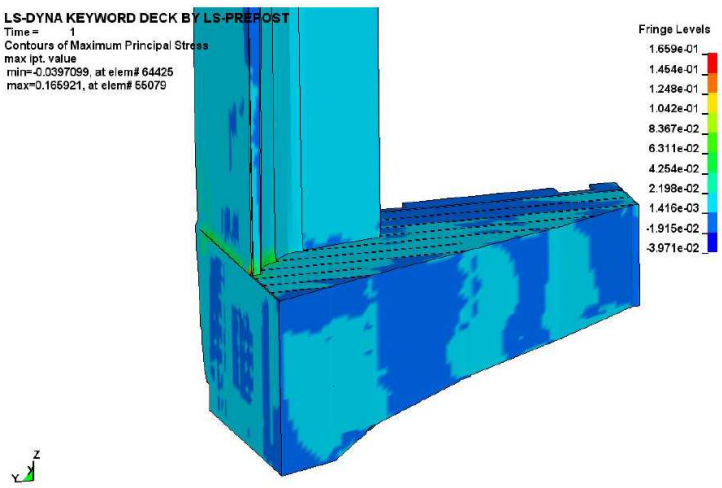

Figure 87: Reaction zone maximum principal stress map for EN12663 static loads [120]

The conclusions drawn from these models is that for the geometries and materials used the structure is compliant with rail vehicle static and dynamic loadings, demonstrating uniform stress distribution throughout the structure [120].

4.4. Novelty of Design: Patent Granted

The work undertaken and described in this chapter represents a unique and innovative approach to the application of composite materials in rail vehicle primary structures. The opportunity to file a patent to protect the design philosophy was investigated and consequently a patent [121] with Bombardier was filed to protect the concept of a "Light-weight compound cab structure for a rail vehicle". The patent was granted internationally with the number WO/2012/038383A1 and is available through the World Intellectual Property Organization (Figure 88).

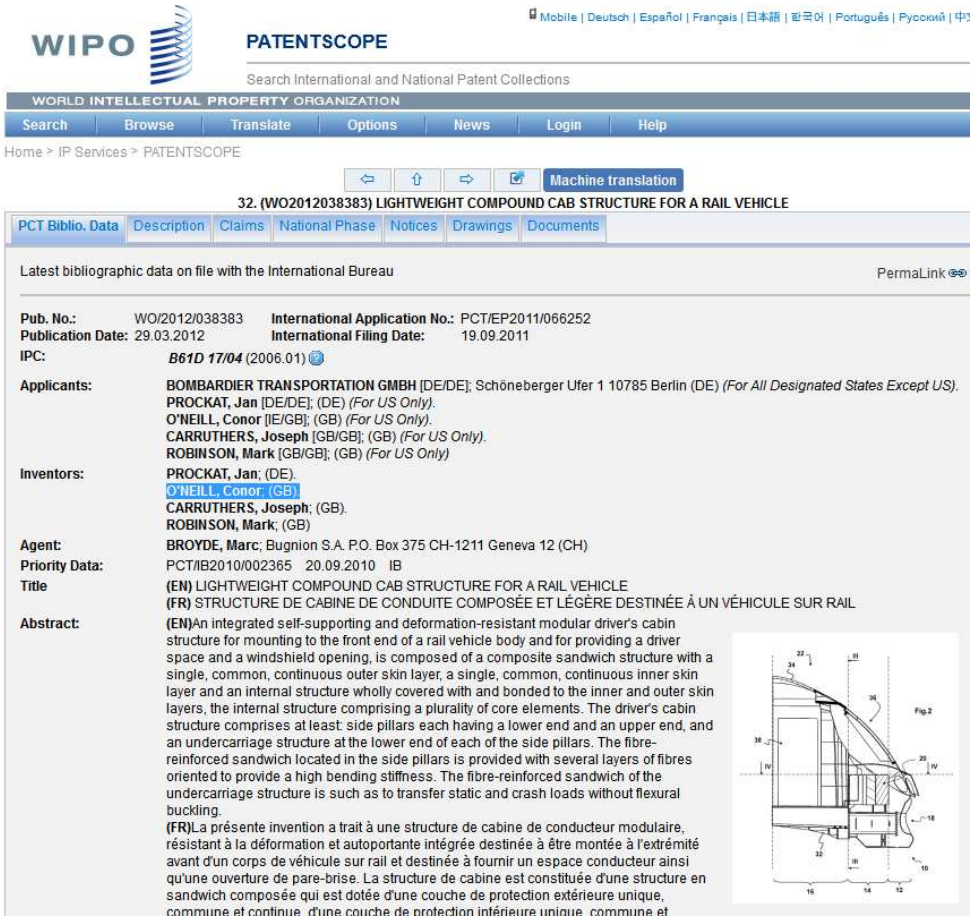

Figure 88: WIPO Patent Search showing this author's name highlighted as inventor (extracted Feb 2016) [122]

This patent application was driven by the industry wide desire by rail vehicle manufacturers to remove weight from rolling stock as discussed in Section 1.5.

Protecting the concept and the design philosophy behind the cab ensured that competitors such as Voith would not be able to adopt such an approach in future vehicles. Indeed, the Galea design produced by Voith [123] stops short of delivering a fully integrated cab, using aluminium honeycomb in a more piecemeal approach to protect the side pillars rather than delivering dedicated energy absorption across the front of the cab for the LDO crash scenario. The composite pillars derived for this design are replacements for existing structures and are not integrated with the side walls or subfloor construction (Figure 89 and Figure 90).

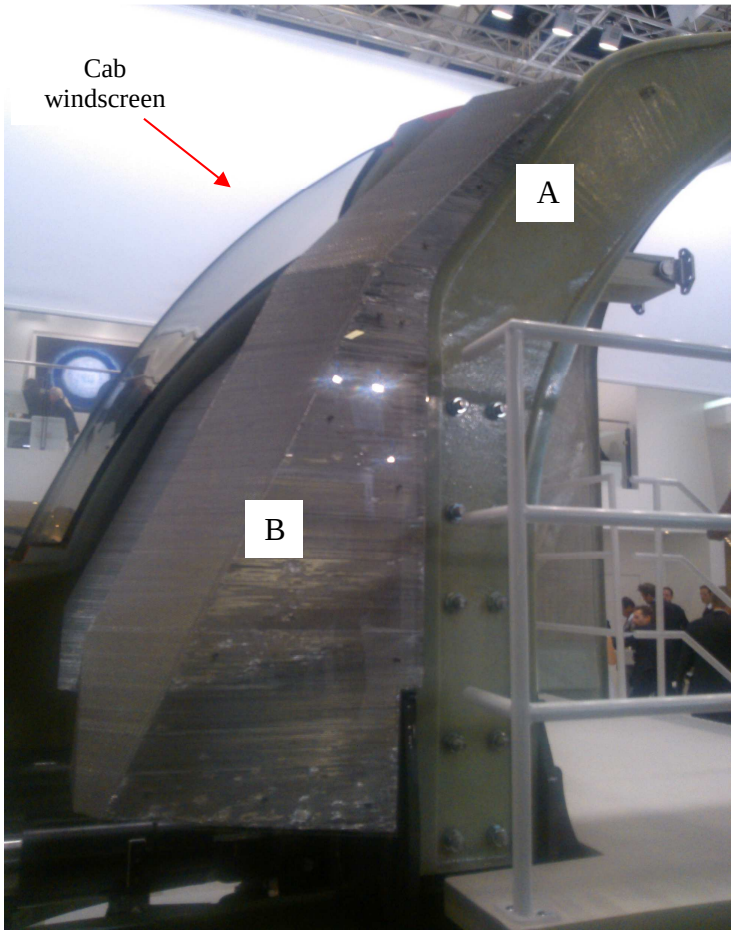

Figure 89: Voith's Galea cab concept showing composite pillars (A) and protecting aluminium honeycomb structure (B) (photo taken at Innotrans 2012, Berlin).

Figure 90: Close-up view of the Galea's roof structure, demonstrating the lack of full structural integration with the cab - the composite pillar (A) is connected to the cab shell (B) by means of a rudimentary composite spacer (C). (photo taken at Innotrans 2012, Berlin).

4.4.1. *Patent Abstract*

"An integrated self-supporting and deformation-resistant modular driver's cabin structure for mounting to the front end of a rail vehicle body and for providing a driver space and a windshield opening, is composed of a composite sandwich structure with a single, common, continuous outer skin layer, a single, common, continuous inner skin layer and an internal structure wholly covered with and bonded to the inner and outer skin layers, the internal structure comprising a plurality of core elements. The driver's cabin structure comprises at least: side pillars each having a lower end and an upper end, and an undercarriage structure at the lower end of each of the side pillars. The fibre-reinforced sandwich located in the side pillars is provided with several layers of fibres oriented to provide a high bending stiffness. The fibre-reinforced sandwich of the undercarriage structure is such as to transfer static and crash loads without flexural buckling."

4.4.2. *Patent Primary Claim:*

“An integrated self-supporting and deformation-resistant modular driver's cabin structure for mounting to the front end of a rail vehicle body, the driver's cabin structure having a front end and a longitudinal direction, the driver's cabin structure providing a driver space and a windshield opening, the driver's cabin structure consisting of a composite sandwich structure with a single, common, continuous outer skin layer, a single, common, continuous inner skin layer and an internal structure wholly covered with and bonded to the inner and outer skin layers, the internal structure comprising a plurality of core elements, the composite sandwich structure comprising a unitary matrix for bonding the internal structure, the inner skin layer and outer skin layer, parts of the outer skin layer being directly exposed to the outside, parts of the inner skin layer being directly used as inner wall for the driver's cabin, the driver's cabin structure comprising at least:

- side pillars each having a lower end and an upper end, comprising a fibre-reinforced sandwich, and
- a reactor structure located towards, and integrated with, the lower end of each of the side pillars, the reactor structure being reinforced such as to transfer static and crash loads to the main body structure of the rail vehicle and including a central cavity open towards the front end of the driver's cabin to accommodate a coupling element for the rail vehicle.”

4.4.3. *Patent Detail*

Referring to Figure 91 and Figure 92, a modular front end structure (10) for a rail vehicle, consists of three modules: a lower strength primary crush zone (12), a higher strength secondary crush zone (14), which is located behind the primary crush zone and contains the majority of the cab’s energy absorption capability, and a reaction zone (16) which is able to resist the collapse loads of the two frontal crush zones whilst protecting the driver and ensuring that any forces are properly transferred to the main part of the coach body.

The nose (12) is designed to be easily detached and re-attached to facilitate repair or replacement following minor collisions and contributes to the overall energy absorption

capability of the cab. Energy absorbing materials and structures are suitably deployed within the available design envelope of the nose.

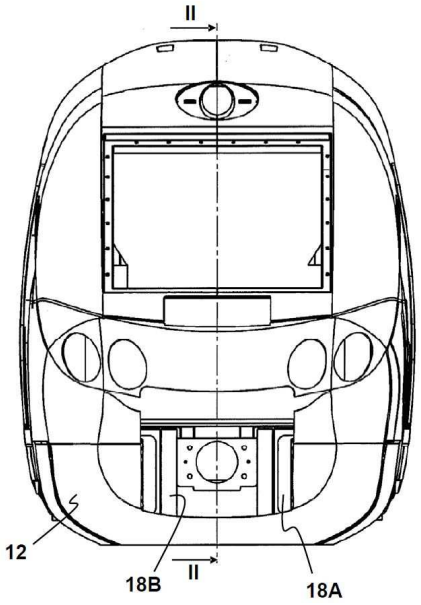

Figure 91: Annotated front view of cab [121]

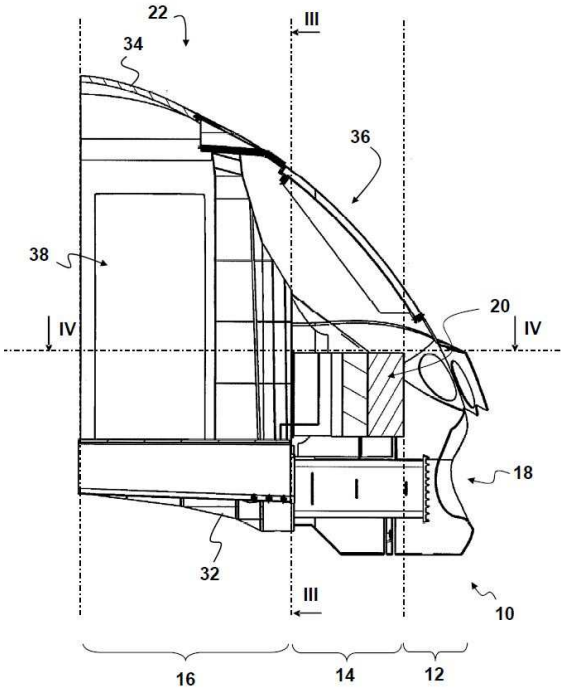

Figure 92: Annotated vertical cross-section of cab [121]

The secondary crush zone (14) includes lower, buffer-level energy absorbers (18) and upper energy absorber (20) – see Chapters 5 and 6 respectively.

The lower, buffer-level energy absorbers are two interchangeable discrete energy absorbers (18A) (18B) with an aluminium honeycomb sandwich construction which provides excellent performance levels in terms of constant and continuous absorbed energy during a crash.

The upper energy absorber (20) consists of a distributed energy absorbing zone, which runs across the width of the cab as illustrated in Figure 93. The main function of the upper energy absorber is to resist the collision with a deformable obstacle. As the deformable obstacle provides a distributed load input to the cab, the use of a distributed energy absorbing zone, i.e. a zone that extends continuously from side to side of the front-end, is preferable to the use of discrete energy absorbing elements. The upper energy absorber is be formed as a multi-layer aluminium honeycomb sandwich (see Section 5.1.1. In addition to providing an energy absorption capability, the crossbeam provides enhanced missile protection for the driver.

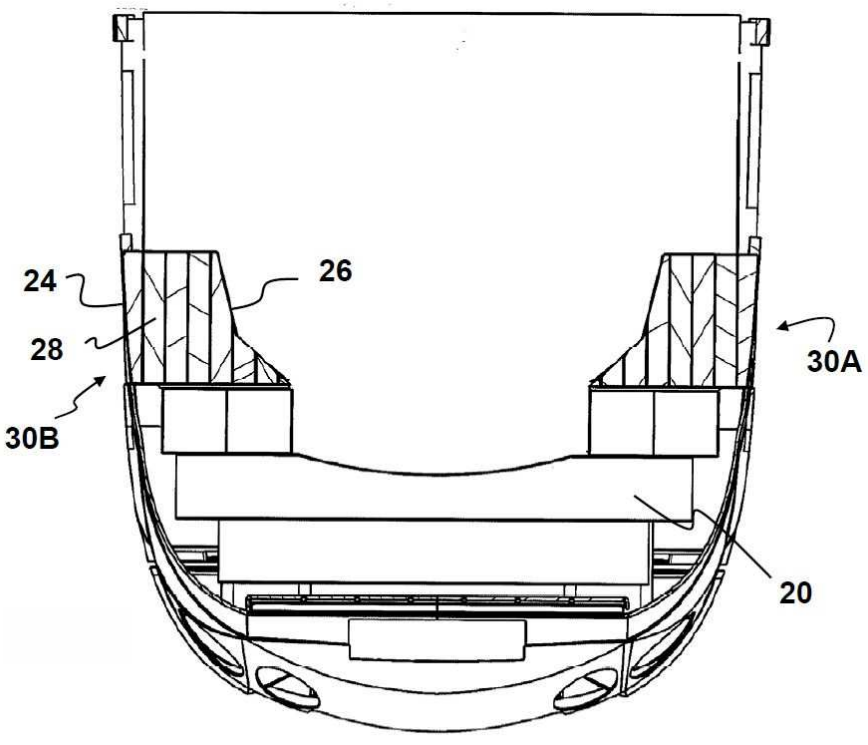

Figure 93: Annotated horizontal cross section of cab [121]

The driver's cabin structure comprises side pillars (30A, 30B) each having a lower end and an upper end, a reactor structure (32) at the lower end of each of the side pillars, and is integral with a roof structure (34).

The reaction zone (16) forms an integrated self-supporting and deformation-resistant driver's cabin structure (22). This structure, depicted in Figure 94, is composed of a sandwich composite structure produced from glass fibre reinforced polymer (GFRP) layers with a single, common, continuous outer skin layer (24), a single, common, continuous inner skin layer (26) and an internal structure produced from and polymer foam (16) wholly covered with and bonded to the inner and outer skin layers.

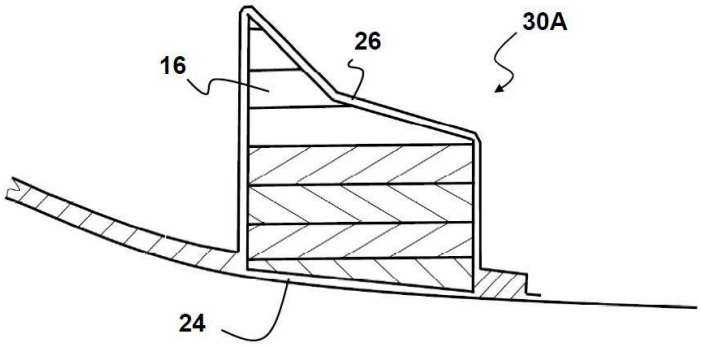

Figure 94: Annotated horizontal cross section of cab pillar [121]

The reactor structure (32) in the lower buffer regions (Figure 95) consists of an array of bonded square-section foam cores wrapped in glass fibre reinforced polymer (GFRP) to produce a macro-cellular structure to transfer loads without flexural buckling. The pillar regions (30A, 30B) above the reactor structure also consist of an assembly of GFRP and foam cores. Each vertical column of foam in the pillars is sandwiched between continuous vertical layers of GFRP to produce a multi-layer sandwich construction to provide a high bending stiffness to the side pillars.

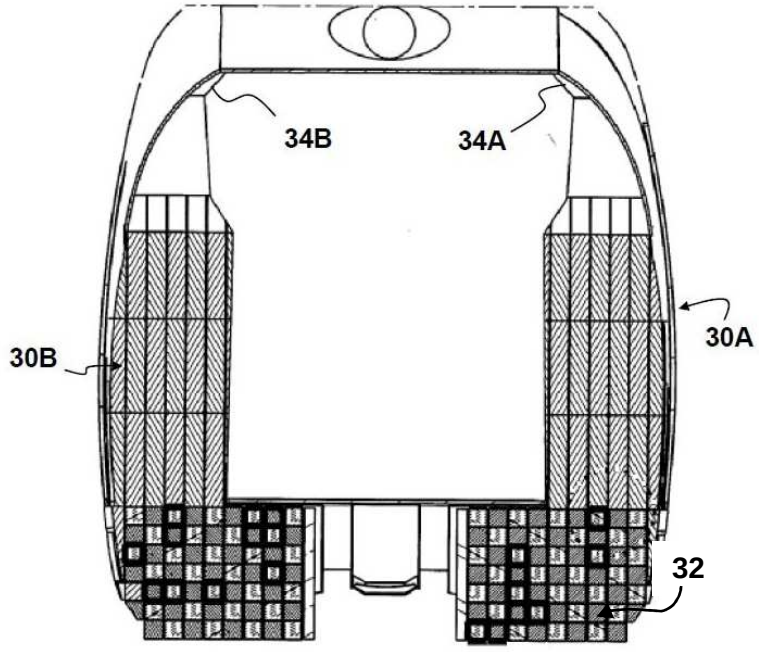

Figure 95: Annotated vertical cross section through cab pillars and reactors [121]

Chapter 5: Design of a lightweight space constrained upper energy absorber

5.1. Design for Crashworthiness

As well as meeting the crash criteria set out in Section 4.1 the upper energy absorber design must also provide the same energy absorption profile as set out in the Bombardier specification [124] and detailed in Figure 96. This will ensure that the absorber meets the same standard as existing cabs in order for it to be deemed a suitable replacement.

It can be seen from Figure 96 that a single absorber has a stroke of approximately 500 mm and a uniform crush plateau of 700 kN. This provides a useful energy absorption capacity of approximately 350 kJ (i.e. area under the graph). For the combined upper absorbers this gives a crush plateau of 1400 kN and an energy absorption capacity of 700 kJ.

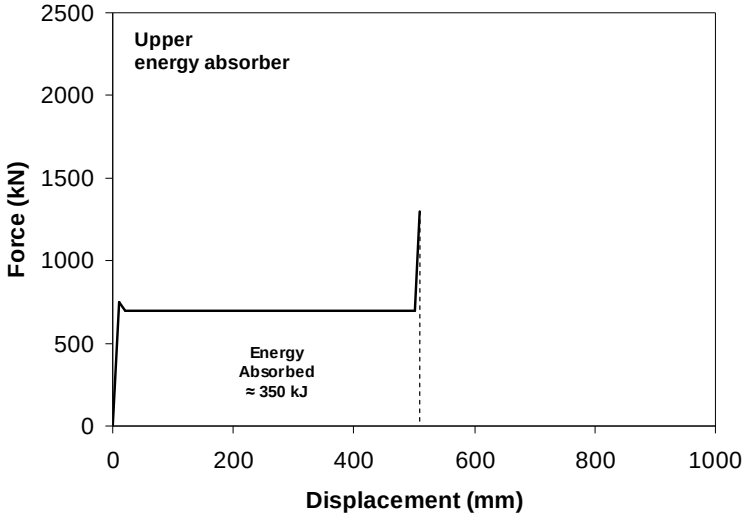

Figure 96: Force-displacement characteristic of a single upper energy absorber in the Bombardier cab design

In addition to the crash loading, the rail vehicle structural loads specified in EN 12663, "Structural requirements of railway vehicle bodies" [35] place a requirement on rail cabs to react longitudinal proof loads of 300 kN in this upper absorber area. This compressive force is distributed across the front of the cab at the same height as the upper energy absorbers and the new design must also satisfy this condition.

5.1.1. *Design Concept*

Based on these European standards and Bombardier requirements a new design concept was created for the upper energy absorbers in which an aluminium honeycomb beam, stabilized by aluminium plate, would be located across the front of the rail cab. It would be positioned at the same location as the existing upper absorbers and designed to fit into the existing cab shell without making changes to the cab's external aerodynamic surface. The beam will be mounted on the two pillars described in Section 4.2.3 which will transmit the loads rearwards into the main vehicle body.

To determine the general dimensions of the beam, the volume available within the design needs to be reconfigured for a rectangular shape. Figure 97 shows a horizontal cross section of the cab of the Bombardier SPACIUM vehicle at the location of the existing upper energy absorbers. The shape can be approximated by a semi-ellipse (red) with major axis of 3.408 m and minor axis of 0.955 m.

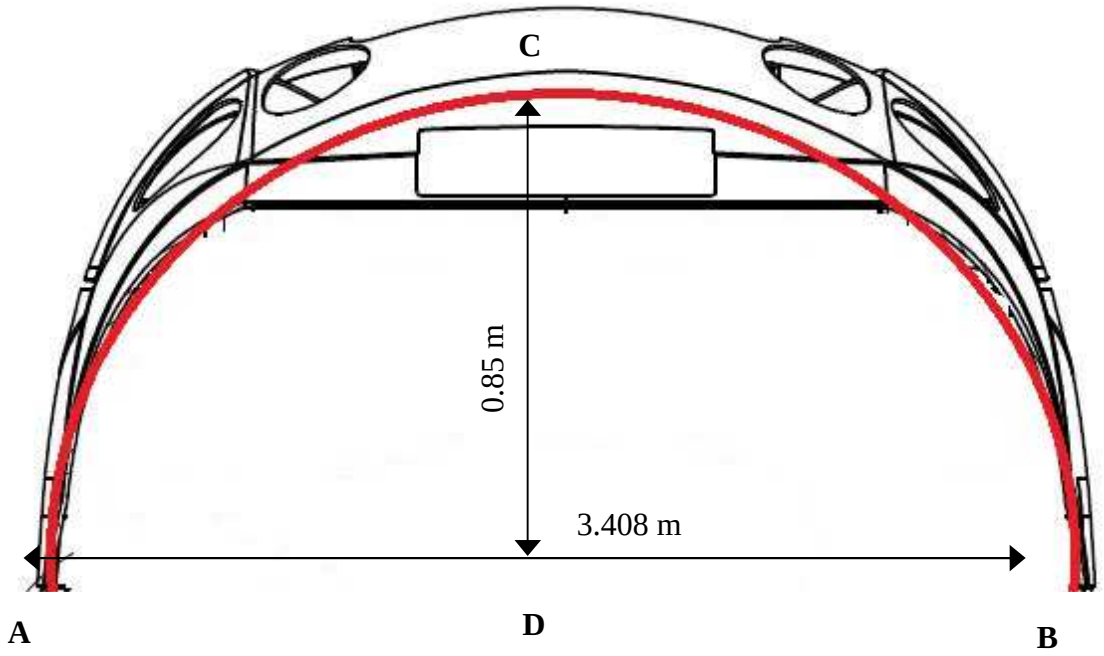

Figure 97: Front of the Bombardier Spacium cab and its semi-elliptical approximation.

The rectangular shape of the new energy absorber can be calculated using equation (35) to determine the length of the base and equation (37) to determine the height (see Section 3.4).

Using equation (35) the base length of the honeycomb beam is:

$$AB = (1.704)\left(\sqrt{2}\right) = 2.41\ m$$

Using equation (37) the height of the honeycomb beam is:

$$CD = \frac{0.85}{\sqrt{2}} = 0.6\ m$$

From these equations the length of the rectangular honeycomb beam was determined to be 2.410 m and the height to be 0.6 m. The maximum depth available was measured to be 0.675 m (i.e. the depth of the existing energy absorber). This is the first iteration and will be assessed as a single beam to identify if a suitable honeycomb can be used to comply with the energy absorbing requirements. If compliant, further iterations as describe in Section 3.4 will not be deemed necessary.

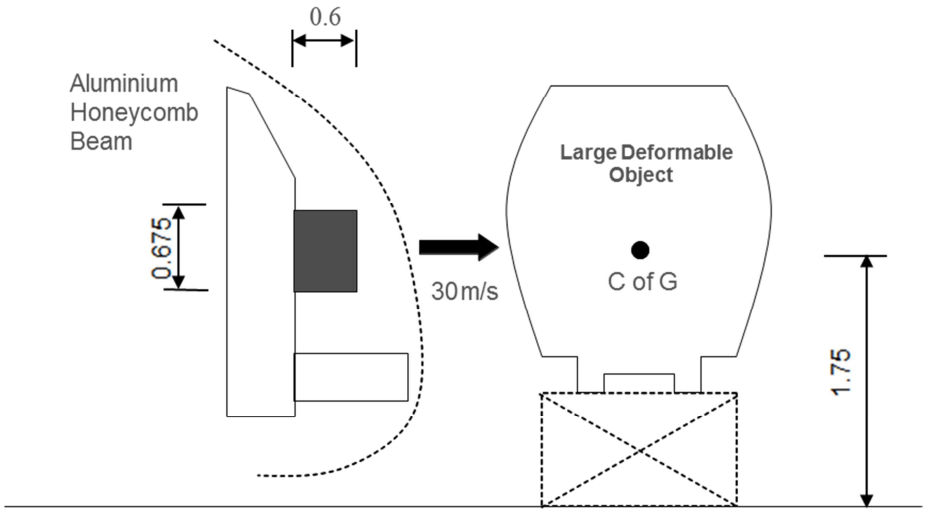

Figure 98: Location of the honeycomb beam absorber with respect to the Large Deformable Object crash scenario

Figure 98 depicts the positioning of the new honeycomb absorber with respect to the LDO crash scenario, and Figure 99 shows the conceptual design with the honeycomb cells axially aligned with the direction of travel.

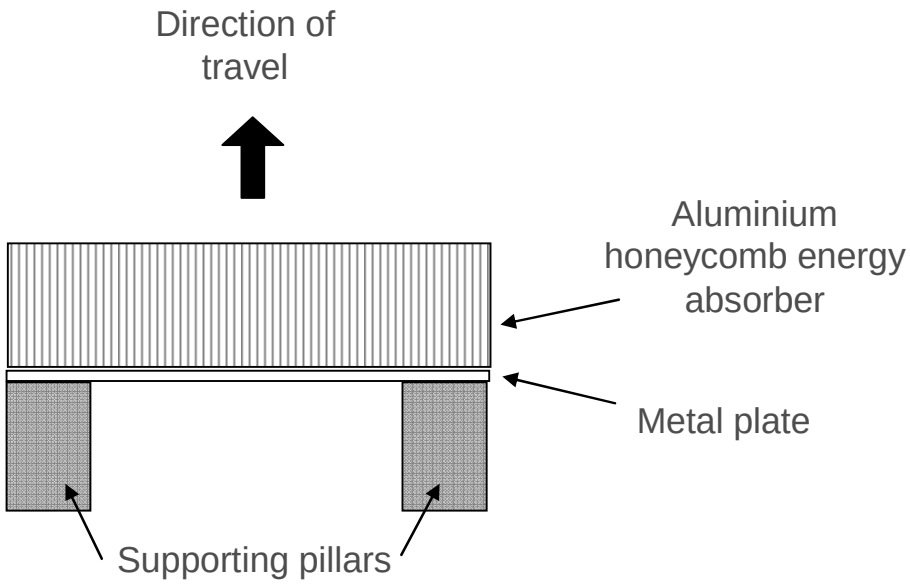

Figure 99: Conceptual design and assembly of honeycomb beam upper absorber

5.1.2. *Honeycomb Selection*

Due to the significant energy absorption requirements of the LDO crash scenario, it is this requirement that drives the honeycomb material selection of the upper energy absorber. The energy absorbed in the collision (E_{abs}) can be approximated as the product of the mean crush load ($P_{crush\text{-}mean}$) and crush distance (s_{crush}) as given in (44).

$$E_{abs} \approx (P_{crush-mean})(s_{crush}) \tag{44}$$

$$\rightarrow E_{abs} = (\sigma_{crush})(A_{upp})(L_{upp})(80\%) \tag{45}$$

where σ_{crush} is the crushing stress, A_{upp} is the area of the upper absorber, L_{upp} is the length of the upper absorber (measured fore to aft) and 80% represents the assumed useful stroke of the absorber.

Rearranging (45) gives:

$$\sigma_{crush} = \frac{E_{abs}}{(A_{upp})(L_{upp})(80\%)} \tag{46}$$

Section 5.1 defines the energy absorption requirement as 700 kJ. Substituting this value and the dimensions in Section 5.1.1 into (46) gives:

$$\sigma_{crush} = 0.896MPa$$

The material chosen to meet this requirement was determined from the selection tables provided by Hexcel for their 5052 Aluminium Alloy Hexagonal Honeycomb [113]. From the Hexcel table in [113] (reproduced here in part as Table 14), the most suitable honeycomb density with a crush strength of 0.896 MPa is CR III 1/8-5052-.0007.

Table 14: Properties for 5052 Aluminium Alloy Hexagonal Honeycomb [113]

CR III 5052 Alloy Aluminium Honeycomb	Density (kg/m^3)	Compressive			Crush Strength (MPa)
		Bare	Stabilised		
		Strength (MPa)	Strength (MPa)	Modulus (MPa)	
1/8-5052-.0007	28.8	1.97	2.07	517.11	**0.896**
1/8-5052-.001	48.1	3.79	3.93	1034.21	1.793
1/8-5052-.0015	64.1	6.76	7.03	1654.74	3.103
1/8-5052-.002	80.1	10.34	10.76	2413.17	5.171
1/8-5052-.0025	96.1	14.48	15.51	3447.38	7.239
1/8-5052-.003	128.1	18.62	19.99	6205.28	9.308

The stress experienced by the absorber under static loading conditions (σ_{stat}) for the absorber can be determined from the proof load (P_{proof}) and the load area (A_{load}) which is assumed to be of 0.1 m height across the front of the absorber.

$$\sigma_{stat} = \frac{P_{proof}}{A_{load}} \tag{47}$$

Using (47) and a value of 300 kN for the proof load from Section 5.1 gives:

$$\sigma_{stat} = 1.24MPa$$

From the Hexcel data sheet [113] it was determined that the compressive strength of CR III 1/8-5052-.0007 honeycomb is 2.07 MPa. This means that the CR III 1/8-5052-.0007 material satisfies both the crash and proof load requirements. However, the compressive strength of the material is significantly higher than required so a less dense material may also fit this requirement. An alternative aluminium honeycomb of CR III 3/8-5050-.002 presented in the Hexcel data sheet [113] has a compressive strength of 1.38 MPa but its crush strength may not be sufficient given the geometry of the conceptual design. Both materials will be investigated to determine their suitability.

5.2. Design Optimisation

The two material options selected in Section 5.1.2 provide the material properties which can be used by finite element analysis software to develop the conceptual design into detailed geometry. Aluminium honeycomb is an orthotropic material and provides the maximum energy absorption when the cells are axially aligned with the load. To determine the feasibility of the beam design it was necessary to understand the load paths through the beam and its supporting structure. Excessive lateral or vertical loads may lead to cell buckling, weakening the structure and reducing its energy absorption properties.

5.2.1. *Load Path Analysis*

The first aspect of the conceptual design investigated was to determine the reaction of a stabilized honeycomb beam under uniform loading supported at two locations by pillars. The beam was modelled using a 10 mm aluminium series 6106-T6 backplate to transmit the loads into the pillars. A static finite element model was created in ANSYS Workbench using the material properties in Table 15.

Table 15: Material properties of aluminium plate and honeycomb used in finite element model

		Aluminium 6106-T6	CR III 1/8-5052-.0007 Aluminium honeycomb
Density (kg/m^3)		2770	49.6
Young's Modulus (MPa)	*z-dir (axial)*	71000	517
	x-dir (lateral)		5.17
	y-dir (vertical)		5.17
Poisson's Ratio		0.33	0.05
Shear Modulus (MPa)	*XZ*	26000	310.3
	YZ		151.7
	XY		2.3
Compressive Yield Strength (MPa)		230	0.9
Relative volume at full compaction			0.2

The backplate was given fixed supports in two locations and the front of the beam was subjected to a 1 mm displacement load (Figure 100).

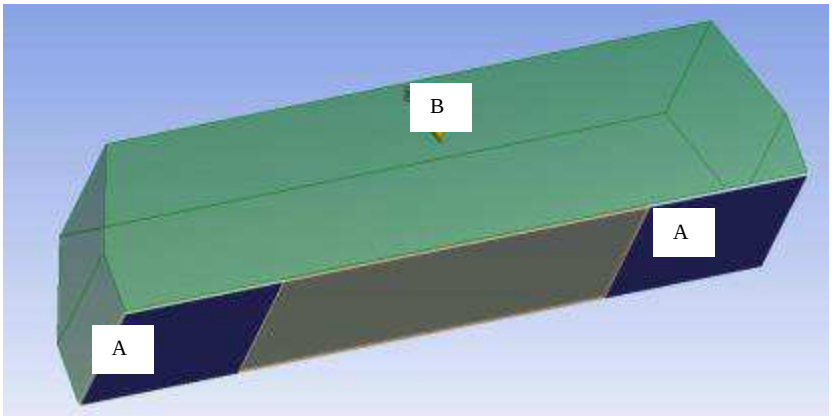

Figure 100: Upper absorber beam in ANSYS showing location of supports (A) and displacement load (B)

The total deformation of the beam was analysed and the proportional displacement vector results are shown in Figure 101. From this figure it is clear that the portion of the honeycomb beam between the supports does not deform as seen by the low magnitude vectors, indicating that the honeycomb will not crush in this region.

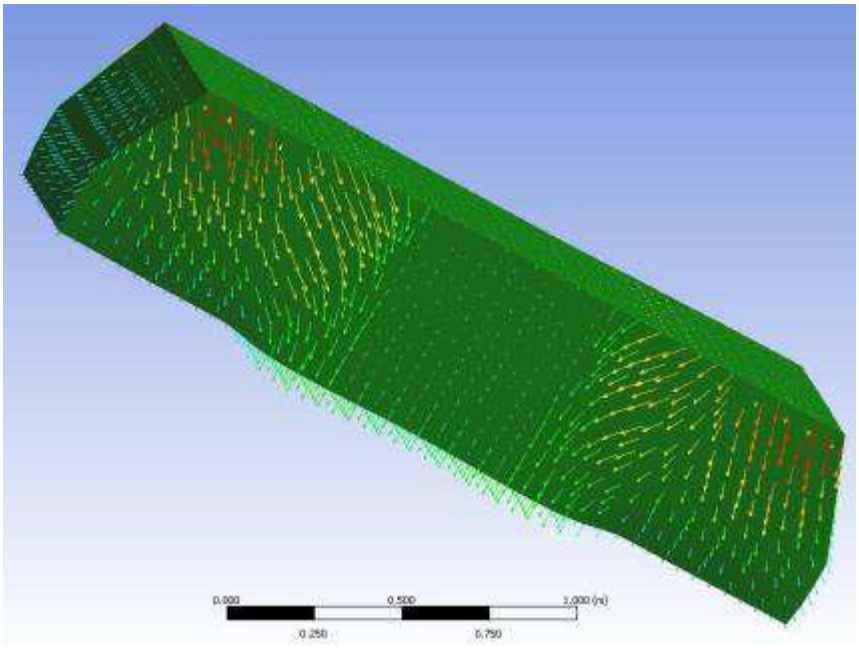

Figure 101: Upper absorber beam with flat backplate showing proportional vectors of total deformation under load

This analysis was confirmed by testing a small sample of stabilized honeycomb under conditions commensurate with the finite element model.

5.2.2. *Test Set-up*

The stabilised honeycomb sandwich specimen was manufactured by Alcore Brigantine to the dimensions in Table 16.

Table 16: Dimensional properties of stabilized honeycomb specimen.

Property	Value (mm)
Length	100
Width	50
Depth	15
Skin thickness	1
Cell wall thickness	0.05

The stabilised honeycomb specimen was mounted on two steel blocks (25 x 25 x100 mm) to represent the non-continuous support of the mounting pillars within the cab design, see Figure 103. The test was carried out on Newcastle University's DARTEC Universal Test Machine (Figure 102).

Figure 102*: DARTEC Universal Test Machine at Newcastle University*

Load was introduced by means of a steel faceplate mounted on the upper load head of the test machine at a rate of 0.5 kN/s until the honeycomb between the mounting blocks and the load head reached a fully compressed state. Displacement and load were measured via the DARTEC's ZWICK controller and associated Workshop 96 software.

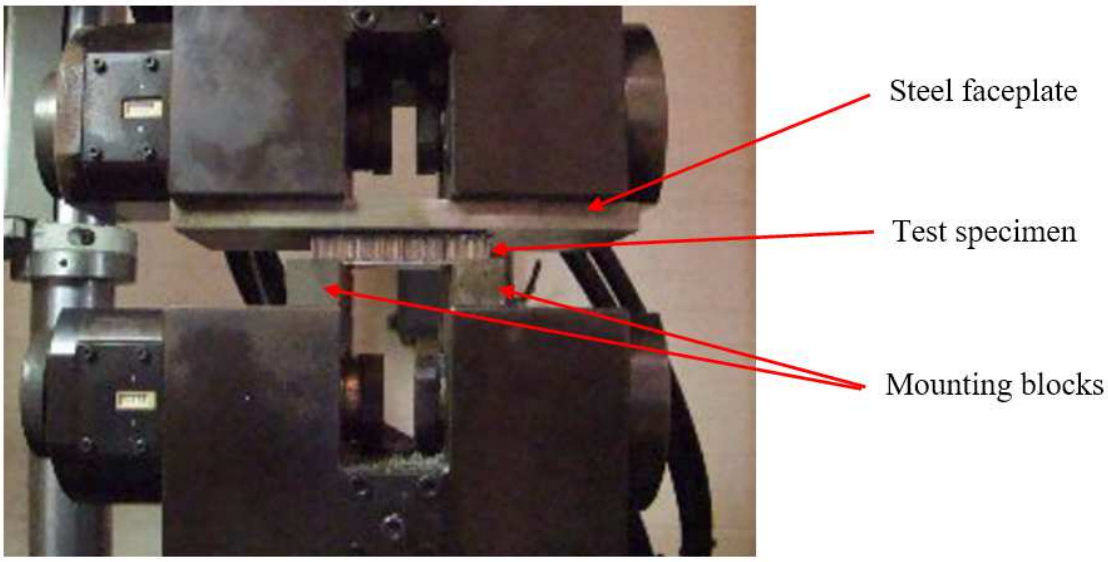

Figure 103: Test set-up for stabilised honeycomb panel.

5.2.3. *Results*

Due to material availability only one specimen was tested and this author recommends more comprehensive test programme to better understand the mechanics of failure in such structures under simply-supported loads. As such, a full statistical analysis is not available, however the indicative nature of the test allows some conclusions to be drawn:

During the test the honeycomb above the mounting blocks crushed while the material between the mounting blocks pushed downwards into the unsupported area. As the crush continued, this movement deformed the lower skin of the sandwich, causing it to be pulled laterally across the mounting blocks. This led to lateral deformation of the honeycomb cells which weakened the structure.

The load-displacement curve for the test specimen is shown in Figure 104. The curve is typical of honeycomb materials, however the lack of crushing in the specimen between the support blocks infers that the total energy absorbed could be considerably higher for the specimen.

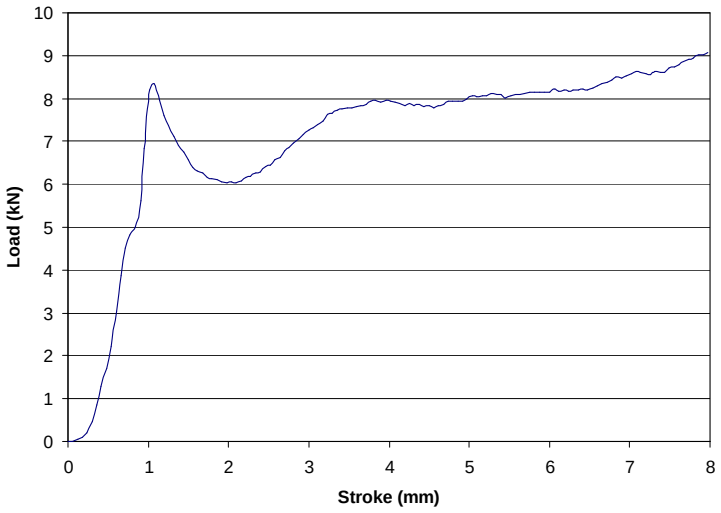

Figure 104: Load-displacement curve for stabilised honeycomb panel.

The test demonstrated that the unsupported portion of the panel, i.e. the region between the mounting blocks, did not exhibit any crushing in the honeycomb (Figure 105a) leading to an arched protrusion. Those regions of the panel which did crush were significantly weakened by the lateral deformation caused by the movement of the sandwich skin (Figure 105b). This

movement caused the walls of the honeycomb cells to buckle rather than fold progressively (the failure mode which absorbs the most energy).

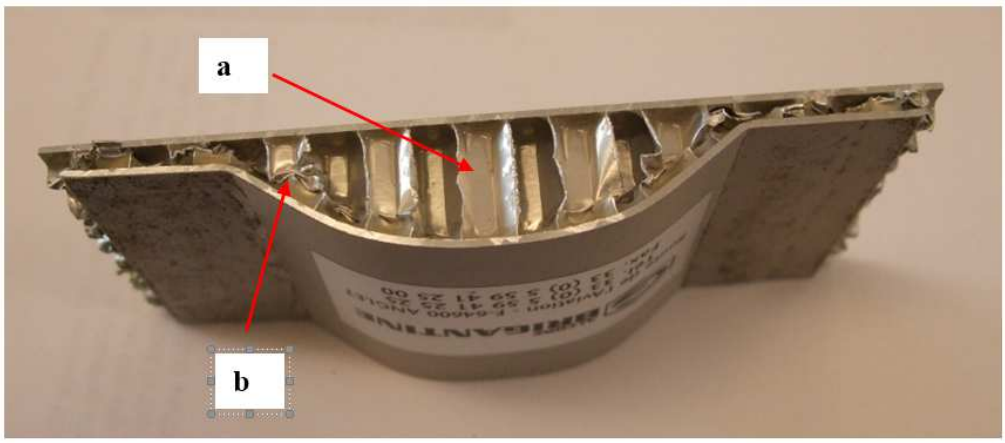

Figure 105: Sandwich panel after testing exhibiting: (a) lack of honeycomb crushing in unsupported region and, (b) lateral deformation of cells due to skin movement.

5.2.4. *Refining the model*

It is concluded from this test that a stabilized honeycomb panel will not react impact loads in the desired manner if it is not sufficiently reinforced with a suitable backing plate, i.e. it will form a hemispherical protrusion which could intrude on the driver's survival space.

The recommendation from this test is to support the central honeycomb beam using a curved steel backplate which will introduce load paths from the centre of the beam out to the pillars. This will ensure that the honeycomb begins crushing in a predictable manner across the entire front face of the beam delivering improved energy absorption. Figure 106 below shows the recommended conceptual design for the upper energy absorber using aluminium honeycomb.

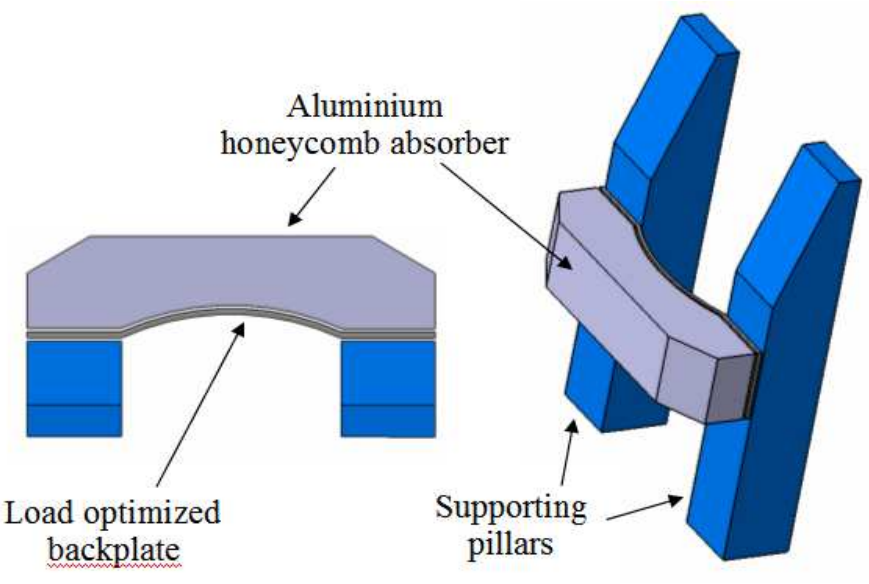

Figure 106*: Optimized upper energy absorber design.*

The CAD model was modified with a curved backplate being introduced to resist the through penetration of the beam between the pillars. As before, a finite element model was created in ANSYS using a mesh size of 50 mm for the aluminium honeycomb and 20 mm for the curved mild steel backplate (Figure 107). Table 17 shows the material properties used in the static structural analysis.

Table 17: Material properties of mild steel and honeycomb used in finite element model

		Mild Steel	**CR III 1/8-5052-.0007 Aluminium honeycomb**
Density (kg/m^3)		7850	49.6
Young's Modulus (MPa)	*z-dir (axial)*	206000	517
	x-dir (lateral)		5.17
	y-dir (vertical)		5.17
Poisson's Ratio		0.27	0.05
Shear Modulus (MPa)	*XZ*	80000	310.3
	YZ		151.7
	XY		2.3
Compressive Yield Strength (MPa)		248	0.9
Relative volume at full compaction			0.2

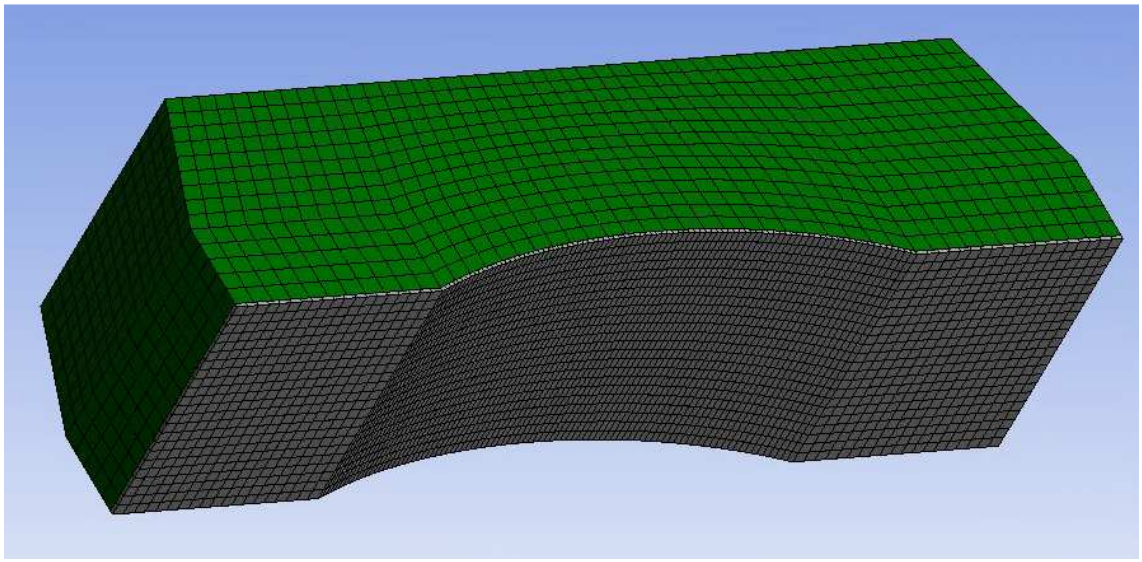

Figure 107: Meshed model of refined upper energy absorber

The same 1 mm displacement was applied to derive vectors to indicate the magnitude of the displacement across the beam (“B” in Figure 108) and two supports (“A” in Figure 108) were located to represent the interface with the pillars.

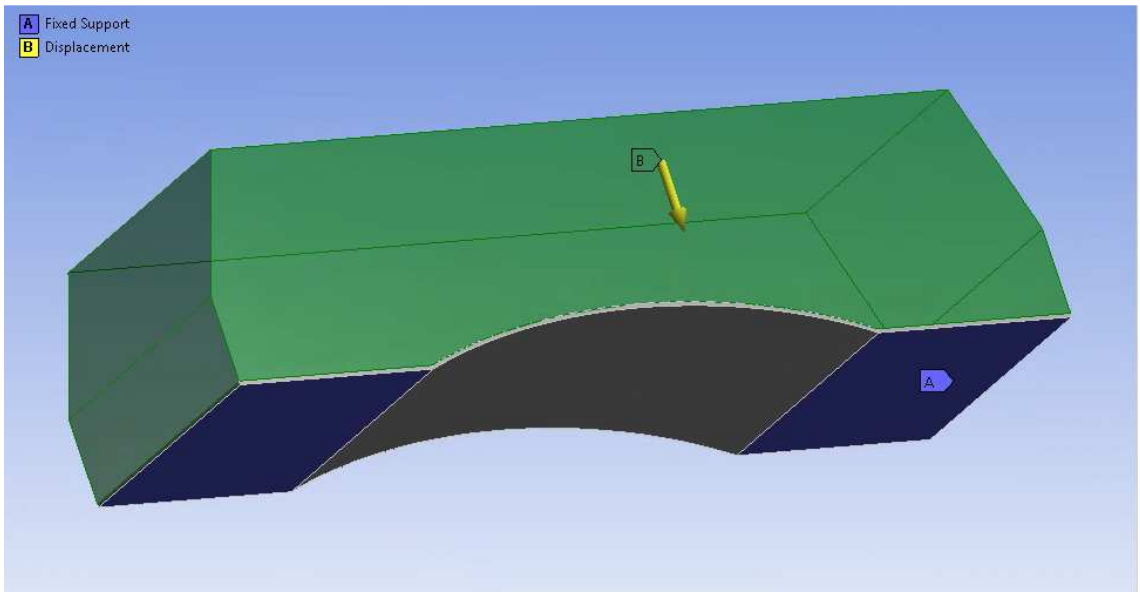

Figure 108: FE model loads and supports for the refined beam

Figure 109 shows the resulting displacement vectors for the refined beam. This figure shows significantly more deformation in the honeycomb across the entire width of the material,

indicating that the curved backplate is resisting the loads and causing the honeycomb to uniformly deform. Higher magnitude vectors between the supports indicate substantial deformation in this region. This improved deformation of the material will ensure that the entire honeycomb in the beam will crush and absorb energy during impact.

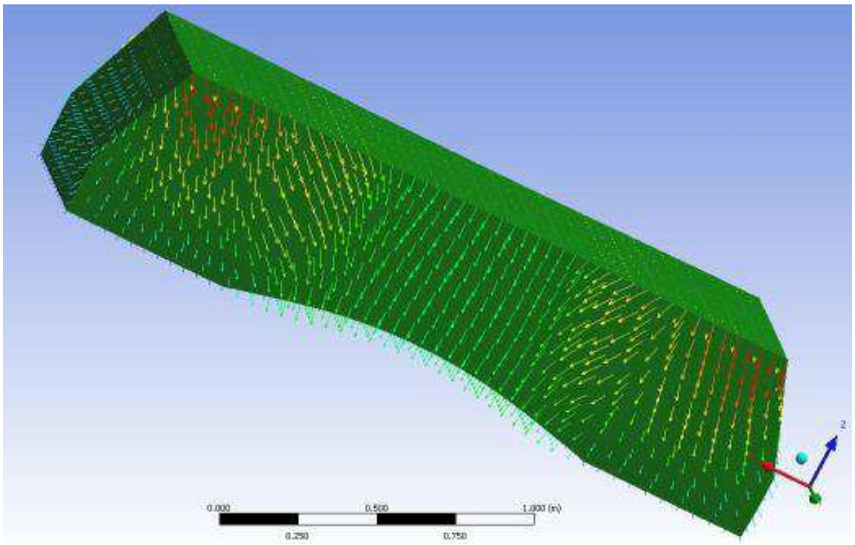

Figure 109: Upper absorber beam with curved backplate showing proportional vectors of total deformation under load

5.2.5. *Energy Absorption*

Using the design developed in Section 5.2.1 the finite element model underwent dynamic analysis by Grasso [120] using an anisotropic model implemented in LS-DYNA using MAT_HONEYCOMB (MAT-26) and the material properties described in Table 17. Two densities of aluminium honeycomb were modelled to determine which was the most suitable and lightweight material that satisfied the crashworthiness requirements; CR III 1/8-5052-.0007 (49.6 kg/m^3) and CR III 3/8-5050-.002 (48.1 kg/m^3)

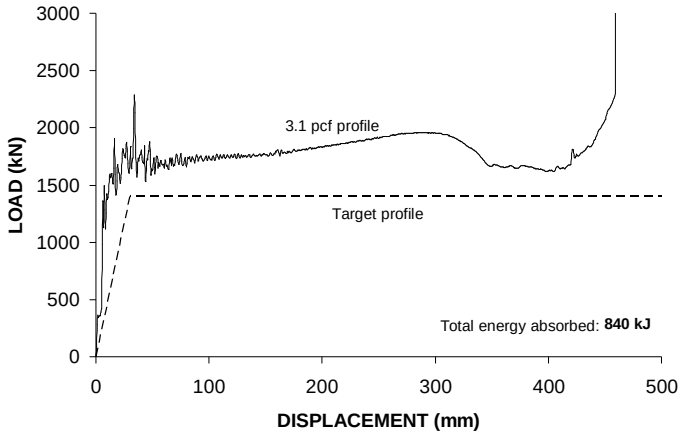

Figure 110: Load displacement curve and target profile for CR III 1/8-5052-.0007 aluminium honeycomb

Figure 110 & Figure 111 show the load displacement curves for the CR III 1/8-5052-.0007 (labelled as "3.1 pcf profile") and CR III 3/8-5050-.002 (labelled as "3.0 pcf profile") honeycomb respectively. Whilst CR III 1/8-5052-.0007 meets the target energy absorption of 700 kJ the profile of the load-displacement curve exceeds the target profile. The CR III 3/8-5050-.002 honeycomb offers the opportunity to further reduce weight and as can be seen in Figure 111 the energy absorbed was 801 kJ *and* the target profile is now achieved. This makes the CR III 3/8-5050-.002 aluminium honeycomb the material of choice for the energy absorber.

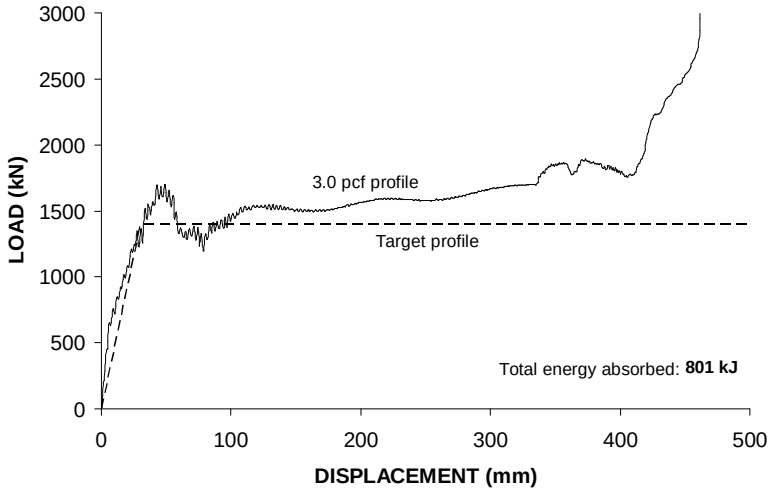

Figure 111: Load displacement curve and target profile for CR III 3/8-5050-.002 aluminium honeycomb

5.3. Conclusions

From the design calculations (Section 5.1.2) the CR III 1/8-5052-.0007 aluminium honeycomb material was chosen as the ideal honeycomb density to meet both the 700 kJ energy absorption and 1400 kN crush plateau targets. However, having optimized the design by identifying the load paths through the upper absorber it can be seen in Figure 110 that the CR III 1/8-5052-.0007 material is providing excess energy absorption. The total energy absorbed is 140 kJ higher than necessary and the crush plateau is approximately 300 kN higher than the target profile.

The load-displacement profile of the CR III 3/8-5050-.002 honeycomb as shown in Figure 111 is a much better match to the target profile. The total energy absorbed is just 101 kJ above the requirement and the crush plateau is only 150 kN higher than the target. This material also meets the 300 kN proof load requirement of EN 12663 (see LS-5 in Figure 19).

Materials of a lower density as detailed in the 5052 Alloy tables in [113] such as the CR III 5/32-5052-.0007 or CR III 1/4-5052-.001 material do not meet the proof load requirements so further optimization is not possible within this material listing.

Based on these findings the CR III 3/8-5050-.002 aluminium honeycomb mounted on a mild steel curved backplate and axially aligned with the direction of travel will provide sufficient energy absorption capacity to react the large deformable object crashworthiness scenario. In addition it will possess sufficient strength to react the proof loads required in this area of the driver's cab.

As a single beam design solution is compliant against the European standards, further iterations (as described in Chapter 3) to maximise the design space are not strictly necessary and would require additional refinement of the material selections based on densities and crush strength which would incur additional costs to the manufacturer without contributing to the achievement of compliance.

The estimated mass of the D-CAB upper energy absorber solution is found to be 128 kg, which is a saving in excess of 60% when compared to the existing SPACIUM upper absorbers.

Chapter 6: Design of lightweight space constrained lower energy absorbers

6.1. Introduction

The design of a pair of buffer or lower-level energy absorbers to meet the crashworthiness requirements described in Section 4.1 can be challenging, especially if the goal of the redesign is to reduce the overall mass of the rail vehicle. Indeed, one of the more difficult crash scenarios defined in EN 15227 [28] is the 40mm offset case for a collision with an identical unit. This requirement is driven by the need to minimise the likelihood of over-riding occurring during impact, i.e. when one of the vehicles is forced over the top of the other.

The Bombardier SPACIUM driver's cab was again used as the basis for the design, and for the lower energy absorbers the intention was to maintain the overall geometry, position and performance of the existing devices.

6.2. Crashworthiness Requirements

Bombardier's required lower level energy absorber performance is defined in Figure 112. Each device should have a crush force of 1,200 kN and a crush stroke of 900 mm. This should provide a useful energy absorption capacity of approximately 1,100 kJ.

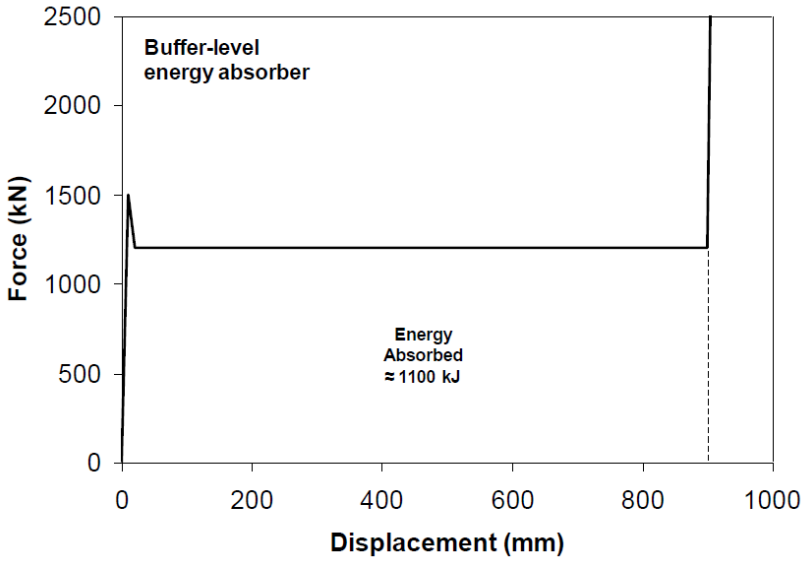

Figure 112: Force-displacement characteristic of a single lower energy absorber in the Bombardier cab design [119]

6.3. Design Considerations

In order to produce a lightweight absorber that meets the crashworthiness requirements aluminium honeycomb was again chosen as the energy absorbing element. The predictable crushing behaviour of the material means that the total energy absorbed by the design can be quickly established (see Section 2.2.3.1).

Unlike the upper energy absorber where a beam of honeycomb was designed to stretch across the front of the vehicle, the volume of space available for the lower absorbers is heavily restricted. This is primarily due to the presence of the coupler which cannot be designed out. As such, the new design must fit within a volume of space no greater than that which is occupied by the original absorbers and must be located in the same position to meet load path requirements. This provided the absorber design envelope which could not be penetrated by the new design.

6.3.1. *Prior Art*

The existing energy absorber design consists of a steel case mounted on supports with bespoke anti-climbers located at the front (Figure 113). The mode of energy absorption for this type of design is through folding of the steel case as the load is applied. The amount of energy absorbed is related to the type and thickness of steel used, the trigger mechanism employed, and the folding mechanism of the casing (axisymmetric or non-axisymmetric) [63].

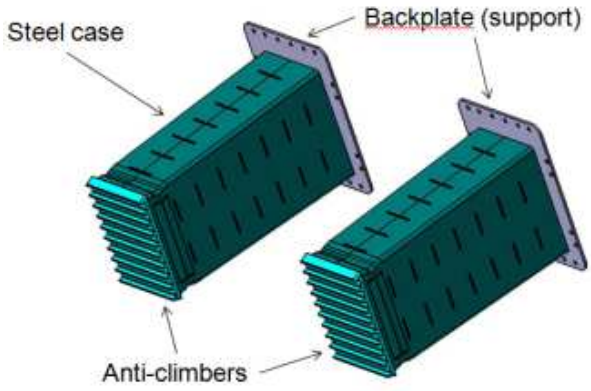

Figure 113: Typical energy absorber design [119]

Crushing is triggered to begin just aft of the anti-climber, progressing rearward until fully collapsed. To ensure the absorbers remain aligned with their counterpart during offset impacts, the internal structure consists of guide pins and guide plates. The pins penetrate through holes in the guide plates, thus keeping the anti-climber in a vertical position throughout the impact.

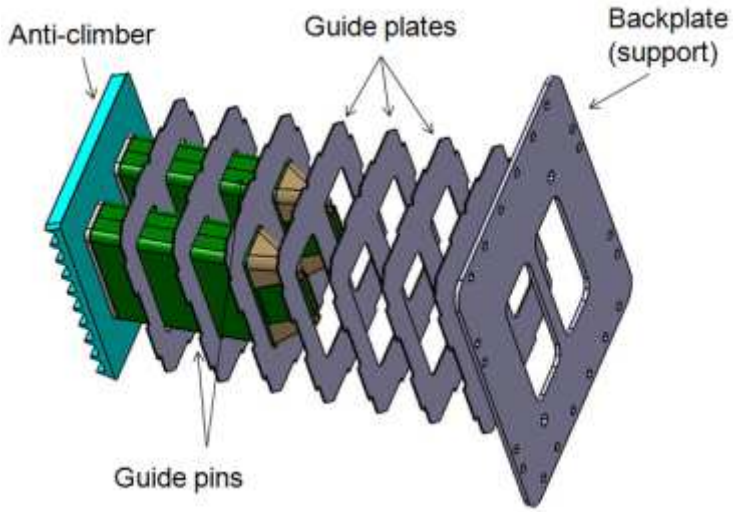

Figure 114: Internal structure of original absorbers [119]

Whilst this design succeeds in meeting the energy absorption requirements for the vehicle there are three key aspects of this design solution which should be noted:

1. **Mass** – These devices are designed primarily to absorb energy and therefore mass has not been a principle design driver. As a result, the materials used and the internal design make it a particularly heavy design solution.
2. **Through penetration** – The guide pin/plate mechanism keeps the anti-climber aligned during impact but as a result the pins penetrate through the support plate and into the space aft of the bulkhead. Whilst this is not a safety concern, it impacts the design of the structure behind the absorber, leading to a heavier design solution in this region to compensate for this phenomenon.
3. **Unused volume** – The method by which energy is absorbed is by means of folding of the steel outer shell of the absorber. The internal structure (pins and guide plates) do

not themselves absorb energy but merely guide the folding process. As such there is a significant volume **within** the design which is not being used to absorb energy.

In the following sections each of these key aspects will be addressed to produce an absorber design that is both lightweight and meets crashworthiness standards.

6.3.2. *The Issue of Mass*

The first step in reducing the mass of the energy absorber design is to investigate the materials currently employed and the method by which these materials are deployed within the design to absorb energy. Steel has traditionally been used due to its known properties, its relatively low cost and its ability to absorb energy through folding. Modifying the thickness of the steel and optimising the trigger mechanism means that this material can be employed to absorb varying amounts of energy as required. However, due to its relatively high density, steel does not represent a lightweight solution to energy absorption requirements.

Aluminium produces a lighter solution from a material perspective, however operationally it lacks the ductility of steel to absorb sufficient energy should a straight swap of materials be implemented. As such, the design needs to be readdressed if aluminium is to be utilised.

Rather than attempting to mimic the large-scale folding mechanism of the prior-art, aluminium can be used in the form of thin-walled tubes of smaller diameter, thereby facilitating energy absorption through folding on a much smaller scale. Individually these tubes absorb a small proportion of energy, but when numerous tubes are combined to function in unison (such as in aluminium honeycomb), large amounts of energy can be absorbed without significantly increasing the mass of the absorber.

6.3.3. *Preventing Through-penetration*

As discussed in Section 6.3.1 the function of the guide pins is to ensure that the anti-climber remains in a vertical position throughout the crush sequence. When the absorber is fully crushed these pins protrude through the bulkhead on which the absorber is attached. On rail vehicles where space is available behind the bulkhead this is not significant issue (although it does require local reinforcement due to stress concentrations around the introduced holes in the bulkhead). However, in space-constrained designs (such as trams), penetration through the bulkhead is undesirable. Therefore a solution is required where the anti-climbers remain in a vertical position by means of a mechanism other than guide pins (Section 6.4 describes in more detail how this can be achieved).

6.3.4. *Optimal use of the Available Volume*

By removing the guide pins as suggested in Section 6.3.3 and the associated guide plates, the volume available within the design is dramatically increased. By introducing an energy absorbing material such as aluminium honeycomb into this volume the design can make optimal use of the available space and thereby increase its energy absorption capabilities. Increasing the potential to absorb energy within the device decreases the requirement to absorb energy through the outer casing, to the point where it is no longer necessary for this part of the structure to absorb energy at all. This completely removes the requirement for a dedicated steel casing which can now be replaced using lighter materials such as aluminium, thereby driving down the mass of the design without compromising its capacity to absorb energy.

6.4. Design of a lightweight Self-correcting Energy Absorber

To address the shortcomings of the original design a new and innovative absorber design was developed. As discussed in Section 2.2.3.1, aluminium honeycomb has excellent and predictable energy absorption properties. In addition to this the material also has one other

key and inherent property, that of self-alignment. When aluminium honeycomb crushes, each cell acts as individual tubes, the folding of which provides the energy absorption (Figure 115).

Figure 115: Folding mechanism of aluminium honeycomb cells

Once fully compressed, the block of honeycomb forms a stiff, rigid panel which can become, through innovative design, a load-bearing structure within the energy absorber.

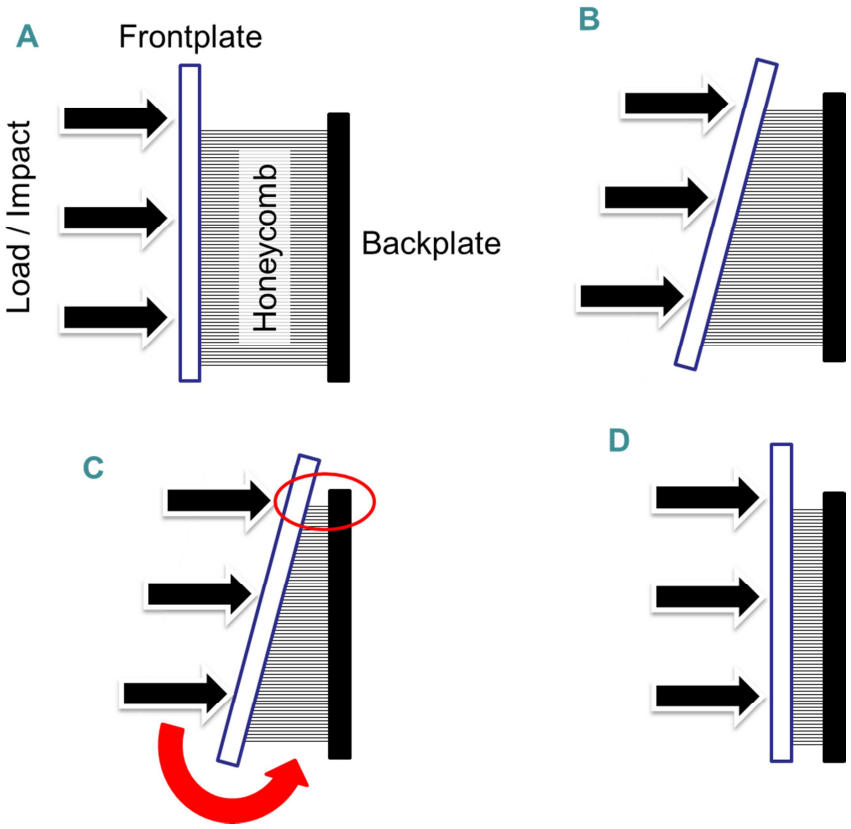

Figure 116: Self-aligning crush sequence of aluminium honeycomb

Figure 116 describes the mechanism by which a block of aluminium honeycomb causes a load to self-align with the axial direction of the cells.

A) Should the applied load be offset (as in the crashworthiness standards), the honeycomb begins crushing at one side of the material.
B) When this area becomes fully crushed, it forms a stiff plate which cannot crush further (see Figure 57 in Section 2.2.3.1).
C) This forces the applied load to be absorbed into the uncrushed portion (area of least resistance) thus causing the absorber to "self-align" bringing the frontplate back into vertical alignment.
D) This process continues until the entire honeycomb block is crushed.

To utilise this unique property to create a self-aligning absorber a new crushing methodology was devised. Rather than having the crush sequence begin at the point closest to the impact (i.e. directly behind the anti-climber) the crush is designed to begin at the point furthest from impact (i.e. at the support plates). This moves the centre of rotation of the anti-climbers to a point furthest away from the point of impact, thereby reducing local rotational effects which could lead to the anti-climbers becoming disengaged. This is especially relevant during a collision with a significant vertical offset between absorbers.

This shifting of the rotational centre can be achieved through intelligent deployment of aluminium honeycomb within the energy absorber. Rather than filling the available volume with a single block of the energy absorbing material, numerous blocks of honeycomb can be arranged inside, stacked on top of each other and inter-layered with thin aluminium sheet (this prevents interpenetration of the honeycomb blocks into each other).

Arranging the energy absorption blocks in order of increasing deformation resistance (and therefore density) in a direction moving away from the backplate provides the advantage of initiating the deformation of the energy absorber at a location furthest from the point of impact. Figure 117 shows a cross-section of the final design for the lower energy absorber, detailing the internal structure using multiple honeycomb blocks of different densities increasing in steps from lowest density (brown), to highest density (orange).

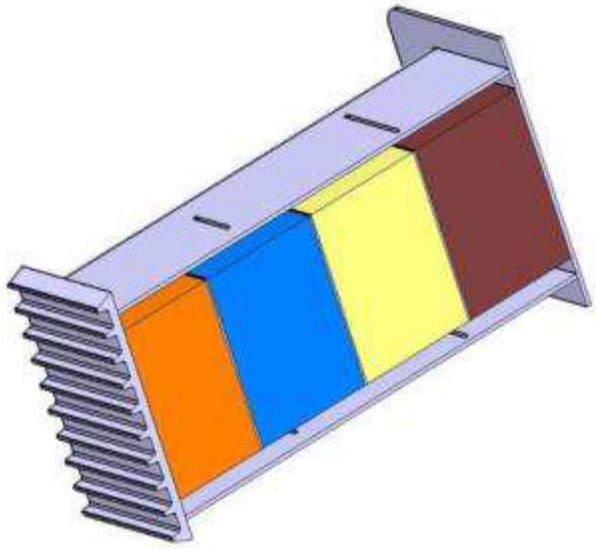

Figure 117: Cross-section of energy absorber design showing individual honeycomb blocks

As a result of this set-up, any rotational component of deformation force will crush the deformable material more on one side than on the other. This in turn causes a tendency for the uncrushed part of the material to become more easily crushed than the crushed part, which in turn initiates a rotational component of deformation force opposite to the original rotational component.

6.5. Simulation

To prove the functionality and capability to the lower energy absorber design a series of simulations were conducted at NewRail [120] against the impact requirements as set out in EN 15227. Achievement of validation of absorber designs for the rail industry is achieved through simulation, with the material properties being determined through physical testing.

To characterise the honeycomb behaviour within dynamic FEA models compression tests were conducted on CR III 1/8-5052-.0007 aluminium honeycomb blocks (Figure 118). Two blocks having dimensions 100 x 75 x 50 mm were tested in a fully supported mode under compression using the University's DARTEC Universal Test Machine (Section 4.3.2 Figure 82).

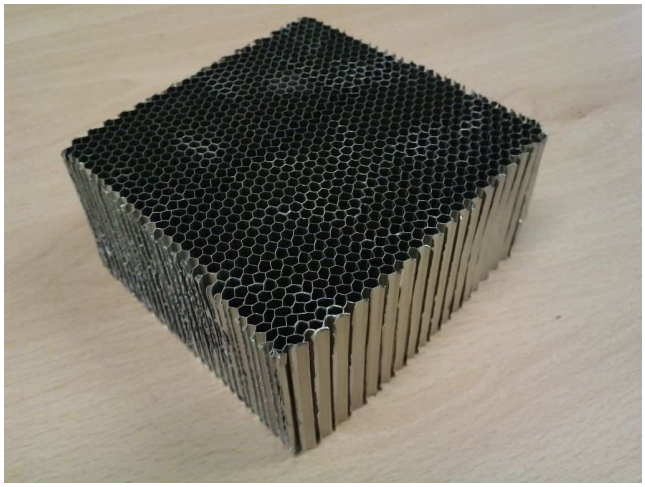

Figure 118: Aluminium honeycomb test specimen

The specimen was aligned within the machine such that it would be uniformly loaded on the upper face and continually supported on the lower face. The specimen was then loaded at a rate of 0.5 mm/s until the honeycomb had reached a fully compressed state (Figure 119).

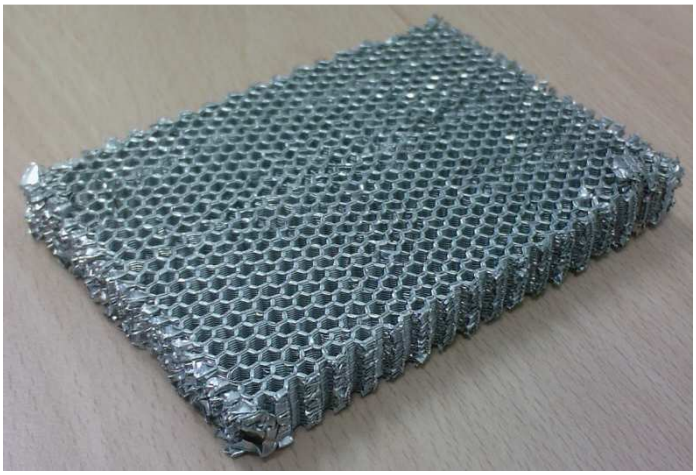

Figure 119: Fully compressed state of aluminium honeycomb block

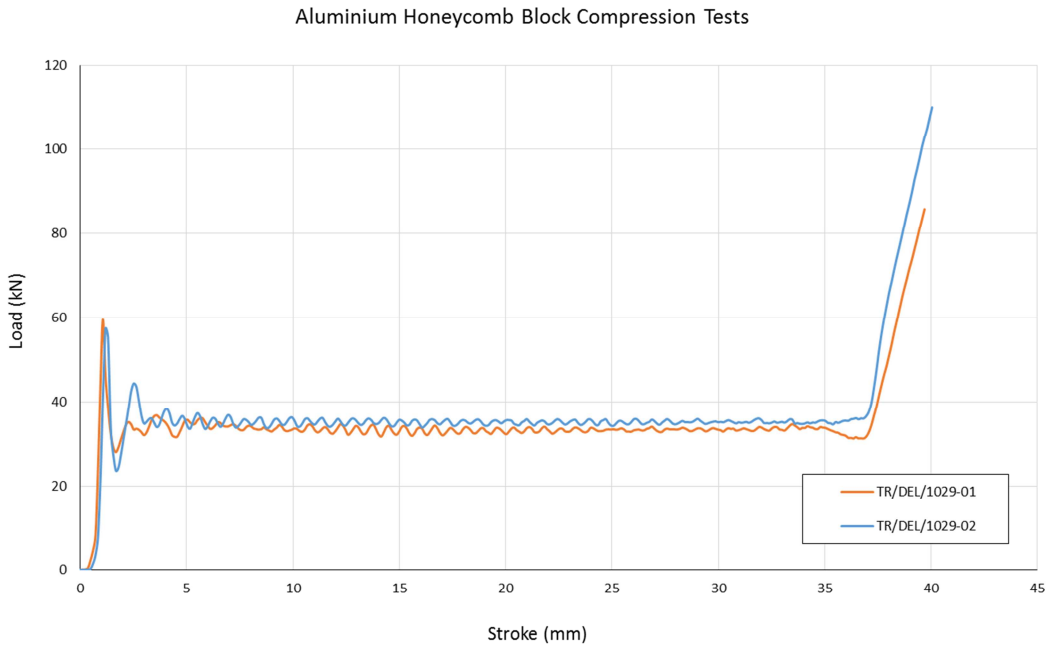

Figure 120: Compression profiles of two aluminium honeycomb blocks.

Using this material data, Grasso [120] derived the numerical curves through simulation and implemented them in the absorber design derived in Section 6.4

To demonstrate the self-correcting capabilities of the absorber design the results of the FEA simulations for the 40mm offset case (see Section 1.3) is detailed below. Figure 121 shows the initial configuration of the energy absorbers for simulation, and the finite element analysis (FEA) mesh is shown in Figure 122 which details the internal configuration of the absorbers.

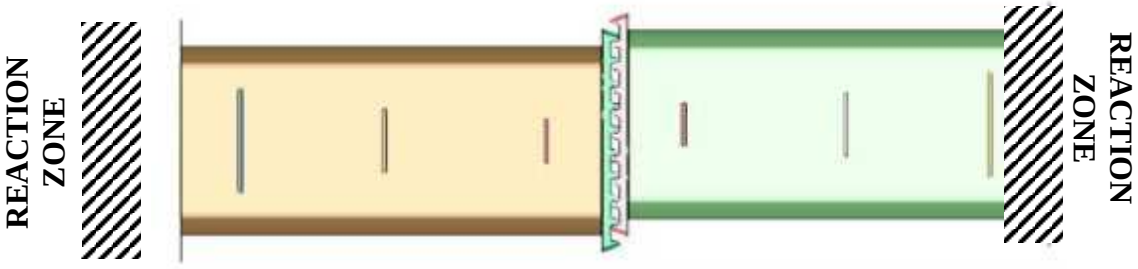

Figure 121: Initial configuration of the FEA model for 40mm offset case

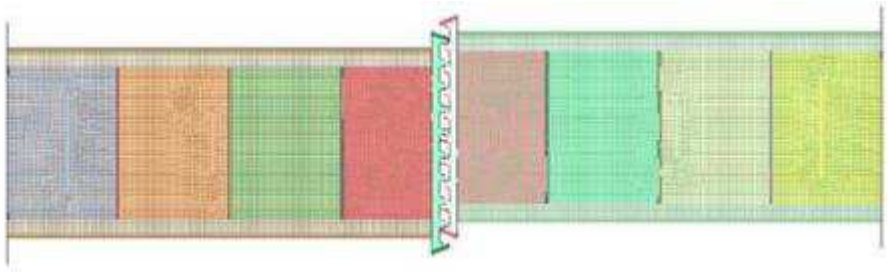

Figure 122: Internal structure of absorbers and FEA mesh

Figure 123 shows the simulated impact mid-way through the collapse sequence. The honeycomb blocks closest to the reaction zone are now completely crushed, forming solid plates against which the remaining honeycomb blocks will crush. The arrows indicate the regions of the honeycomb which are in the process of being crushed (see Figure 116c for comparison).

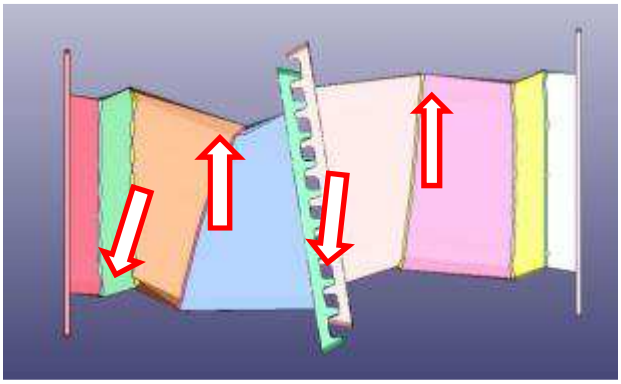

Figure 123: Mid-way through crush sequence (note fully compressed honeycomb blocks furthest from point of impact)

When fully crushed (Figure 124) the final configuration of the energy absorber is such that the anti-climbers remain engaged and in a vertical position, thus assisting in preventing overriding of the coaches.

Figure 124: Fully crushed absorbers (note anti-climbers remain in a vertical position)

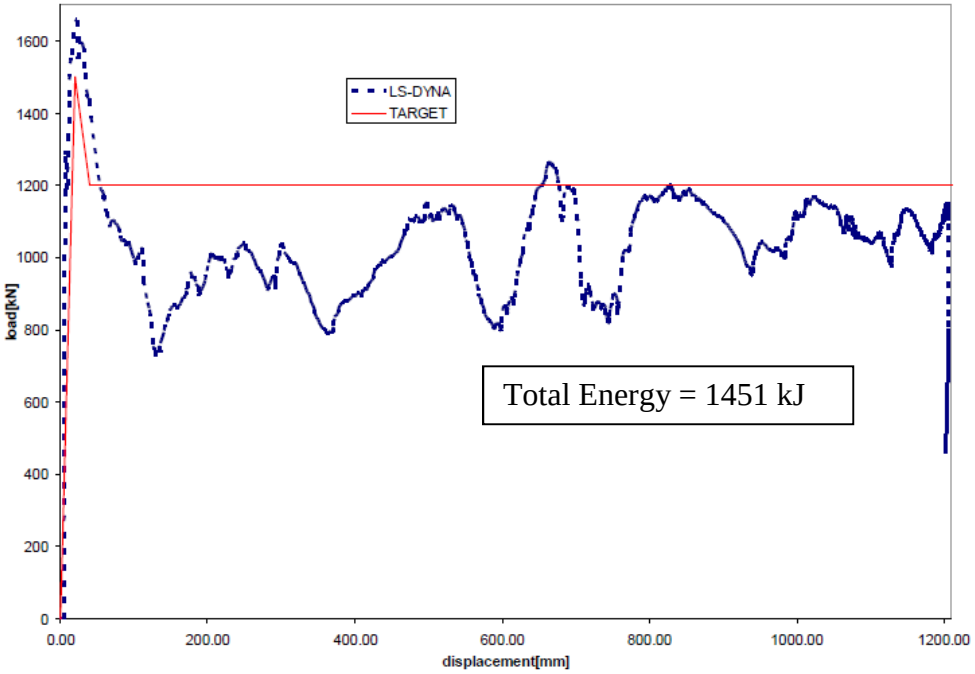

Figure 125: Load-Displacement curve for D-CAB lower absorbers [120]

The total energy absorbed by the energy absorbers was determined to be 1,451 kJ, which when combined with the other energy absorbing elements of the design (Section 7.1.1) deliver a complete and compliant crashworthy structure which meets rail industry standards.

6.6. Conclusions

Within this chapter it has been shown that through optimal use of the volume within existing absorber designs a lightweight, fully functional and effective energy absorber can be developed. By introducing aluminium honeycomb in a manner such that it begins crushing at the point furthest from impact it inherently begins to self-align, keeping the anti-climbers engaged throughout the crush stroke thereby preventing overriding of the vehicles.

The estimated mass of a single D-CAB buffer-level energy absorber is 113 kg. This represents a mass saving of more than 50% when compared to the existing SPACIUM device.

6.7. Novelty of Design: Patent Granted

As a result of the work undertaken and described in this chapter, a patent [125] was registered to protect the innovative concept of a “Self-correcting crash energy absorber”. The patent was granted internationally with the number WO/2011/012884A1 and is available through the World Intellectual Property Organization (Figure 126)

Figure 126: WIPO Patent Search showing this author’s name highlighted as inventor (extracted Feb 2016) [126]

6.7.1. *Patent Abstract*

“An energy absorber for absorbing kinetic energy of a vehicle is disclosed. The energy absorber comprises a housing adapted to be mounted to a vehicle body, and energy absorber blocks, each of which has at least one respective deformable material adapted to absorb

energy by being deformed and having a respective deformation resistance. The energy absorber blocks are arranged substantially in order of sequentially increasing deformation resistance, and the energy absorber is adapted to be mounted to the vehicle body such that the energy absorber blocks are arranged substantially in order of increasing deformation resistance in a direction moving away from the vehicle body."

6.7.2. *Patent Primary Claim*

"An energy absorption apparatus for absorbing kinetic energy of a vehicle, the apparatus comprising: a support adapted to be mounted to a vehicle body; and energy absorption means mounted to the support and comprising a plurality of energy absorption portions, each of which has at least one respective deformable material adapted to absorb energy by being deformed and having a respective deformation resistance, wherein the energy absorption portions are arranged substantially in order of sequentially increasing deformation resistance, and the apparatus is adapted to be mounted to the vehicle body such that the energy absorption portions are arranged substantially in order of increasing deformation resistance in a direction moving away from the vehicle body."

6.7.1. *Patent Detail*

Referring to Figure 127 and Figure 128, an energy absorber (102) for mounting to a rail vehicle has a support in the form of an aluminium housing (104) having a steel anti-climber plate (106) mounted to one end of the housing, and an aluminium back plate (108) mounted to the other end of the housing. The back plate 108 is arranged to be mounted to a body of the rail vehicle. The housing is provided with a series of weakened regions (110) spaced apart along the length of the housing, to enable it to collapse and progressively fold in the event of a sufficiently large impact on the anti-climber plate.

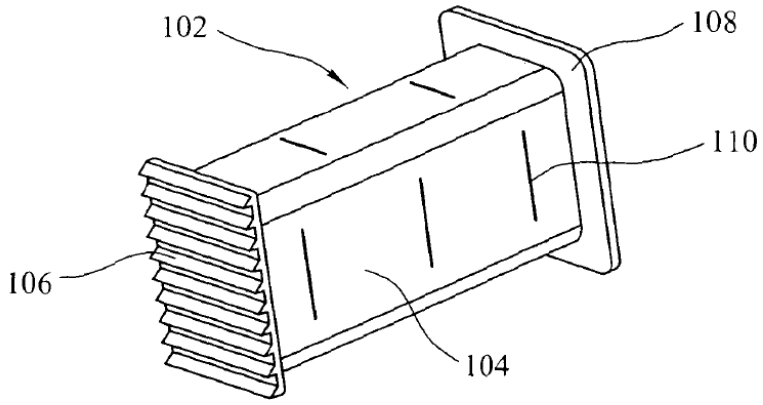

Figure 127: Perspective view of an energy absorber embodying the present invention [125]

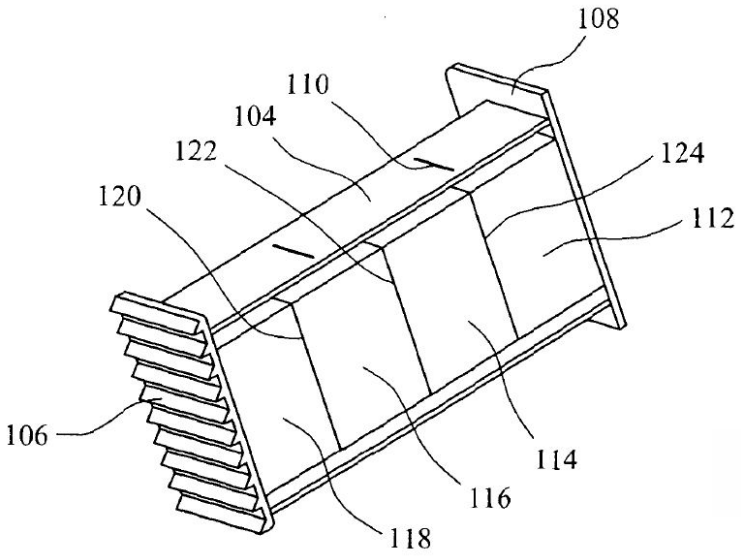

Figure 128: Partly cut away view of the energy absorber [125]

A series of energy absorber blocks (112, 114, 116, 118) are arranged inside the housing and are each formed from a crushable material such as aluminium honeycomb material or crushable foam material. The energy absorber blocks have different crush resistances and are arranged in order of increasing crush resistance in a direction from the back plate to the anti-climber plate, so that the block of weakest material (112) is in contact with the back plate, and the block of strongest material (118) is in contact with the anti-climber plate. Aluminium support plates (120, 122, 124) are positioned in between the energy absorption blocks to prevent the blocks interpenetrating one another.

In the event of a collision between two rail vehicles provided with identical energy absorbers of the type shown in Figure 127 and Figure 128, the anti-climber plates of the energy absorbers initially engage each other such that ridges on the anti-climber plates engage and

resist vertical sliding motion to minimise the risk of one vehicle climbing onto the other vehicle. Since the energy absorber block of smallest crush resistance of each energy absorber is arranged adjacent the back plate, crushing, and therefore energy absorption, occurs initially in the block adjacent the back plates. When complete crushing of the energy absorber block 112 has occurred, crushing of the remaining blocks (114, 116, 118) occurs in order of increasing crush resistance, i.e. progressively in a direction from the back plate towards the anti-climber plate.

If, as a result of the two rail vehicles being slightly offset in position relative to each other causing an offset in height between the anti-climber plates, the impact force is applied unevenly to the energy absorbers, producing rotational movement of the anti-climber plates relative to the back plates. If this rotational movement is as shown in Figure 129, the upper part of the block of crushable material (112) will be crushed more than the lower part of the block, as a result of which complete crushing of the upper part will occur before the lower part has been completely crushed.

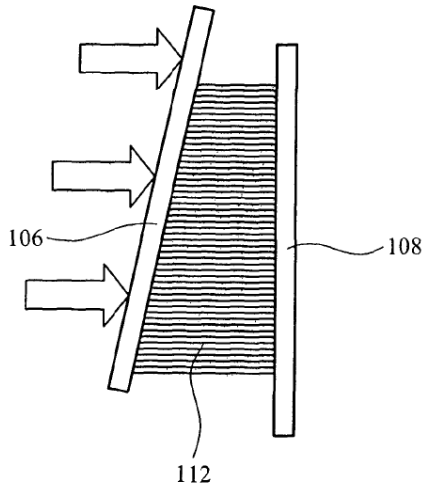

Figure 129: Crushing of aluminium honeycomb in offset case [125]

Because the upper part of the block becomes more resistant to deformation as a result of crushing, and therefore less prone to crushing than the lower part, further crushing of the block tends to cause an anticlockwise component of rotational motion of the anti-climber plate relative to the back plate and further crushing of the energy absorber block tends to correct any rotational component of movement of the anti-climber plates relative to the back plate (108).

Chapter 7: Key attributes, conclusions, impact and recommendations for further work

7.1. Key attributes of the cab – Energy Absorption, Mass, Part Count, Cost

7.1.1. *Energy Absorption*

There are five distinct elements of the D-CAB structure that contribute to its overall energy absorption capability, summarised in Table 18.

For the coupler, the energy absorption characteristics of the original SPACIUM coupler are determined to be 500 kJ [119]. The energy absorption characteristics of the upper and lower energy absorbers are those derived from the dynamic simulation in Figure 111 and Figure 125. For the nose and cab shell walls an average material energy absorption capability of 10 kJ/kg was adopted, a conservative value based on previous work on the crushing of glass fibre reinforced polymer (GFRP) / foam sandwich structures [127]. The useful crush stroke of the nose and the secondary module cab shell walls was conservatively estimated to be approximately 80% of their total length.

Table 18: Design elements that contribute to the D-CAB's overall energy absorption.

Energy Absorbing Element	Initial Peak Load (kN)	Effective Crush Stroke (mm)	Energy Absorption (kJ)
Coupler	1,800	1,000	500
Nosecone	-	450	160[1]
Lower energy absorbers (combined)	2,663	700	1,451
Upper energy absorber	1,577	400	801
Cab shell walls	-	500	400[2]
Total Energy Absorption Capability:			**3,351**

[1] Measured mass of nosecone structure = 20 kg
[2] Estimated mass of crushable cab shell wall = 50 kg (5mm facings, 10 mm core)

The energy absorption capacity of the original SPACIUM cab was 3.3 MJ as described in Section 4.1, so the figure of 3.351 MJ for the D-CAB is highly commensurate with this target and demonstrates that the design meets EU standards and industry requirements.

Based on the data presented in Table 18 and the overall layout of the cab, Figure 6.4 shows a combined load-displacement characteristic for the first metre of D-CAB's collapse. The dotted line shows the target (i.e. the existing SPACIUM design) performance as defined in Section 4.1, Figure 71.

It can be seen that the overall profiles are broadly similar.

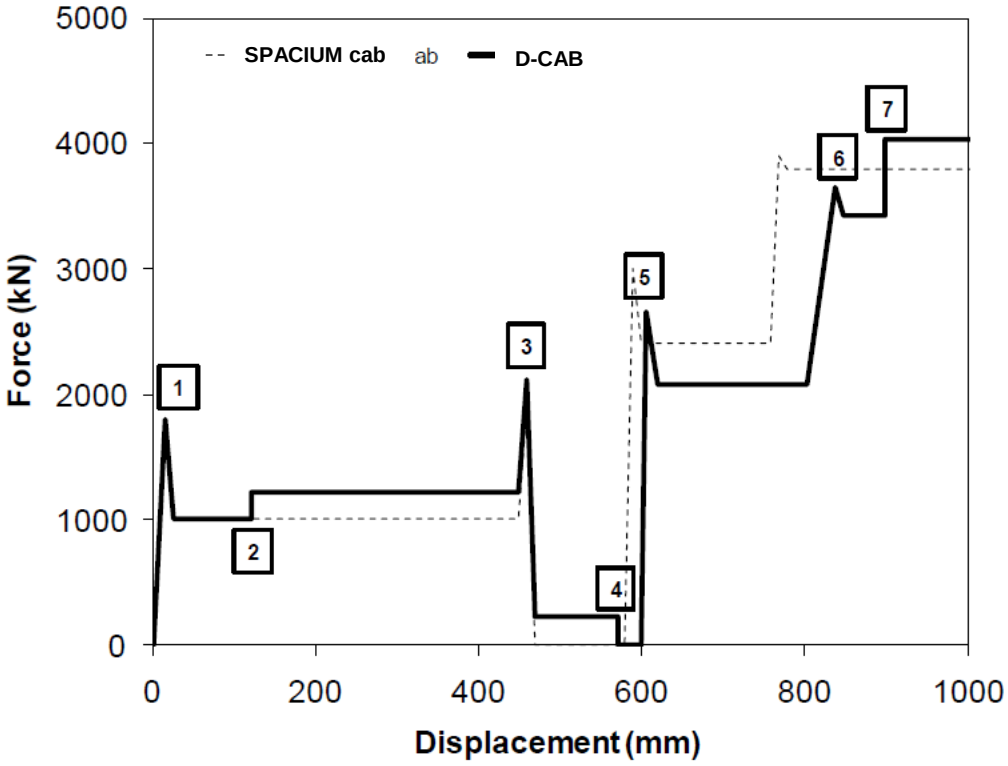

Figure 130: Load-Displacement profile of SPACIUM and D-CAB

The sequence of collapse (as labelled in Figure 130) is as follows:

1. Engagement of the coupler. The coupler has its own in-built collapse mechanism.
2. Engagement of D-CAB's nosecone. This will fail by the stable, high energy brittle fracture of the constituent GFRP material.
3. Exhaustion of the useful collapse stroke of the coupler.
4. Exhaustion of the useful collapse stroke of the nosecone.
5. Engagement of the buffer-level energy absorbers. These will fail by the stable, high energy plastic deformation.

6. Engagement of the upper energy absorber. This will fail by the stable, high energy plastic deformation.
7. Engagement of the cab shell walls. These will fail by the stable, high energy brittle fracture of the constituent GFRP / polymer foam material.

The primary differences between the collapse response of the existing SPACIUM cab and D-CAB can be summarised as follows:

- D-CAB provides two additional sources of energy absorption – the nose (between points 2 and 4 in Figure 130) and the secondary module cab shell walls (point 7 onwards).
- The D-CAB lower energy absorbers engage slightly later (after 600 mm, as opposed to 579 mm for the SPACIUM cab) – point 5 in Figure 130.
- The mean collapse load of the D-CAB lower energy absorbers is slightly lower (1,036 N for each absorber, as opposed to 1,100 N for the SPACIUM cab) – point 5 in Figure 130.
- Although it is not shown in Figure 130, the D-CAB upper absorber have a lower useful crush stroke than the SPACIUM absorbers (300 mm vs. 500 mm for the upper energy absorber).

7.1.2. *Mass*

The estimated mass of the D-CAB sandwich structure (i.e. pillars, reactors, outer sandwich shell and nosecone) is 600 kg. Add to this the mass of the two buffer level energy absorbers (226 kg, Section 6.6) and the mass of the upper energy absorber (128 kg, Section 5.3). This gives a total estimated mass for D-CAB of 954 kg.

While a measured mass was not available for the SPACIUM cab, its mass could be estimated by applying representative steel density to the CAD geometry. Using this method, the mass of the SPACIUM cab's steel structure was approximated as 2,300 kg. Add to this figure the mass of the fibreglass shell, estimated to be 100 kg, and the overall estimate for the mass of the SPACIUM cab is 2,400 kg.

Comparing the masses of both cabs gives an overall **mass reduction of 60%**.

7.1.3. *Part Count*

As a result of the design methodology and material choice for the D-CAB there is a significant reduction in the number of parts required to complete a cab assembly.

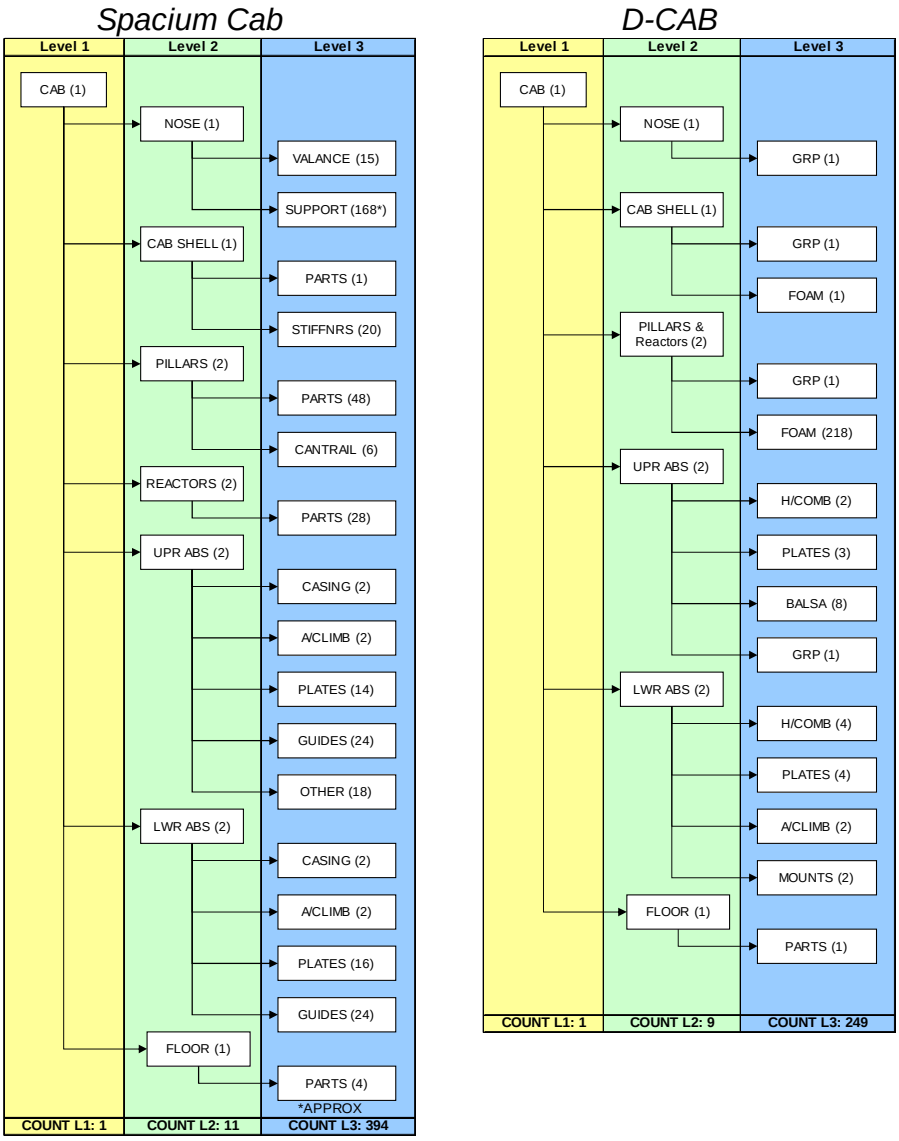

Figure 131: Part count comparison between SPACIUM and D-CAB

Figure 131 gives a part-by-part breakdown of the major components that comprise the SPACIUM driver's cab and the D-CAB design.

The numbers indicate a **part count reduction of approximately 37%**, primarily due to the merging of the outer shell of the cab with the inner load-bearing components (reactors and pillars). This movement towards a more monocoque construction lends itself to outsourcing

the cab as a single part to a first tier supplier. This would greatly reduce the assembly time required as manufacturers could purchase cabs as individual units which could be quickly aligned and jointed with the mainframe prior to systems installation and final equipping.

7.1.4. *Cost*

It is worth highlighting that whilst the cost of the composite materials and their processing might be expected to be somewhat higher for the D-CAB, savings in secondary assembly and outfitting costs due to the reduced part would be a reasonable expectation. A previous study by Ingleton [128] estimated some of the likely cost differences between the two approaches. A summary of the findings are presented in Figure 132.

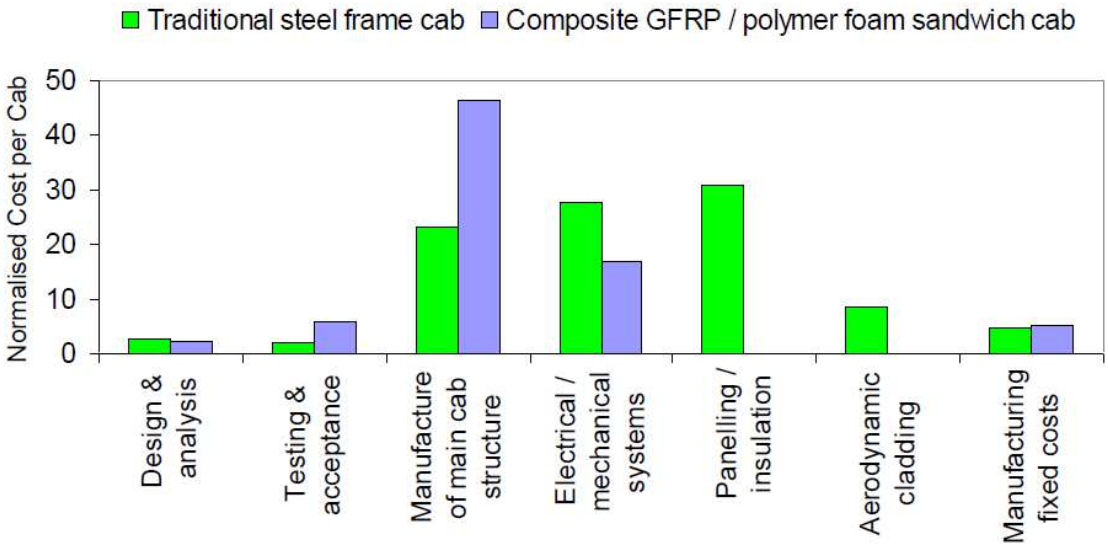

Figure 132: Cost analysis of traditional and GFRP cab designs. Data from Ingleton [128]

Detailed D-CAB costings

Based on a quotation of £816 for a 2440 x 1220 x 250mm honeycomb block (3.4-1/4-15 - 3003 AL) this gives a cost of approximately £20/kg. The cost of the aluminium honeycomb used in the absorber design can be estimated as per Table 19.

Table 19: Costings for aluminium honeycomb

Density (kg/m^3)	Cost ($/kgm^{-3}$)	Quantity	Volume (m^3)	Unit cost
77	£1,538	1	0.029	£44.60
53	£1,057	1	0.037	£39.11
37	£737	1	0.037	£27.27
29	£576	1	0.037	£21.31

For the 6000 series aluminium tube it was assumed that this can be simplified by costing for four plates of 10mm thick aluminium (Table 20).

Table 20: Costings for aluminium plate

Thickness (mm)	Width (mm) x Length (mm)	Quantity	Unit cost	Total cost
10	410 x 1100	2	£68.61	£137.22
10	470 x 1100	2	£77.48	£154.96

Aluminium end plate, 650 x 600 x 10mm = £60.42
Steel anti-climber (machined) = £800.00 (estimate)
Assembly costs of 10 hrs at £50/hr = £500 (estimate)

Total cost of single lower absorber = £1,785 (€2,117[1])

This figure compares very favourably with the cost of the existing units (€3,500), giving a potential cost saving of 41% per unit.

For the upper energy absorber the cost of the honeycomb is estimated to be £938 based on a volume of 0.976 m^3 and a cost of £961 /kg m^{-3}. The cost of producing the curved steel backplate and aluminium plates was quoted as £1550.

Total cost of upper absorber = £2488 (€2,950[1])

[1] Based on a rate of 1 GBP = 1.18611 EUR, correct as of Dec. 2013

The estimated cost of producing the D-CAB sandwich structure is approximately £11,000 based on the prototype manufactured using the design developed in this thesis (Figure 140). Adding the cost of the upper and lower absorbers gives:

Estimated cost of D-CAB of approximately £15,273 (€12,8771).

The manufacturers of the SPACIUM fibreglass shell quoted a price of around £13,000 for manufacture. Cost estimates for the SPACIUM steelwork and absorbers are £20,000.

Total for the SPACIUM cab of £33,000 (€27,8261).

Therefore, the cost saving associated with the D-CAB is estimated to be **54%**.

7.1.5. *Manufacturing the prototype*

Using the designs produced by this thesis a full scale prototype of the patented D-CAB was built by AP&M, a composites specialist company based in Lagos, Portugal. The completed structure was a true and accurate representation of the SPACIUM elements with respect to outer surface geometries and driver's survival space. However it incorporates within this volume all the lightweight, crashworthy, energy-absorbing and structural elements developed and described by this thesis.

Being a prototype build, AP&M adopted a hand-lay-up approach to reduce costs and allow for the introduction of design changes as the analysis matured. This complimented the manufacturing approach used in the production of the test specimens "A" in Section 4.3.1. While this method reduced the cost of the manufacture of the prototype and suited the scope of the De-Light project, for higher production volumes this author would recommend the use of processes such as vacuum assisted resin transfer moulding to produce the cab outer shell to desired tolerances.

The photographs in Figure 133 to Figure 140 are presented in sequence to describe the process by which the cab and its associated moulds were manufactured.

Figure 133: Cab shell from the existing SPACIUM vehicle

The starting point for the manufacturing process was a cab shell assembly from the existing SPACIUM vehicle (Figure 133). This was used to provide a reference outer surface from which a “splash” (female mould) was taken to produce the main D-CAB.

Figure 134: D-CAB mould made from original cab

The splash is completed and the original cab shell removed to produce a mould which conforms to the shape and geometry of the original cab (Figure 134). The composite components of the D-CAB will be laid into this mould as part of the manufacturing and assembly process.

Figure 135: Polyurethane foam beams for reactor structure

Figure 135 shows the polyurethane foam (HD-PUR) beams that were used as the core elements for the reactor structure that supports the lower energy absorbers. These cores were cut from block using a band-saw and the edges were rounded by hand using trimming knives and sandpaper. Each of these foam cores was wrapped in M705 CSM using a mandrel to hold and rotate the pieces and subsequently brush-saturated using the SR1500/SD2507 epoxy resin system delivering layers of fibres and epoxy resin which are gradually applied and built up to the required thickness. These are then bonded together (Figure 136) using the epoxy resin to produce the structure commensurate with that described in Section 4.2.3.

Figure 136: Reactor beams wrapped in GFRP

Figure 137: Polyurethane foam parts for one of the D-CAB pillars

A kit of polyurethane foam components (Figure 137) for the pillars that support the upper energy absorber were produced, hand cut from blocks of HD-PUR using a band-saw.

The reactors and pillars are laid into the cab mould and the whole construction is built up layer by layer working from the mould surface outwards, with GFRP bonding the reactor tubes to the pillar structure. Continuous vertical layers of GFRP were inserted between the foam pieces to produce a multilayer sandwich structure as described in Section 4.2.3, Figure 78. The process is continued until all the reactor and pillar structures are completed and bonded in-situ.

Figure 138: Assembly of the pillar/reactor structure in the mould, arrow shows layered construction direction.

Figure 138 (left) shows the ongoing assembly of the pillar/reactor structure with four layers completed. Figure 138 (right) shows the addition of the final layers of the structure comprising seven layers of polyurethane foam core and GFRP. A final layer of GFRP encapsulates the entire structure and is cured in-situ Figure 139.

Figure 139: Pillars and reactors fully installed.

When cured the D-CAB was removed from the mould and painted in accordance with rail standards. The nosecone section was cut away and the energy absorbing elements were connected to the main structure before the nosecone was bolted back onto the structure as shown in Figure 140.

Figure 140: Prototype D-CAB on display at INNOTRANS, Berlin 2010

7.2. Conclusions and recommendations for future work

The intention of the work described in this thesis is to provide an indication of the feasibility of making optimal use of the space envelope of a rail vehicle driver's cab to achieve lightweight crashworthy capabilities. A crashworthy cab was designed from lightweight sandwich materials and aluminium honeycomb energy absorbers which meet structural and crashworthiness standards. The design is supported by two granted international patents.

With respect to the adoption of composites in a primary structural role within rolling stock, there is still a number of key items that will have to be addressed before the design philosophy presented here can be implemented in rail vehicles:

7.2.1. *Design Optimisation*

It is recommended that the following areas would require further design and development effort:

- Rationalisation of the foam core geometries for the pillar and reactor structures with a view to reducing the overall part count. This could include the use of the prefabricated pultruded box sections (see Section 4.3.1) in place of the GFRP-wrapped foam beams.
- Enhanced driver missile protection in vulnerable areas and validation of overall missile protection capability.
- Consideration of the optimum material selection to balance the required level of fire performance against cost, processing and surface finish.
- The development of improved standards to certifiy the use of structural composites in the rail industry.

7.2.2. *Simulation*

It is recommended that the following areas would require further simulation effort:

- Validation of static load compliance through finite element analysis.
- Further refinement of D-CAB's energy absorbers, particularly in terms of their crushing stroke and off-axis stiffness.
- Further refinement of the lower absorber casings to ensure they do not encroach upon and impact the functionality of the internal honeycomb structure.
- Fatigue analysis of the cab structure backed-up by material testing
- Structural lifetime performance in adverse environments.

7.2.3. *Testing*

It is recommended that the following areas would require further testing:

- Validation of crash compliance through experimental testing. Upper and lower energy absorber elements should be tested individually or in unison to confirm their capability and functionality.
- Validation of fatigue performance (joints, aerodynamic loads and mounted equipment). This should be conducted on a sub-assembly level to provide life cycle data for in-service application.

For the purposes of monitoring and inspection during the operational lifetime of the vehicle the following non-destructive testing technologies should be investigated further for rail vehicle applications:

- Phased array ultrasonic testing.
- Pulsed thermography.
- Laser shearography.
- Passive wireless embedded sensors.
- Health-monitoring using PZT thin film sensors.

7.2.4. *Certification*

Adopting composite materials for primary structural roles within rail rolling stock will require an assessment of the suitability of current European Standards to fulfil the certification and homologation requirements. These standards will require intensive interrogation to determine whether they can adequately accommodate the different susceptibilities of composite materials (as opposed to more traditional steel and aluminium constructions) such as: water ingress; crack propagation; repair procedures; fault detection; crush mechanics; extreme environment performance.

7.2.5. *Manufacturing considerations*

The implementation of more advanced manufacturing techniques (than the hand lay-up method used in this body of work) for rail vehicle composite components would deliver products of improved consistency and thus improved performance. Irregularities in the hand lay-up process and the risk of inclusions could lead to a much reduced structural response under load. Other manufacturing options available to the industry include:

- Automated lay-up and tape-laying.
- Spray-up (mixture of resin and chopped strands).
- Filament Winding.
- Pultrusion.
- Resin Transfer Moulding.

Whilst these manufacturing techniques have the potential to deliver consistent products in a cost-effective manner, a careful balance needs to be struck to ensure that the fibre volume fraction (V_f) remains within the specified design range. Increased V_f can deliver thinner and lighter structures but they can be more susceptible to buckling as a result. At lower V_f values there is a tendency for the structure to delaminate - which would make them more suitable for energy absorption/ballistic roles. Choosing the correct V_f range for the indented design

purpose and consistently manufacturing to that range will deliver material solutions that can meet the specific needs of the rail industry.

7.2.6. *Risk mitigation for implementation*

Table 21 describes some of the potential risks and barriers to the industrial uptake of the lightweight rail driver's cab design described in this body of work. Mitigation and contingencies are described to negate the effect of these risks which should be addressed prior to implementation.

Table 21: Potential risks to lightweight cab implementation

Risk	**Likelihood**	**Impact**	**Mitigation / Contingency**
Lightweight energy absorbers underperform.	Medium	Low	Existing (proven) steel energy absorbers could be used, albeit with a weight penalty
Difficulties in properly validating the performance of the cab using computer simulation because of the complexities of modelling composites.	Medium	Medium	Experimentally-based validation methods should be used instead, however this would lead to higher development costs.
Key joints fail unexpectedly under statutory loadings.	Medium	High	Critical joints should be thoroughly analysed and/or tested as part of the design refinement process to validate performance and minimise the risk of failure.
Lack of relevant rail industry standards for certifying composite designs.	Low	Medium	Regular communication should be maintained with relevant standards committees and certification bodies.
Difficulties in reassuring potential customers of the longer term fitness-for-purpose (durability) of the breakthrough design.	Medium	High	Planned duration of certification and approval process should be extended, and there should be close ongoing liaison with customers.

7.3. Impact

7.3.1. *Bombardier*

Notwithstanding the two filed patents already produced by this body of work (Sections 4.4 and 6.7) the composite cab design has had a significant impact on the rail industry and the acceptance of new and novel materials in primary structural roles.

The current D-CAB prototype now resides with Bombardier at their Crespin facility in France. It is being reviewed with respect to the potential weight and cost savings that could be realised by implementing the design whilst the impact on their assembly process and the readiness of the supply chain (via Tier 1 suppliers) to deliver the product is ongoing.

For this body of work it is the design philosophy with respect to the tailored application of composite materials that forms the primary output for industrial applicaiton. I have already used the principles presented in this thesis to develop a lightweight solution for tram driver's cabs (Figure 141), in response to a specific request from Bombardier for their Flexity 2 vehicle.

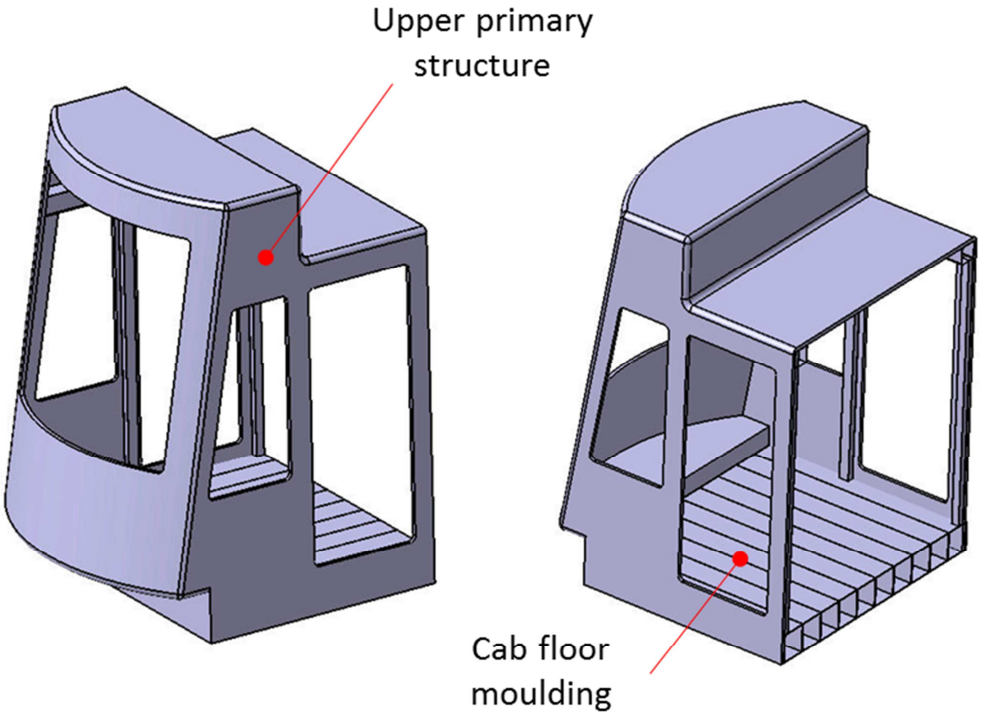

Figure 141: Lightweight tram cab proposal for Bombardier Flexity 2 vehicle

All the structural steelwork of the existing design, as well as the exterior glass reinforced polymer (GRP) shell are replaced by just two parts moulded from structural composite sandwich materials:

- A cab floor moulding consisting of a tubular composite sandwich structure similar to that used in the reaction zone of the cab presented in Section 4.2.3.
- A single moulding for the remainder of the upper primary structure.

These two sandwich structures would be designed to accommodate all the required static loads of EN 12663. The implementation of this concept would provide a very significant reduction in part count and assembly time and associated costs. It would also provide more flexibility in the aesthetic design of the cab as the design envelope would no longer be dictated by an underlying steel structure.

Alternative (lower cost, lighter, more efficient) energy absorbers using aluminium honeycomb could achieve the required crash performance without any intrusion rearward through the bulkhead as detailed in Chapter 4. Coupler access would be provided by a hinged moulding at the front of the cab and the structural floor moulding would provide a robust mounting point for a lower obstacle deflector.

7.3.2. *Effect on European standards*

As a result of this work and the De-Light project the rail industry was compelled to undertake a full and comprehensive interrogation of current rail vehicle standards in preparation for the adoption of composite materials into the industry. This led to the launch of the EU-funded project ***REFRESCO*** *– Towards a Regulatory Framework for the use of Structural New Materials in Railway Passenger and Freight Carbodyshells*. The objective of this on-going multi-million Euro project is to set the framework for the rapid, efficient and safe implementation of new materials in the railway sector through the evolution of certification processes for rolling stock.

7.3.3. *Recognition by the European Commission*

In 2012 the European Commission recognised the achievements of the lightweight rail cab design described in this thesis as an example of "Investing in success" [129]. The brochure produced by the European Commission to launch the Horizon 2020 funding programme selected the cab for inclusion in their publication detailing research success stories (Figure 142).

DE-LIGHT

Adapting Formula 1 technology to aid the rail industry

At first sight, train drivers' cabs and Formula 1 cars may not seem to have much in common. But a research project funded by the European Commission has led to a potential breakthrough for the rail industry - by adapting technology most commonly found in high performance racing cars.

The results promise to provide the rail industry with trains that are more environmentally-friendly, easier and cheaper to produce, and less costly for rail companies in terms of track maintenance. An all round win-win situation.

The rail industry's needs are clear: lightweight materials for trains in order to increase energy efficiency and reduce the damage to tracks, and reduced costs. All, of course, without compromising safety.

The problem is that conventional train cabs, made from welded steel units, can weigh up to one tonne each. With a cab at each end of the train, the potential for weight reduction is clear. On top of that, traditional cab designs tend to be very complex, incorporating a large number of parts, all made from different materials. That is because they need to meet a range of physical demands, including strength, crashworthiness, aerodynamics and insulation. As a result, assembly costs are high.

Formula 1 cars use extremely strong, lightweight materials known as carbon composites to help achieve the high performance they need. But such materials are highly specialised and uneconomic for extensive use in trains.

The answer for the rail industry came through a multi-year project funded under the European Commission's DE-LIGHT programme, which was aimed at developing improved light-weight

materials for use in a wide range of transport systems. After three years of research, a team from Newcastle University in the UK, working in collaboration with Bombardier Transportation and Portuguese manufacturing firm AP&M, succeeded in producing a prototype lightweight train cab which reduces the weight of the traditional cab by a remarkable 40%.

The breakthrough technology behind the new cab takes the form of a 'sandwich' construction, in which an aluminium honeycomb structure and a polymer foam core are enclosed in outer layers of special glass-reinforced plastic. The effect is similar to the composites used in Formula 1 - but at much lower unit cost.

Crucially, the inherent strength of the new construction eliminates the need for steel elements. This reduces not only the weight, but also the number of separate parts required. In addition to the 40% weight reduction, the new cab reduces the number of separate component parts by up to 75%. And this in turn reduces overall costs by up to 20%, as assembly and outfitting are far simpler than before.

All of this is achieved while still meeting stringent crashworthiness requirements.

"It's great to finally see the cab in real life," says lead designer Conor O'Neill of Newcastle University's rail research centre. "I've been staring at a virtual model on my computer screen for the last three years, and it's very satisfying to see the real thing."

It is intended that the cab will first go into commercial use in Bombardier's Spacium trains on suburban services in Paris.

Figure 142: The European Commission selects the De-Light Rail Driver's Cab research as an example of "Investing in Success" [129]

7.4. Concluding remarks

Within this thesis I have presented an overview of the aims and objectives of crash energy management and the methods by which this can be embodied within rail vehicles. Current and state-of-the-art energy absorber designs and materials are reviewed identifying the pros and cons of each solution with respect to rail applications. Using aluminium honeycomb as the basis for energy absorption, 2D shapes and 3D volumes are reconfigured based on the material's key characteristics and identified design or manufacturing constraints.

A practical application of this material in a rail vehicle has been undertaken, with Bombardier's SPACIUM vehicle forming the basis of the design. The upper and energy absorbers have been replaced with aluminium honeycomb which makes optimal use of the available space and provides a crushing capability which meets the requirements of the EN standards. A composite cab has been developed which fills the available space with lightweight materials which have the capability to react rail vehicle static and impact loadings.

Two patents have been successfully filed by the author to protect the design of the lower energy absorbers and the composite cab.

The benefits of such a solution have been identified though the mass and part-count savings, as well as an overall reduction in the total cost of production for the driver's cab.

This thesis has shown that lightweight energy absorbing structures can be successfully applied within a rail vehicle's driver's cab to provide an economically viable solution which meets crashworthiness requirements.

References

[1] Railways Archive, “Accident Returns: Extract for the Accident at Nottingham - Beeston on 21st November 1844.” [Online]. Available: http://www.railwaysarchive.co.uk/docsummary.php?docID=4269. [Accessed: 04-May-2017].

[2] National Transportation Safety Board, *Collision of Metrolink Train 111 with Union Pacific Train LOF65-12 Chatsworth, California, September 12, 2008 - Accident Report*. 2010.

[3] Boster Kobayashi & Associates, “LA-area commuter trains get crash-avoidance system.” [Online]. Available: http://www.boster-kobayashi.com/la-area-commuter-trains-get-crash-avoidance-system/. [Accessed: 25-Mar-2016].

[4] D. Parent, D. Tyrell, K. Jacobsen, and K. Severson, “Crashworthiness Analysis of the January 26, 2005 Glendale, California Rail Collision,” in *ASME/ASCE/IEEE Joint Rail Conference*, 2011, pp. 1–10.

[5] B. Siuru, “Metrolink’s New CEM Trains,” *Mass transit*. [Online]. Available: http://www.masstransitmag.com/article/10158425/metrolinks-new-cem-trains. [Accessed: 12-Jan-2017].

[6] R. Forsberg, “Train Crashes - Consequences for Passengers,” Umeå University, 2012.

[7] UK Department of Transport, “Railway accidents: train accidents, annual from financial year ending 2002,” 2014. [Online]. Available: https://www.gov.uk/government/uploads/system/uploads/attachment_data/file/385175/rai0503.xls. [Accessed: 06-Apr-2014].

[8] European Commission, “EURailSafe.” [Online]. Available: http://www.eurailsafe.net/. [Accessed: 13-Feb-2016].

[9] R. Palacin, “SAFEINTERIORS - Project Overview,” *EURailSafe*, 2007. [Online]. Available: http://www.eurailsafe.net/projects.php?id=2. [Accessed: 13-Feb-2016].

[10] D. F. Shanahan, “Determination of Injury Mechanisms,” in *Injury Research: Theories, Methods, and Approaches*, G. Li and S. P. Baker, Eds. Springer Science & Business Media, 2012, pp. 111–138.

[11] J. Roberts, A. M. Robinson, and G. Kotsikos, “Safety Development of Rail Crashworthiness in Europe,” 2015.

[12] M. S. Pereira, “Structural Crashworthiness of Rail Vehicles,” in *World Congress for Railway Research*, 2006.

[13] Railway Technical Web Pages, “ATP Beacons and Moving Block.” [Online]. Available: http://www.railway-technical.com/sigtxt3.shtml. [Accessed: 04-May-2017].

[14] R. Palacin, “Interior Passive Safety for Europe - Researching Ahead,” *EURAILmag Business and Technology*, no. 22, pp. 30–33, 2006.

[15] K. Jacobsen, K. Severson, and B. Perlman, “Effectiveness of Alternative Rail Passenger Equipment,” in *Joint Rail Conference*, 2006, pp. 121–129.

[16] D. Tyrell, E. Martinez, and B. Perlman, “Development of Crash Energy Management Designs for Existing Passenger Rail Vehicles,” in *ASME International Mechanical*

Engineering Congress, 2004, pp. 1–9.

[17] D. Tyrell, K. Jacobsen, E. Martinez, and A. B. Perlman, "A Train-to-Train Impact Test of Crash Energy Management Passenger Rail Equipment : Structural Results," in *ASME International Mechanical Engineering Congress and Exposition*, 2006, pp. 1–10.

[18] Y. C. Yeh, "Triple-triple redundant 777 primary flight computer," *1996 IEEE Aerosp. Appl. Conf. Proc.*, vol. 1, pp. 293–307, 1996.

[19] Federal Aviation Authority, "Chapter 13 - Aircraft Landing Gear Systems," in *Aviation Maintenance Technician Handbook - Airframe*, 2014, pp. 1–96.

[20] Wings of History Air Museum, "American Eagle A-101," 2015. [Online]. Available: http://wingsofhistory.org/exhibits/aircraft-on-display/american-eagle-exhibit?showall=1&limitstart=. [Accessed: 28-Jun-2015].

[21] S. Kellas, "Design , Fabrication and Testing of a Crushable Energy Absorber for a Passive Earth Entry Vehicle," NASA. Fairfax, Virginia, 2002.

[22] D. F. Shanahan, "Basic Principles of Crashworthiness," in *RTO-EN-HFM-113 Pathological Aspects and Associated Biodynamics in Aircraft Accident, The Human Factors and Medicine Panel (HFM) Lecture Series*, 2004.

[23] C. M. Kindervater and H. Georgi, "Composite strength and energy absorption as an aspect of structural crash resistance," in *Structural Crashworthiness and Failure: Proceedings of the Third International Symposium on Structural Crashworthiness*, 1993, pp. 162–203.

[24] J. D. Cronkhite, T. J. Hass, and R. W. Mort, "Energy absorbing composite aircraft structure," Pat. No. 4593870-, 1986.

[25] Fédération Internationale de l'Automobile, "Formula One Technical Regulations - Article 16," 2014.

[26] C. Bisagni, G. Di Pietro, L. Fraschini, and D. Terletti, "Progressive crushing of fiber-reinforced composite structural components of a Formula One racing car," *Compos. Struct.*, vol. 68, no. 4, pp. 491–503, May 2005.

[27] S. Collins, "Sauber C34," *Racecar Engineering*, 2015. [Online]. Available: http://www.racecar-engineering.com/cars/sauber-c34/#. [Accessed: 11-Mar-2016].

[28] British Standard, "BS EN 15227: Railway applications — Crashworthiness requirements for railway vehicle bodies." pp. 1–39, 2010.

[29] Deutsche Welle, "Woman dies from injuries from Amsterdam train crash," 2012. [Online]. Available: http://www.dw.de/woman-dies-from-injuries-from-amsterdam-train-crash/a-15903665. [Accessed: 22-Sep-2015].

[30] A. Klanac, S. Ehlers, and J. Jelovica, "Optimization of crashworthy marine structures," *Mar. Struct.*, vol. 22, no. 4, pp. 670–690, Oct. 2009.

[31] A. Erskine, "Literature review of rail vehicle structural crashworthiness," 2003.

[32] L. Lim, "Some aspects of the crashworthiness of rail vehicles: Volume 1," University of Sheffield, 1996.

[33] X. Xue, S. Ingleton, J. Roberts, and M. Robinson, "Qualitative comparison of the characteristics of articulated and non-articulated trains and their effects on impact," *Proc. Inst. Mech. Eng. Part F J. Rail Rapid Transit*, vol. 225, pp. 24–37, Jan. 2011.

[34] ReasonRail's channel, "FRA crash energy management collision tests." [Online]. Available: http://www.youtube.com/watch?v=NUpUJrk4QBE. [Accessed: 30-Jun-2012].

[35] British Standard, "BS EN 12663: Railway applications — Structural requirements of railway vehicle bodies." pp. 1–39, 2010.

[36] Office of Rail Regulation, "ORR's Sustainable Development & Environment Duties - A Consultation Document," 2006.

[37] R. Ford, "Transport Mass," in *Institution of Mechanical Engineers Seminar: Weight Saving and Structural Integrity of Rail Vehicles*, 2007.

[38] Rail Safety and Standards Board, "Rail Technical Strategy 2012," 2012.

[39] A. Garcia, "High speed, energy consumption and emissions," 2010.

[40] B. Eickhoff and R. Nowell, "Determining the benefit of train mass reduction," in *World Congress on Railway Research*, 2011, no. 1405, pp. 1–9.

[41] Association of Train Operating Companies (ATOC), "Baseline Energy Statement – Energy consumption and carbon dioxide emissions on the railway," 2007.

[42] A. Cortesi, T. Issenmann, and T. Kalbermatten, "Light nose for fast locomotives.," *Schweizer Eisenbahn Review*, pp. 435–442, 1991.

[43] Bombardier, "SPACIUM commuter train - Ile-de-France," 2013. [Online]. Available: http://www.bombardier.com/en/transportation/projects/project.spacium-paris-france.html. [Accessed: 15-Oct-2014].

[44] Bombardier, "Spacium Electric Multiple Unit," 2015. [Online]. Available: http://www.bombardier.com/content/dam/Websites/bombardiercom/Projects/spacium-electric-multiple-unit-paris-4486.jpg/_jcr_content/renditions/cq5dam.web.750.750.jpeg. [Accessed: 15-Oct-2014].

[45] J. Carruthers, S. Ingleton, C. O'Neill, and J. Roberts, "De-Light Transport: Deliverable Report – WP4F Rail Vehicle Driver's Cab," 2010.

[46] British Standard, "BS EN 45545:Railway applications - Fire protection on railway vehicles." 2013.

[47] Seventh Framework Programme - Grant agreement 246037, "Fire-Resist." .

[48] "EasyComposites," 2017. [Online]. Available: http://www.easycomposites.co.uk. [Accessed: 10-Apr-2017].

[49] EasyComposites, "Technical Data Sheet Product : High Density Polyurethane Foam Block," 2017.

[50] Owens Corning, "M705 Chopped Strand Mat Datasheet," 2014.

[51] Owens Corning, "Advantex ® Boron-Free E-CR Glass Reinforcement Specification," 2010.

[52] Sicomin Epoxy Systems, "SR 1500 Technical Datasheet," 2014.

[53] J. Roberts, "Passive Safety - Bombardier presentation." 2012.

[54] M. Bak, "New FEA Tools Tackle Composite Challenges," 2017. [Online]. Available: http://www.machinedesign.com/materials/new-fea-tools-tackle-composite-challenges. [Accessed: 08-Jul-2017].

[55] Livermore Software Technology Corporation, “Material selector for LS-DYNA,” 2017. [Online]. Available: http://www.lstc.com/dynamat/. [Accessed: 02-Jul-2017].

[56] B. Z. Hague and J. W. J. Gillespie, “Rate Dependent Progressive Composite Damage Modeling,” in *13th International LS-DYNA Users Conference Session:*, 2014, pp. 1–15.

[57] A. Onder, C. O’Neill, and M. Robinson, “Flying ballast resistance for composite materials in railway vehicle carbody shells,” *Transp. Res. Procedia*, vol. 14, pp. 595–604, 2016.

[58] S. Barre, T. Chotard, and M. L. Benzeggagh, “Comparative study of strain rate effects on mechanical properties of glass fibre- reinforced thermoset matrix composites,” *Compos. Part A*, vol. 27A, pp. 1169–1181, 1996.

[59] J. J. Carruthers, “Some aspects of the energy absorption of composite materials,” University of Sheffield, 1997.

[60] G. L. Farley, “Energy Absorption of Composite Materials,” *J. Compos. Mater.*, vol. 17, no. May, pp. 267–279, 1983.

[61] A. G. Mamalis, Y. B. Yuan, and G. L. Viegelahn, “Collapse of thin-wall composite sections subjected to high speed axial loading,” *Int. J. Veh. Des.*, vol. 13, no. 5–6, pp. 564–579, 1992.

[62] D. W. Schmueser and L. E. Wickliffe, “Impact Energy Absorption of Continuous Fiber Composite Tubes,” *J. Eng. Mater. Technol.*, vol. 109, pp. 72–77, 1987.

[63] F. . Bardi, H. . Yun, and S. Kyriakides, “On the axisymmetric progressive crushing of circular tubes under axial compression,” *Int. J. Solids Struct.*, vol. 40, no. 12, pp. 3137–3155, Jun. 2003.

[64] S. R. Reid, “Plastic deformation mechanisms in axially compressed metal tubes used as impact energy absorbers,” *Int. J. Mech. Sci.*, vol. 35, no. 12, pp. 1035–1052, 1993.

[65] F. C. Bardi and S. Kyriakides, “Plastic buckling of circular tubes under axial compression—part I: Experiments,” *Int. J. Mech. Sci.*, vol. 48, no. 8, pp. 830–841, Aug. 2006.

[66] A. Alghamdi, “Collapsible impact energy absorbers: an overview,” *Thin-Walled Struct.*, vol. 39, no. 2, pp. 189–213, Feb. 2001.

[67] M. A. Aleitani, M. A. Alzahrani, and A. A. Aljinidi, “Blast Loading of Triangular Conical Truncated Energy Absorber,” in *IMPLAST Conference*, 2010, pp. 1–9.

[68] L. Czechowski and J. Jankowski, “Failure Analysis of an Energy Absorber Subjected to Pressure Pulse,” *Mech. Mech. Eng.*, vol. 14, no. 2, pp. 193–199, 2010.

[69] A. G. Olabi, E. Morris, and M. S. J. Hashmi, “Metallic tube type energy absorbers: A synopsis,” *Thin-Walled Struct.*, vol. 45, no. 7–8, pp. 706–726, Jul. 2007.

[70] P. Feraboli, C. Norris, and D. McLarty, “Design and certification of a composite thin-walled structure for energy absorption,” *Int. J. Veh. Des.*, vol. 44, no. 3/4, pp. 247–267, 2007.

[71] J. N. Price and D. Hull, “Axial crushing of glass fibre-polyester composite cones,” *Compos. Sci. Technol.*, vol. 28, no. 3, pp. 211–230, Jan. 1987.

[72] S. B. Bodlani, S. C. K. Yuen, and G. N. Nurick, “The Energy Absorption Characteristics of Square Mild Steel Tubes With Multiple Induced Circular Hole

Discontinuities—Part I: Experiments," *J. Appl. Mech.*, vol. 76, no. 4, p. 41012, 2009.

[73] S. T. S. Al-Hassani, W. Johnson, and W. T. Lowe, "Characteristics of inversion tubes under axial loading," *J. Mech. Eng. Sci.*, vol. 14, pp. 370–381, 1972.

[74] P. Rosa, R. Baptista, J. Rodrigues, and P. Martins, "An investigation on the external inversion of thin-walled tubes using a die," *Int. J. Plast.*, vol. 20, no. 10, pp. 1931–1946, Oct. 2004.

[75] L. R. Guist and D. P. Marble, "NASA Technical Note: Prediction of the inversion load of a circular tube," 1966.

[76] M. Shakeri, S. Salehghaffari, and R. Mirzaeifar, "Expansion of circular tubes by rigid tubes as impact energy absorbers: experimental and theoretical investigation," *Int. J. Crashworthiness*, vol. 12, no. 5, pp. 493–501, Oct. 2007.

[77] K. Ahn, J. S. Kim, H. Huh, and S. Engineering, "The effects of local buckling on the crash energy absorption of thin-walled expansion tubes," *Int. J. Mod. Phys. B*, vol. 22, no. 31, pp. 799–804, 2008.

[78] J. S. Kim, H. S. Jung, and T. S. Kwon, "Train Crash Test Facilities and Application," in *WCRR*, 2013, pp. 1–6.

[79] J. S. Kim, H. S. Jung, and T. S. Kwon, "Effect of punch angle on energy absorbing characteristics of tube-type crash elements," vol. 12, no. 3, pp. 383–389, 2011.

[80] X. Huang, G. Lu, and T. X. Yu, "Energy absorption in splitting square metal tubes," *Thin-Walled Struct.*, vol. 40, no. 2, pp. 153–165, Feb. 2002.

[81] X. Huang, G. Lu, and T. X. Yu, "Collapse of square metal tubes in splitting and curling mode," *Proc. Inst. Mech. Eng. Part C J. Mech. Eng. Sci.*, vol. 220, no. 1, pp. 1–13, Jan. 2006.

[82] Axtone Group, "CRASH Technology," 2014. [Online]. Available: http://www.axtone.eu/en/crash-technology.html. [Accessed: 03-Aug-2014].

[83] D. P. Taylor, "Energy Management Utilizing the Hydraulic Shock Absorber."

[84] Oleo International, "Oleo Hydraulic Principle," 2014. [Online]. Available: http://www.oleo.co.uk/hydraulic-principle. [Accessed: 03-Aug-2014].

[85] Oleo International, "Rail products and services catalogue," 2013.

[86] S. Ramakrishna and D. Hull, "Energy absorption capability of epoxy composite tubes with knitted carbon fibre fabric reinforcement," *Compos. Sci. Technol.*, vol. 49, pp. 349–356, 1993.

[87] D. Hull, "A unified approach to progressive crushing of fibre-reinforced composite tubes," *Compos. Sci. Technol.*, vol. 40, no. 4, pp. 377–421, Jan. 1991.

[88] V. M. Karbhari and J. E. Hailer, "Rate and architecture effects on progressive crush of braided tubes," *Compos. Struct.*, vol. 43, pp. 93–108, 1998.

[89] G. Pitarresi *et al.*, "A comparative evaluation of crashworthy composite sandwich structures," *Compos. Struct.*, vol. 78, no. 1, pp. 34–44, 2007.

[90] L. Pilon, A. G. Fedorov, and R. Viskanta, "Gas Diffusion in Closed-Cell Foams," *J. Cell. Plast.*, vol. 36, no. 6, pp. 451–474, 2000.

[91] Zhiling International Industrial Limited, "Polyurethane foams," 2013. [Online]. Available: http://zhilint.com/images/Panels.jpg. [Accessed: 17-Jun-2015].

[92] Australian Urethane Systems, “Polyisocyanurate systems for pour and block foam,” 2014. [Online]. Available: http://www.ausurethane.com/pir.html. [Accessed: 17-Jun-2015].

[93] Poliuretanos, “PIR ALU-T,” 2014. [Online]. Available: http://www.poliuretanos.com/en/images/productes/productes/PIR-ALU-T.jpg. [Accessed: 17-Jun-2015].

[94] Federation of European Rigid Polyurethane Foam Associations, “Thermal insulation materials made of rigid polyurethane foam,” 2006.

[95] M. Avalle, G. Belingardi, and R. Montanini, “Characterization of polymeric structural foams under compressive impact loading by means of energy-absorption diagram,” *Int. J. Impact Eng.*, vol. 25, no. 5, pp. 455–472, May 2001.

[96] J. Banhart, “Manufacture, characterisation and application of cellular metals and metal foams,” *Prog. Mater. Sci.*, vol. 46, no. 6, pp. 559–632, Jan. 2001.

[97] J. U. Baumeister, J. Banhart, and M. Weber, “Aluminium foams for transport industry,” *Mater. Des.*, vol. 18, pp. 217–220, 1998.

[98] S. Santosa and T. Wierzbicki, “Crash behavior of columns filled with aluminum honeycomb or foam,” *Comput. Struct.*, vol. 68, no. 4, p. 343−367, 1998.

[99] S. S. Cheon and S. A. Meguid, “Crush Behavior of Metallic Foams for Passenger Car Design,” *Int. J. Automot. Technol.*, vol. 5, no. 1, pp. 47–53, 2004.

[100] A. Rabiei and M. Garcia-Avila, “Effect of various parameters on properties of composite steel foams under variety of loading rates,” *Mater. Sci. Eng. A*, vol. 564, pp. 539–547, Mar. 2013.

[101] E. Cardoso and B. F. Oliveira, “Study of the use of metallic foam in a vehicle for an energy-economy racing circuit.,” *Materwiss. Werksttech.*, vol. 41, no. 5, pp. 257–264, Jun. 2010.

[102] B. E. Maine and M. F. Ashby, “Cost Estimation and the Viability of Metal Foams,” *Adv. Eng. Mater.*, no. 4, pp. 205–209, 2000.

[103] B. H. Smith, S. Szyniszewski, J. F. Hajjar, B. W. Schafer, and S. R. Arwade, “Steel foam for structures: A review of applications, manufacturing and material properties,” *J. Constr. Steel Res.*, vol. 71, pp. 1–10, Apr. 2012.

[104] J. Baron, “Finding the Softer Side of Steel,” *North Carolina State University*, 2014. [Online]. Available: http://www.mae.ncsu.edu/rabiei/Archive/online_NEWS_articles/America_gov_article.htm. [Accessed: 18-Feb-2016].

[105] F. C. Campbell, *Manufacturing Technology for Aerospace Structural Materials*. Elsevier, 2006.

[106] T. N. Bitzer, *Honeycomb Technology - Materials, Design, Manufacturing, Applications and Testing*. Chapman & Hall, 1997.

[107] Q. Liu, “Literature Review : Materials with Negative Poisson’s Ratios and Potential Applications to Aerospace and Defence,” *Australian Government Department of Defence*, pp. 1–47, 2006.

[108] C. O’Neill, “De-Light Transport: Honeycomb crush tests (Test Report),” 2008.

[109] T. Jost, T. Heubrandtner, C. Ruff, and B. Fellner, “A New Method to Model

Aluminium Honeycomb Based Crash Barriers in Lateral and Frontal Crash Load Cases," in *LS-DYNA Anwenderforum*, 2008, pp. 13–24.

[110] Applied Vehicle Technology, "Nomex Honeycomb," 2014. [Online]. Available: http://www.avtcomposites.com/PDGImages/catalog12711 079.jpg. [Accessed: 18-Feb-2016].

[111] Southern Bracing Systems, "Kraft honeycomb panel," 2014. [Online]. Available: http://www.southernbracing.com/images/products/honey/Honeycomb_panel_widths_med.jpg. [Accessed: 18-Feb-2016].

[112] S. Abrate, B. Castanie, and Y. Rajapakse, *Dynamic Failure of Composite and Sandwich Structures*. Springer, 2013.

[113] HEXCEL Composites, "HexWeb honeycomb attributes and properties." p. 16, 1999.

[114] Universal Metaltek, "Design Criteria & Fixing Techniques: Aluminium Honeycomb Panel," 2014.

[115] L. H. Lange, "What Is the Biggest Rectangle You Can Put Inside a Given Triangle?," *Coll. Math. J.*, vol. 24, no. 3, pp. 237–240, 1993.

[116] ErcumentGorgul, "Shinkansen 500 Kyoto," 2005. [Online]. Available: http://de.wikipedia.org/wiki/Shinkansen#mediaviewer/Datei:Shinkansen_500_Kyoto_2005-04-05.jpg. [Accessed: 15-Mar-2016].

[117] P. Christener, "Talgo 350," 2003. [Online]. Available: http://commons.wikimedia.org/wiki/File:Talgo_350.jpg. [Accessed: 15-Mar-2016].

[118] Sukhoi37, "E6," 2011. [Online]. Available: http://de.wikipedia.org/wiki/Shinkansen-Baureihe_E6#mediaviewer/Datei:E6系新幹線電車(2011.11.9)-2.jpg. [Accessed: 15-Mar-2016].

[119] Bombardier Transportation, "Private communication, Presented at the DE-LIGHT Transport WP4F Kick-Off Meeting, Brussels." 2006.

[120] M. Grasso, "PhD Thesis - Modeling of Lightweight Crashworthy Rail Components," Università degli Studi di Napoli Federico II, 2009.

[121] J. Prockat, C. O'Neill, J. Carruthers, and M. Robinson, "Lightweight compound cab structure for a rail vehicle," *WIPO Pat. No. WO2012038383*, 2011.

[122] World Intellectual Property Organization, "LIGHTWEIGHT COMPOUND CAB STRUCTURE FOR A RAIL VEHICLE," 2016. [Online]. Available: https://patentscope.wipo.int/search/en/detail.jsf?docId=WO2012038383&recNum=32&office=&queryString=ALLNAMES%3A%28conor+o%27neill%29&prevFilter=&sortOption=Pub+Date+Desc&maxRec=45. [Accessed: 01-Feb-2016].

[123] Voith, "Connect and Protect. GALEA." pp. 1–6, 2012.

[124] Bombardier, "Futur Train des Franciliens - Analyses Crash." Presentation, personal communication, 2006.

[125] C. O'Neill and A. M. Robinson, "Self-correcting crash energy absorber," *EPO Pat. No. EP2459429 A1*, 2010.

[126] World Intellectual Property Organization, "SELF-CORRECTING CRASH ENERGY ABSORBER," 2016. [Online]. Available: https://patentscope.wipo.int/search/en/detail.jsf?docId=EP46615664&recNum=31&office=&queryString=ALLNAMES%3A%28conor+o%27neill%29&prevFilter=&sortOpti

on=Pub+Date+Desc&maxRec=45. [Accessed: 01-Feb-2016].

[127] G. Pitarresi *et al.*, “A comparative evaluation of crashworthy composite sandwich structures,” *Compos. Struct.*, vol. 78, no. 1, pp. 34–44, 2007.

[128] S. Ingleton, “Design of Composite Cabs in Railway Rolling Stock for Structural Applications,” University of Sheffield, 2006.

[129] European Commission, “Investing in success,” *Horizon 2020 publication*, vol. 1, no. 1. pp. 28–29, 2012.